MECHANISTIC STUDIES OF THE METAL CATALYZED FORMATION OF POLYCARBONATES AND THEIR THERMOPLASTIC ELASTOMERS

A Dissertation

by

WONSOOK CHOI

Submitted to the Office of Graduate Studies of
Texas A&M University
in partial fulfillment of the requirements for the degree of

DOCTOR OF PHILOSOPHY

August 2007

Major Subject: Chemistry

MECHANISTIC STUDIES OF THE METAL CATALYZED FORMATION OF POLYCARBONATES AND THEIR THERMOPLASTIC ELASTOMERS

A Dissertation

by

WONSOOK CHOI

Submitted to the Office of Graduate Studies of
Texas A&M University
in partial fulfillment of the requirements for the degree of

DOCTOR OF PHILOSOPHY

Approved by:

Chair of Committee,	Donald J. Darensbourg
Committee Members,	Michael B. Hall
	John P. Fackler
	Hong Liang
Head of Department,	David H. Russell

August 2007

Major Subject: Chemistry

ABSTRACT

Mechanistic Studies of the Metal Catalyzed Formation of Polycarbonates and Their Thermoplastic Elastomers. (August 2007)

Wonsook Choi, B.S., Sogang University;

M.S., Sogang University;

M.S., University of New Mexico

Chair of Advisory Committee: Dr. Donald J. Darensbourg

Studies concerning the formation of industrially useful polycarbonates are the focus of this dissertation. Of particular importance is the biodegradable polymer, poly(trimethylene carbonate) which has a wide range of medical applications. The production of polycarbonates can be achieved by the ring-opening polymerization of cyclic carbonate, or the copolymerization of carbon dioxide and oxiranes or oxetanes. For the production of polycarbonates from these monomers, Schiff base metal complexes have been designed, synthesized, and optimized as catalysts. Detailed kinetic and mechanistic studies have been performed for the ring-opening polymerization of cyclic carbonates, as well as the copolymerization of carbon dioxide and oxiranes or oxetane. In addition, the copolymerization of cyclic carbonates and cyclic esters to modify the mechanical and biodegradable properties of materials used for medical devices has been studied using biocompatible metal complexes.

In the process for ring-opening polymerizations of trimethylene carbonate or lactides, Schiff base metal complexes (metal = Ca(II), Mg(II) and Zn(II)) have been shown to be very effective catalysts to produce high molecular weight polymers with narrow polydispersities. Kinetic studies demonstrated the polymerization reactions to proceed via a mechanism first order in [monomer], [catalyst], and [cocatalyst] if an external cocatalyst is applied, and to involve ring-opening by way of acyl-oxygen bond cleavage. The activation parameters ($\Delta H^{\neq}$, $\Delta S^{\neq}$ and $\Delta G^{\neq}$) were determined for ring-opening polymerization of trimethylene carbonate, ring-opening polymerization of lactides, and copolymerization of trimethylene carbonate and lactide.

In the process for copolymerization of carbon dioxide and oxetane, metal salen derivatives of Cr(III) and Al(III) along with cocatalyst such as n-Bu_4NX or PPNX (PPN = *bis*(triphenylphosphine)iminium, and X = Br, Cl and N_3) have been shown to be effective catalysts to provide poly(trimethylene carbonate) with only trace amount of ether linkages. The formation of copolymer is proposed not to proceed via the intermediacy of trimethylene carbonate, which was observed as a minor product of the coupling reaction. To support this conclusion, ring-opening polymerization of trimethylene carbonate has been performed and kinetic parameters have been compared with those from the copolymerization of carbon dioxide and oxetane.

DEDICATION

This dissertation is dedicated to my parents, my parents-in-law and my husband. Thanks to my family who has loved and supported me forever.

ACKNOWLEDGEMENTS

I would first and foremost like to thank my advisor, Dr. Donald J. Darensboug. For four years he has lavished his time and effort on my research. He always encouraged and inspired me, and let me feel comfortable even with my many shortcomings. I would also like to thank my other committee members, Dr. Michael Hall, Dr. John Fackler and Dr. Hong Liang for their precious time, valuable guidance and excellent advice.

I feel thankful for all DJD group members and have experienced great happiness working with them. Eric Frantz and Shawn Fitch helped me determine molecular weights of polymers. Eric's suggestions and comments helped me to conduct more concrete presentations. Jeremy Andreatta spared no pain whenever I needed his help in many quarters. I also thank Adriana Moncada for sharing in the project of copolymerization of oxetane and carbon dioxide, and Angela Jones for the biodegradation studies. Pop (Osit Karroonnirun) also helped me synthesize ligands for numerous Ca(II) complexes.

I want to especially thank former DJD group members, Dr. Poulomi Ganguly and Cass Richers for working on the ring-opening polymerization of cyclic monomers. Poulomi's exceptional mentoring and guidance and Cass's dedicated assistance helped me to perform more precise research. I also thank Dr. Ryan Mackiewicz for his help when I started my research in the DJD group, Dr. Damon Billodeaux for crystal structure

determination, and both Dr. Andrea Phelps and Dr. Jody Rodgers for their mentoring, and of course Sue Winters for her advice during my graduate study.

My gratitude also goes out to the MYD group members for their support and advice. Adriana Moncada, Elky Almaraz, and Roxanne Jenkins are thanked for the unforgettable friendship and enjoyable memories in College Station. All of the DJD and MYD group members were very nice to me and I really appreciate it.

Finally, I am grateful to my family and Jinho for their everlasting love and concerns.

TABLE OF CONTENTS

CHAPTER page

LIST OF TABLES

TABLE Page

LIST OF FIGURES

FIGURE Page

FIGURE Page

FIGURE Page

FIGURE Page

FIGURE Page

FIGURE Page

FIGURE Page

CHAPTER I

INTRODUCTION

Polycarbonates are very useful materials in industry because of their numerous applications. Polycarbonates are easily processed engineering plastics of high quality with a unique combination of properties including strength, lightness, durability, high transparency, and high heat resistance. Due to their outstanding properties (Table 1-1), polycarbonate plastics are used in many diverse applications, providing a range of benefits to consumers. They are found in thousands of everyday products such as automobiles, cell phones, computers and other business equipment, sporting goods, consumer electronics, household appliances, CDs, DVDs, food storage containers and plastic bottles. The tough, durable, shatter and heat resistant material is ideal for a myriad of applications.[1] The global market for polycarbonate has grown from 600,000 tons in 1990 to 1,800,000 tons in 2000. Market growth is expected to continue with an average growth rate of approximately 10% as new developments and applications contribute to the quality of life for consumers.[2] Polycarbonates also find use in biomedical applications due to their stability and biological inertness. They are generally environmentally friendly and readily degraded. They also have a low heat of combustion due to the number of oxygens in the polymer chain.

This dissertation follows the format and style of *Inorganic Chemistry*.

The industrial method for producing the most useful polycarbonate, Lexon, involves the polycondensation or melt polymerization of Bisphenol A and phosgene at very high temperature (< 300°C) (Figure 1-1). However, this process involves highly toxic and hazardous starting materials as well as the high cost of chlorinated solvents or produces highly toxic phenol byproducts. Moreover, the process is limited to affording aromatic polycarbonates of high molecular weight.[3] Aliphatic polycarbonates with high molecular weight cannot be obtained by polycondensation from aliphatic diols. All these factors have given impetus to the production of polycarbonates by more environmentally benign routes.

Table 1-1. Typical tensile strength, elongation and tensile modulus of polymers.[4]

polymer type	tensile strength (MPa)	elongation (%)	tensile modulus (GPa)
Acrylic	70	5	3.2
Nylon 6	70	90	0.8
Polyamide-Imide	110	6	4.5
Polycarbonate	**70**	**100**	**2.6**
Polyethylene, HDPE	15	500	0.8
Polyethylene Terephthalate (PET)	55	125	2.7
Polyimide	85	7	2.5
Polypropylene	40	100	1.9
Polystyrene	40	7	3

One such a route to produce polycarbonates is copolymerization of carbon dioxide and epoxides in the presence of an organometallic catalyst (Figure 1-2). Unfortunately, the concomitant formation of the thermally stable five-membered ring cyclic carbonate from aliphatic epoxides and carbon dioxide has hindered the wide scale use of this approach (Figure 1-3).[5]

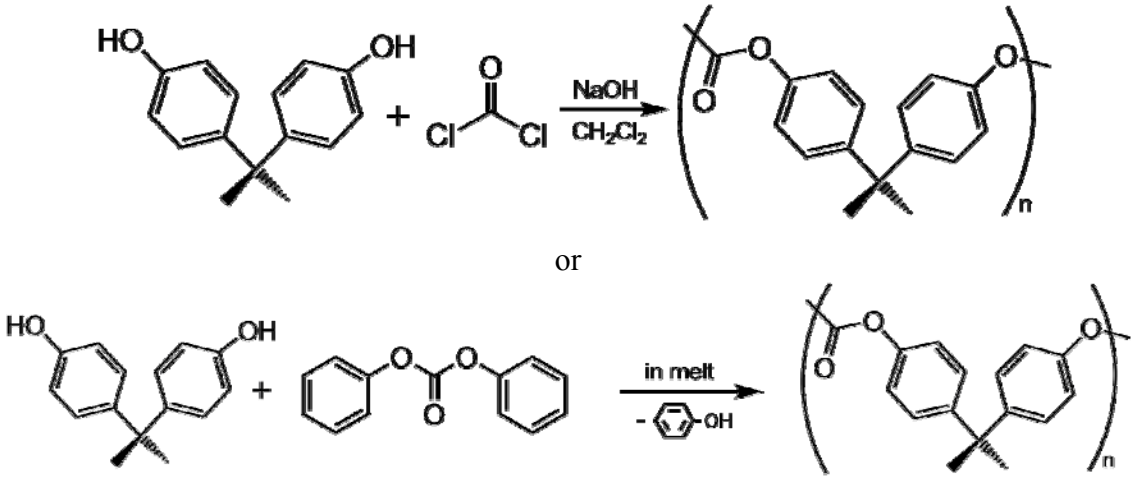

Figure 1-1. Industrial methods for the production of polycarbonate.

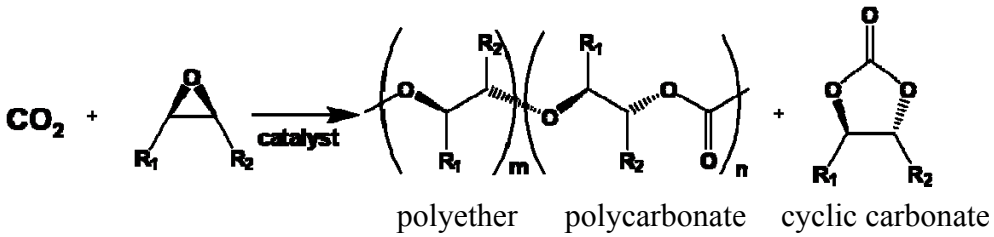

Figure 1-2. Copolymerization of carbon dioxide and epoxides.

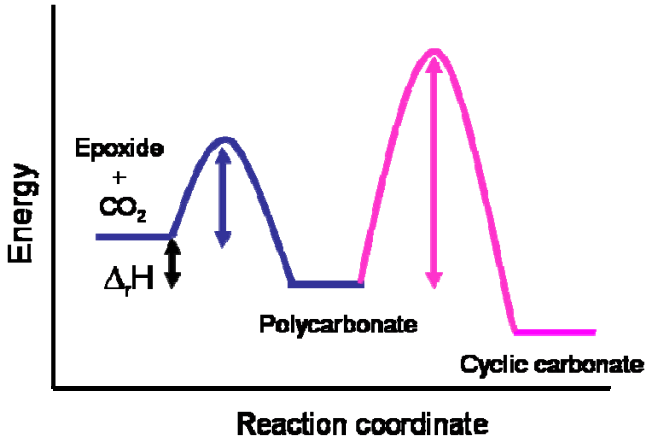

Figure 1-3. Reaction coordinate diagram for the coupling reaction of CO_2 and epoxide.

An alternative pathway to aliphatic polycarbonates is the ring-opening polymerization (ROP) of six-membered cyclic carbonates such as trimethylene carbonates (Figure 1-4). The analogous process involving five-membered cyclic carbonates affords polycarbonates with a significant quantity of ether linkages.[6] Five-membered cyclic carbonates afforded from CO_2 / epoxide are thermodynamically stable towards polycarbonate formation without loss of carbon dioxide. However, six-membered cyclic carbonates such as trimethylene carbonate (TMC) can under certain catalytic conditions provide aliphatic polycarbonates with complete retention of their CO_2 contents. That is, for six- and seven-membered cyclic carbonates ΔH_p is negative and ΔS_p is positive, hence, unlike their five-membered analogs, the polymerization of these cyclic carbonates is spontaneous at all temperatures (Figure 1-5).[7]

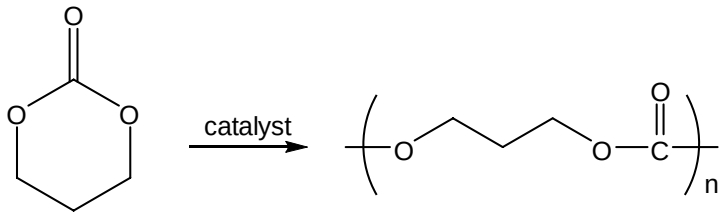

Figure 1-4. Ring-opening polymerization of trimethylene carbonate.

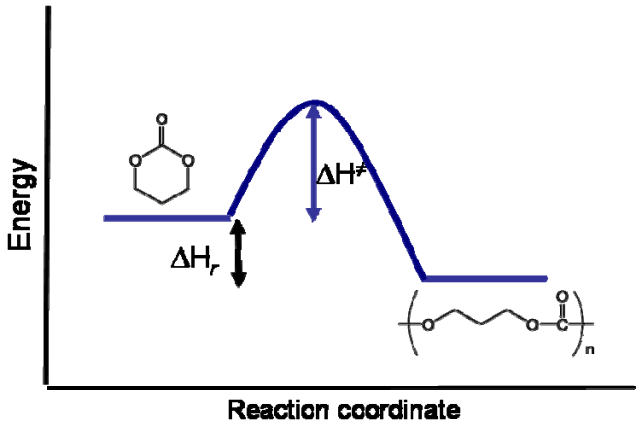

Figure 1-5. Reaction coordinate diagram for ring-opening polymerization of TMC.

Polymers from trimethylene carbonate (TMC) have unique properties with low glass transition temperature, and in conjunction with other comonomers are currently in use for biomedical applications.[8] However, poly(TMC) is a very soft and rubbery amorphous polymer with inappropriate mechanical properties for application in biomedical materials. To improve the mechanical properties, thermoplastic elastomers afforded from other biodegradable crystalline monomers such as glycolide, lactide, caprolactone, and *p*-dioxanone with TMC are ideal copolymers (Figure 1-6). These

cyclic esters can be polymerized via ring-opening polymerization similarly to ROP of TMC (Figure 1-7).

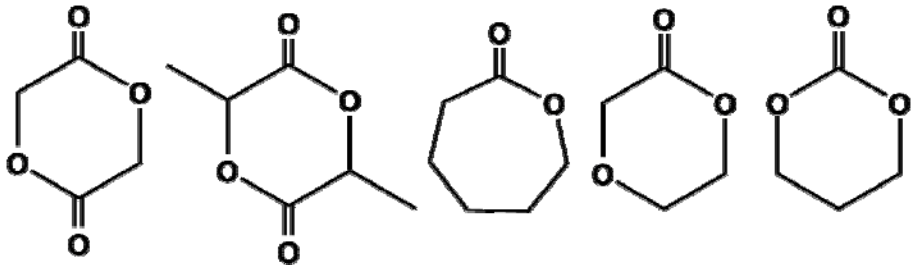

Figure 1-6. Biodegradable monomers (a) glycolide, (b) lactide, (c) caprolactone, (d) *p*-dioxanone, and (d) trimethylene carbonate (TMC).

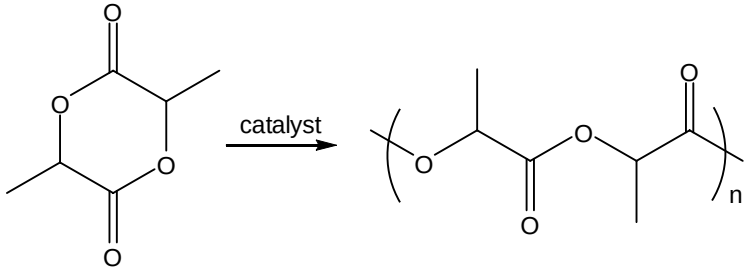

Figure 1-7. Ring-opening polymerization of lactide.

Polymers for use as biomaterials should have appropriate mechanical properties and should be degraded without inflammatory or toxic response. Mechanical properties are demanded for polymer processing and should match the application, remaining sufficiently strong until the surrounding tissue has healed. Biodegradation is need for these polymers to be used as implants, thereby, not requiring a second surgical

intervention for removal. Copolymers as biomaterials can be engineered to degrade at a rate that will slowly transfer load from the support to the healing bone since the bone has not been able to carry sufficient load during the healing process. Mechanical properties are related to the polymer's hydrophilicity, crystallinity, melt and glass-transition temperatures, molecular weight, molecular-weight distribution, end groups, and sequence distribution (random or block). Therefore, the mechanical properties can be improved by monomer selection, initiator selection, and process conditions. For the polymer degradation, polymers should have hydrolytically unstable linkages. Homopolymers or copolymers from the monomer shown in Figure 1-6 have proven to be degradable.

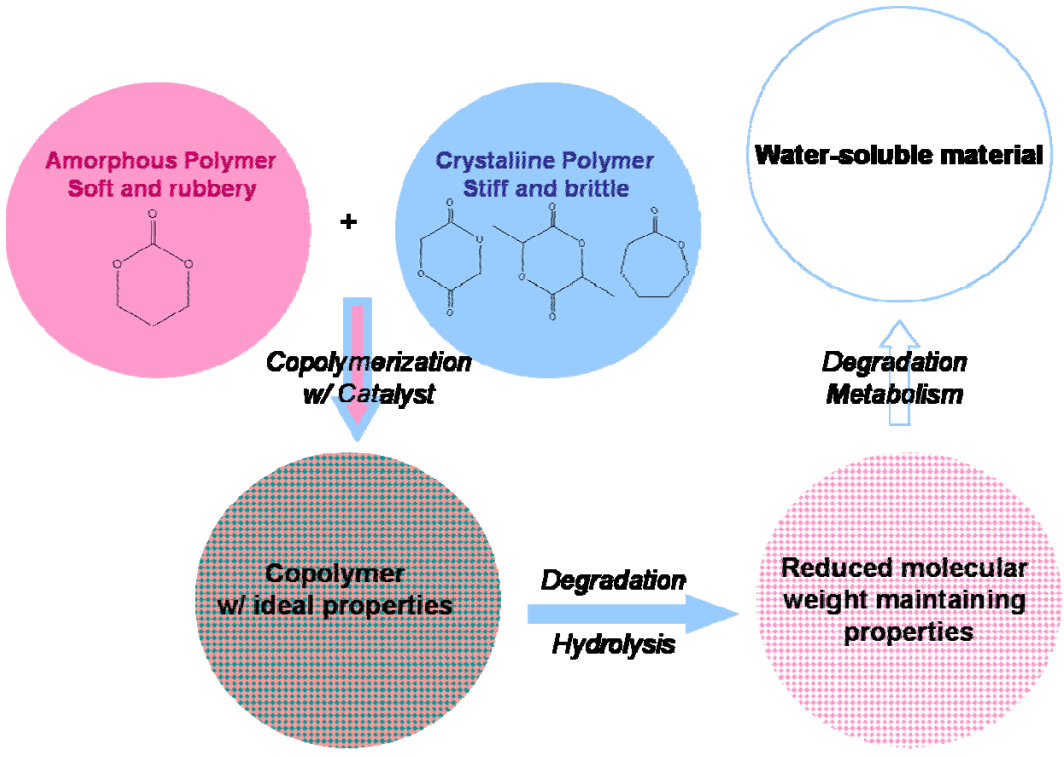

Figure 1-8. Biodegradation of thermoplastic elastomers.

Thermoplastic elastomers afforded from amorphous poly(TMC) and crystalline polymers degrade in 2 steps (Figrue1-8). The first step is hydrolysis by water. In this step, hydrolysis occurs mostly in hydrophilic region, thereby the copolymer becomes a matrix with reduced molecular weights. However, the remaining region of the copolymer maintains its mechanical properties to support surrounding tissue. The second step is metabolism by enzymes. In this step, the rest of the polymer becomes fragmented and turns into water soluble material.

Another method of producing poly(TMC) is from the copolymerization of carbon dioxide and a four membered cyclic ether (Figure 1-9). Unlike epoxides, such investigations have been rarely reported in the case of oxetane (trimethylene oxide) due to its lower reactivity. The products from the copolymerization of carbon dioxide and oxetane are poly(TMC) and TMC, the latter can also produce poly(TMC) via ring-opening polymerization since TMC is thermodynamically less stable than poly(TMC) (Figure 1-10).

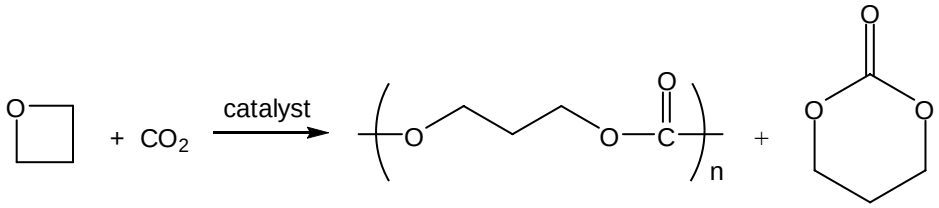

Figure 1-9. Copolymerization of carbon dioxide and oxetane.

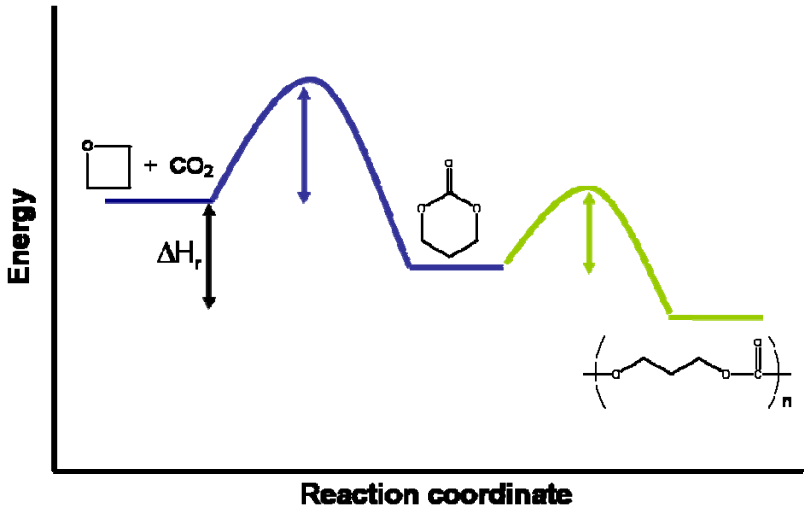

Figure 1-10. Reaction coordinate diagram for copolymerization of oxetane and carbon dioxide.

Our group has focused on alternating copolymerization of epoxides and carbon dioxide to produce polycarbonates using metal salen complexes as catalysts. Metal salen complexes are robust, easily synthesized and can be tuned among multiple electronic and steric variations by varying R, R^1, R^2 and X (Figure 1-11). Cocatalysts are required for this process and can be varied to enhance the catalytic activity.

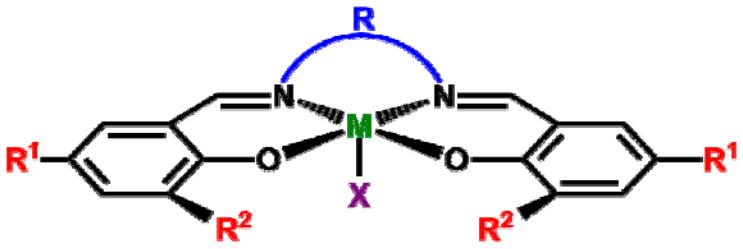

Figure 1-11. Metal salen complex.

Tridentate Schiff base ligands are easily synthesized and they have various applications as catalysts for ring-opening polymerization,[9] ethylene polymerization,[10] and atomic transfer radical polymerization.[11] Compared to salen ligands, they are tridentate and have a -1 charge while salen ligands are tetradentate and have a -2 charge. Modifications of the Schiff base ligands are readily achieved by variations of the aldehyde (variations of R^1 and R^2) and diamine (variation of R) starting reagents.[9,12] The structure of metal salen and tridentate Schiff base metal complexes are well established (Figure 1-12).[8-10]

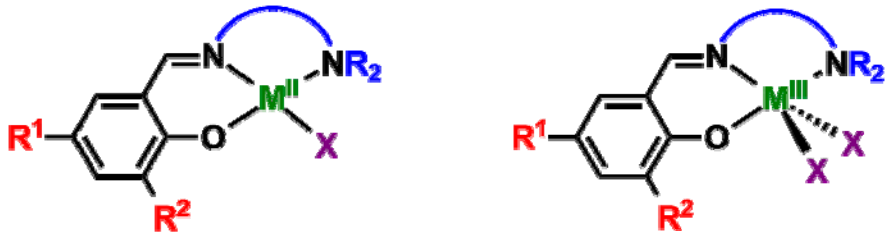

Figure 1-12. Tridentate Schiff base metal complex.

This dissertation will focus on mechanistic studies of formation of polycarbonates catalyzed by metal salen and tridentate Schiff base metal complexes. Kinetic and mechanistic studies have been performed for copolymerization of carbon dioxide and epoxides or oxetanes as well as ring-opening polymerization of cyclic carbonates and esters.[5,13]

CHAPTER II

RING-OPENING POLYMERIZATION OF CYCLIC MONOMERS: PRODUCTION OF POLY(LACTIDE), POLYCARBONATES AND THEIR COPOLYMERS*[#]

INTRODUCTION

Biodegradable polymers have become interesting in the last three decades due to their potential use as sutures, dental devices, orthopedic fixation devices, drug delivery system,[14] and tissue engineering.[15] Important among these materials are thermoplastic elastomers obtained from lactides and trimethylene carbonate.[16] These latter copolymers are prominently used as biodegradable internal fixation devices for repair of fractures to small bones and joints, such as feet / hands or ankles / wrists.[17] The aforementioned orthopedic fixation devices afford a natural healing process, where the copolymers degrade at a rate to progressively transfer the load from the device to the broken bone to aid in bone regeneration, at the same time eliminating the need for a second surgery.

Six-membered cyclic carbonates such as trimethylene carbonate (TMC) can under certain catalytic conditions provide aliphatic polycarbonates with complete retention of their CO_2 contents (eq. 2-1). Presently, the most widely employed catalysts

---

for the anionic ring-opening polymerization of TMC are salts of aluminum and tin.[18] Our group,[19] as well as Cao and coworkers,[20] have reported the use of well-defined, effective salen derivatives of aluminum for the ring-opening polymerization of trimethylene carbonate. Previously, studies have demonstrated organozinc, calcium, and magnesium compounds to be active catalysts for lactide polymerization. Dibutylmagnesium has been used as a catalyst for the ring-opening polymerization of DMC (2,2-dimethyltrimethylene carbonate) by Keul and coworkers.[21] Also in a recent report Dobrznski and coworkers have employed acetylacetonate derivatives of zinc, iron, and zirconium as catalysts for the polymerization of both TMC and DMC.[22] Recently, special attention has been given to exploring biocompatible metal catalysts, e.g., calcium complexes for the ring-opening polymerization of cyclic esters or cyclic carbonates due to the difficulty of removing trace quantities of catalyst residues from the thereby produced polycarbonates.[23]

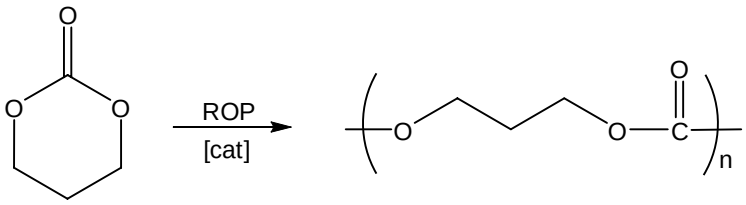

2-1

Poly(lactide) as a biodegradable polymer has been intensively studied with wide range of applications, and ring-opening polymerization of lactides has been investigated using Sn,[24] Y,[25] Ln,[26] Fe,[27] Ti,[28] Mg,[29] Al,[19,30] and Zn[9,31] complexes (eq. 2-2). Lactide is a cyclic dimer produced from the dehydration of lactic acid, which can be obtained on

the basis of renewable starch containing resources (e.g. corn, wheat or sugar beet) by fermentation, or by chemical synthesis (Scheme 2-1). Lactide has the three isomers, *L*-lactide, *D*-lactide and *meso*-lactide where *L* and *D*-lactide are enantiomers that comprise the *rac*-lactide (Figure 2-1). Pure *L*-lactide or *D*-lactide forms crystalline isotactic polymer (Figure 2-2) while *rac*-lactide without control of stereocenters forms amorphous atactic polymer which is inappropriate for the commercial application (Figure 2-3).

Scheme 2-1. Poly(lactide) as a renewable resource

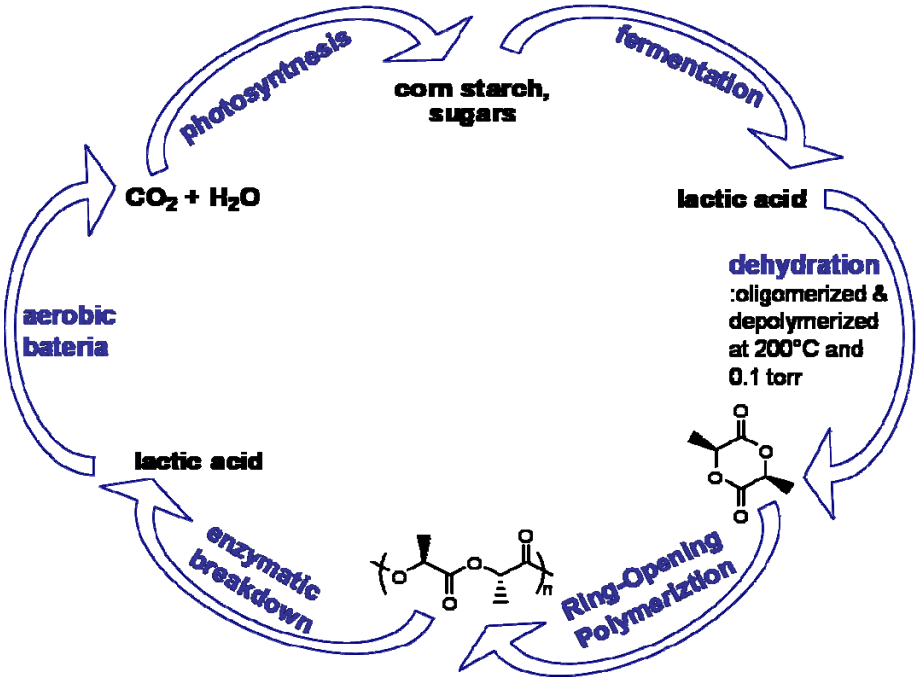

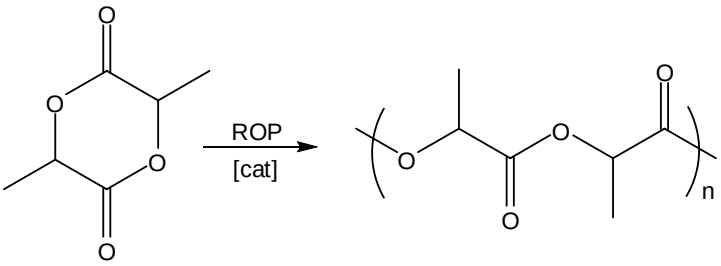

2-2

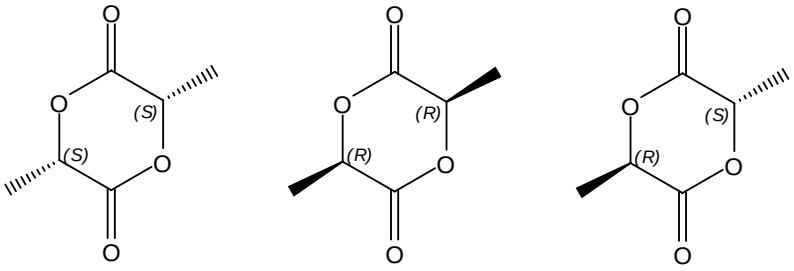

L-lactide *D*-lactide *meso*-lactide

Figure 2-1. The three lactide isomers.

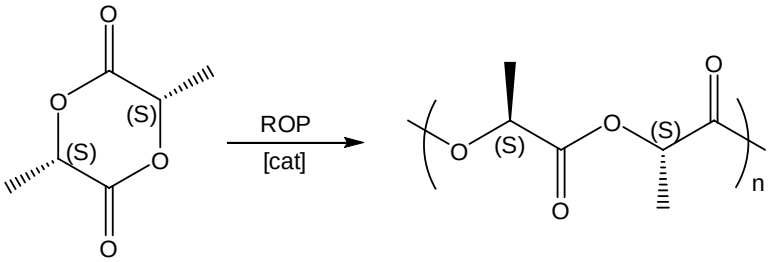

L-lactide isotactic poly(lactide)

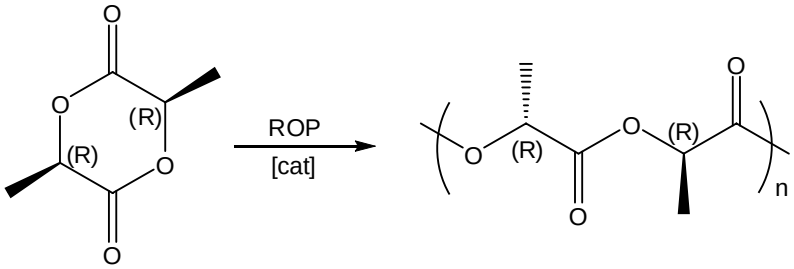

D-lactide isotactic poly(lactide)

Figure 2-2. Isotactic poly(lactide) from ring-opening polymerization of *L*- or *D*-lactide.

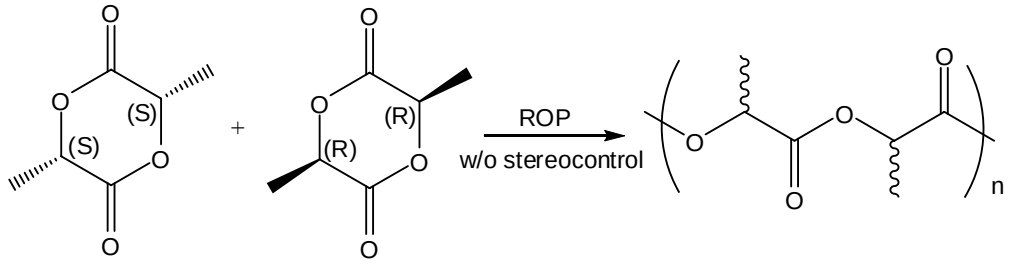

rac-lactide atactic poly(lactide)

Figure 2-3. Atactic poly(lactide) from ring-opening polymerization of *rac*-lactide without stereocontrol.

The control of stereoregularity in polymers by catalysts is an important feature for applications since the tacticity of the polymer leads to different properties. The selectivity for lactide polymerization has been studied.[32] Spassky *et al*. reported chiral binaphthyl Schiff base aluminum methoxide for stereoselectivity in the polymerization of *rac*-lactide where the aluminum methoxide complex demonstrated a preference for *D*-lactide over *L*-lactide to produce an optically active isotactic poly(*D*-lactide) from *rac*-lactide in toluene at 70 °C at low conversion of polymerization (Figure 2-4).[33]

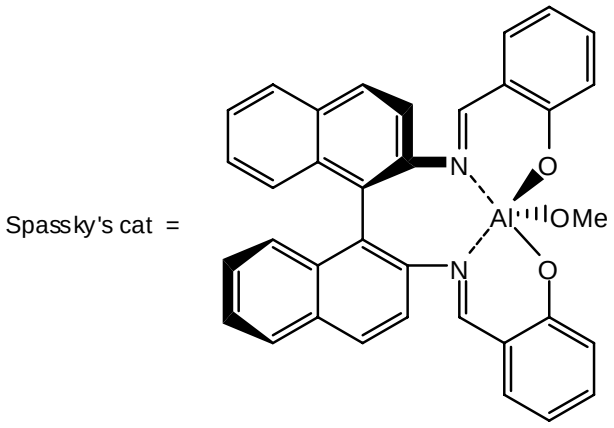

(chiral binaphthyl Schiff base)AlOMe

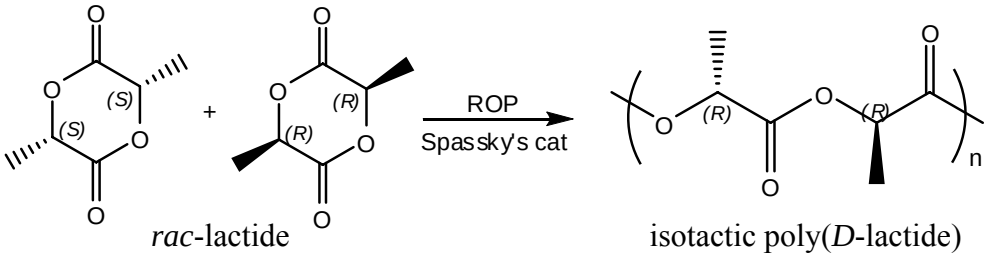

rac-lactide isotactic poly(*D*-lactide)

Figure 2-4. Isotactic poly(*D*-lactide) from the ring-opening polymerization of *rac*-lactide with Spassky's catalyst.

Similar chiral aluminum alkoxide by Coates *et al.*[34] produces highly syndiotactic polylactide from *meso*-lactide (Figure 2-5), and Feijen *et al*. employed chiral salen ligand to aluminum which demonstrated the polymerization of *L*-lactide to be faster than that of *D*-lactide (k_L/k_D = 14) and mostly yields isotactic poly(*L*-lactide) from *rac*-lactide with a selectivity factor of 5.5 (Figure 2-6).[30a] Since these catalysts have chiral centers, an enantiomorphic site control mechanism is possible. Recently, Chisholm and coworkers have shown that calcium complexes containing bulky *tris*-pyrazolyl borate

ligands and phenolate or $N(SiMe_3)_2$ initiators polymerize *rac*-lactide with a high degree of heteroactivity in THF (Figure 2-7).[31]

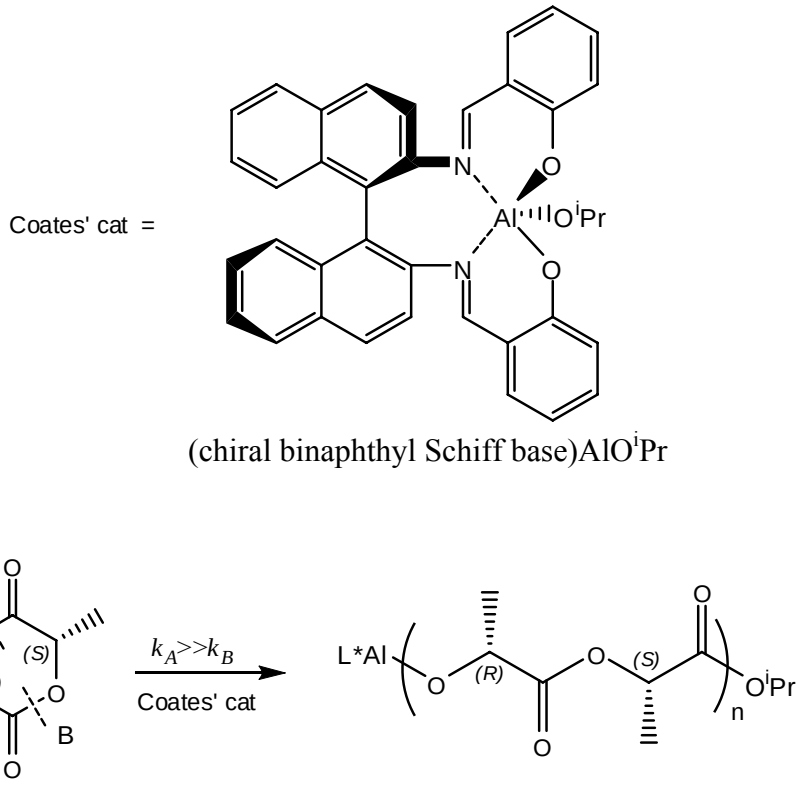

Figure 2-5. Syndiotactic poly(lactide) from the ring-opening polymerization of *meso*-lactide using Coates' catalyst.

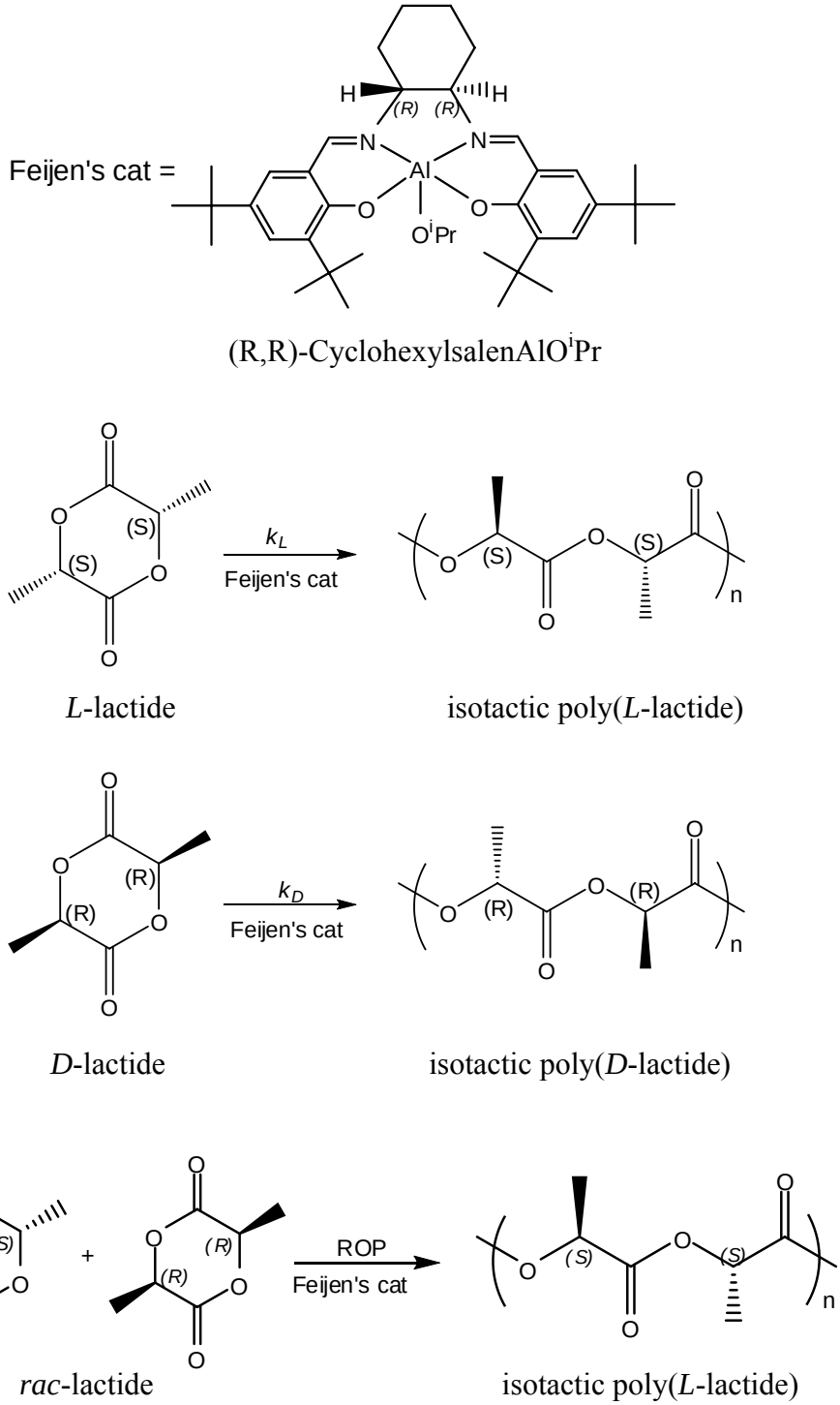

Figure 2-6. Stereoselectivity for poly(lactide) toward *L*-lactide with Feijen's catalyst.

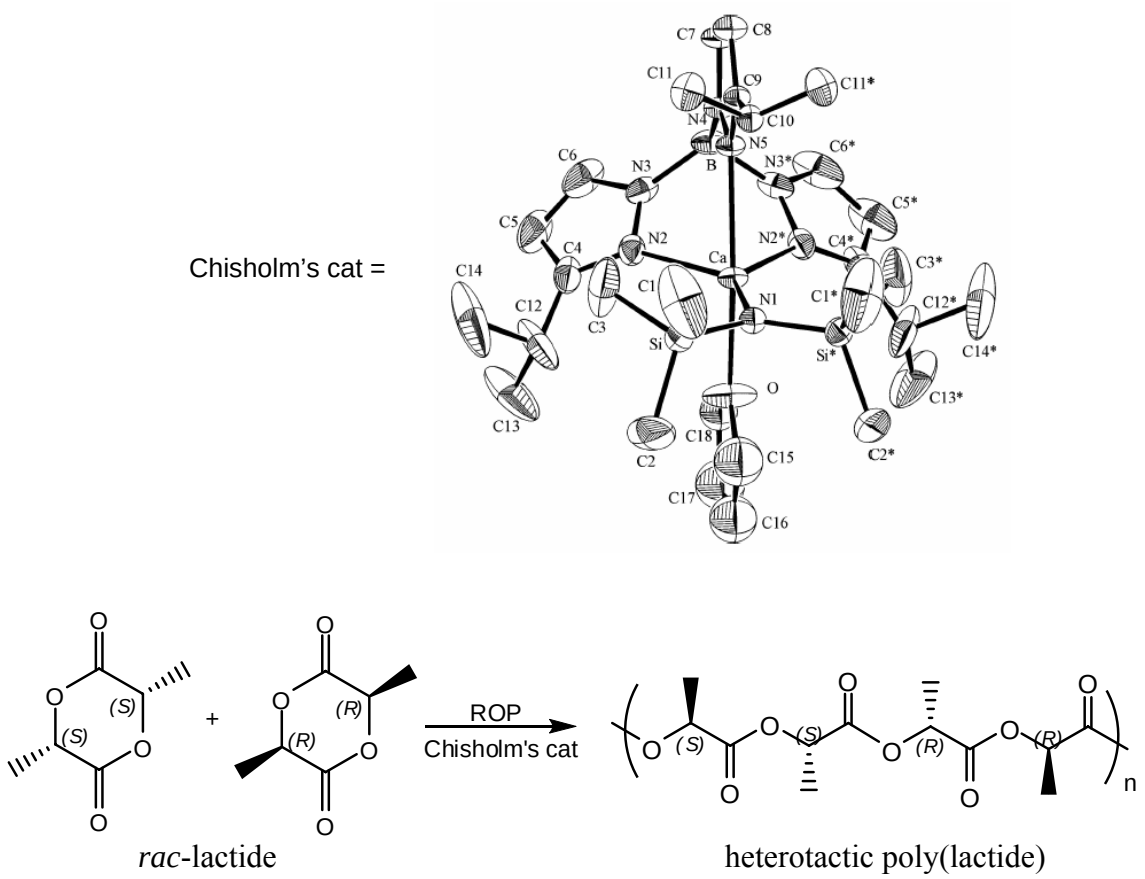

Figure 2-7. Heterotactic poly(lactide) from the ring-opening polymerization of *rac*-lactide with Chisholm's catalyst.

Copolymerization reactions of cyclic carbonate and cyclic ester have been studied using Sn,[24] Y[25] and Ln[26] catalysts. However, these catalysts cannot tailor ideal copolymers, resulting in random or block copolymer with low molecular weight and broad or bimodal molecular distributions. Due to the difficulty to control copolymer's composition and molecular weight, these catalysts yield copolymer with poor mechanical properties and biodegradability. Furthermore, kinetic or mechanistic studies for the copolymerization process have rarely been reported although these studies are

very important to control copolymer's composition and molecular weights which affect mechanical properties and biodegradation of these potential biomaterials.

Degradation of polymers is related to hydrophilic linkages in the polymer, and copolymers with higher hydrophilicity degrade faster. Degradation processes for polyester and polycarbonate are shown in Scheme 2-2 and 2-3, respectively.[24e] It is known that copolymers with increasing lactide content degrade faster since copolymers containing more lactide produce more acidic products, which accelerated the copolymer degradation reaction.

Scheme 2-2. Polyester degradation process.

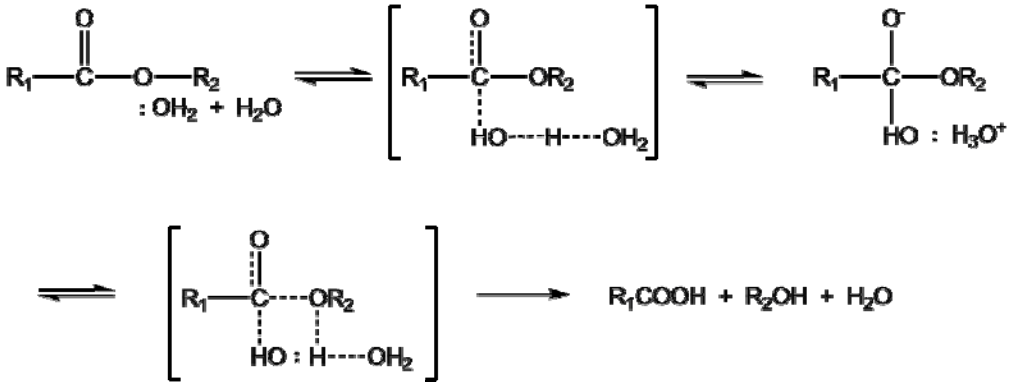

Scheme 2-3. Polycarbonate degradation process.

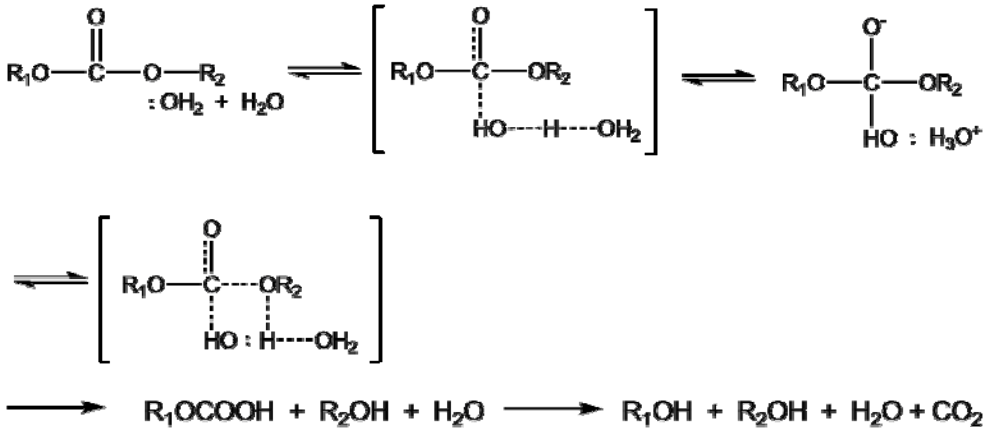

In this chapter, ring-opening polymerization of trimethylene carbonate and lactide will be addressed mostly using biocompatible metal complexes. The details of our investigation of the polymerization reactions of trimethylene carbonate (1,3-dioxan-2-one) and lactide catalyzed by a series of biometal salen complexes (Figure 2-8) and tridentate Schiff base biometal complexes (Figure 2-9) will be described. Importantly, in biometal salen complexes, it is necessary in these processes to employ a cocatalyst since these M(II) salen derivatives do not possess internal nucleophiles for the chain initiation step as is present in the M(III) derivatives previously reported upon, i.e., (salen)AlCl.[19] For this purpose we have generally utilized anions derived from PPN^+ (μ-nitrido-*bis*(triphenylphosphine)(1+)) or *n*-Bu_4N^+ salts (Figure 2-10). Optimization of catalyst, kinetic and mechanistic studies and stereoselectivity toward *L*- or *D*-lactide will be described.

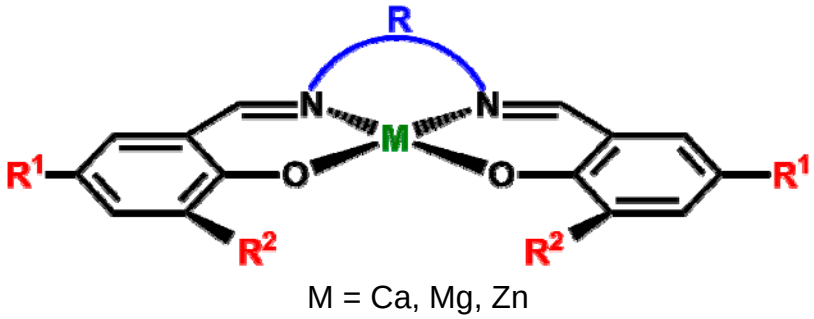

Figure 2-8. General structure of biometal salen complexes utilized as catalysts for the ring-opening polymerization of cyclic monomers.

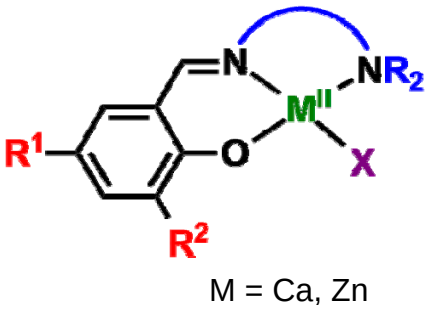

Figure 2-9. General structure of tridentate Schiff base biometal complexes utilized as catalysts for the ring-opening polymerization of cyclic monomers.

(a) (b)

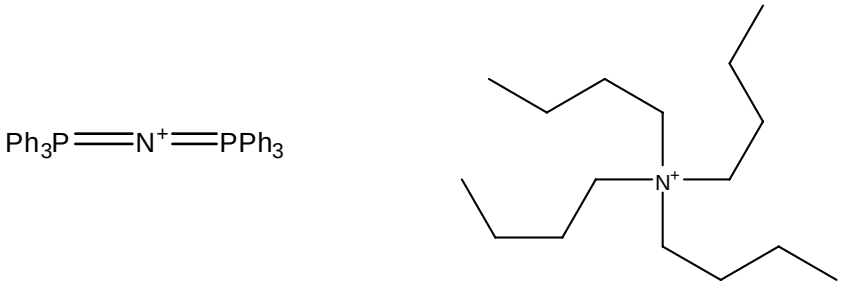

Figure 2-10. Structures of (a) PPN^+ (μ-nitrido-*bis*(triphenylphosphine)(1+)) and (b) *n*-Bu_4N^+ salts.

EXPERIMENTAL

Methods and Materials

Unless otherwise specified, all manipulations were performed using a double manifold Schlenk vacuum line under an atmosphere of argon or an argon filled glovebox. Dichloromethane, tetrahydrofuran and methanol were freshly distilled from CaH_2, sodium / benzophenone and magnesium, respectively. 1,1,2,2-tetrachloroethane (TCE) were freshly distilled from CaH_2. Deutrated chloroform from Aldrich was stored in glovebox and used as received. Trimethylene carbonate was purchased from Boehringer Ingelheim. It was recrystallized from tetrahydrofuran and diethyl ether, dried under vacuum and stored in the glovebox. *L*- and *D*-lactide were gifts from PURAC America Inc. and *rac*-lactide was purchased from Aldrich. These lactides were recryrstallized from toluene twice, dried under vacuum at 40°C overnight, and stored in the glovebox. Sodium *bis*(trimethylsilyl)amide and sodium hydride purchased from Lancaster and Aldrich, respectively, were stored in the glove box and used as received. Salicylaldehyde, ethylenediamine, 1,2-phenylenediamine and 1,2-napthylenediamine were purchased from Aldrich and used as received. *N,N'*-bis(3,5-di-*tert*-butylsalicylidene)-1,2-cyclohexene diimine was purchased from Strem and used without further purification. *N,N*-dimethylethylenediamine, *N,N*-diethylethylenediamine, 2-(aminomethyl)pyridine, and 8-aminoquinoline were purchased from Acros and used as received. PPN^+Cl^- ($PPN^+ = (Ph_3P)_2N^+$) were purchased from Aldrich and recrystallized from dichloromethane / ether before use, and $PPN^+N_3^-$ was synthesized according to published procedure.[35] Tetra-*n*-butylammonium halides (Aldrich) were recrystallized

from acetone / ether twice before use. Tetra-*n*-butylammonium azide (TCI) was stored in the freezer of the glovebox immediately upon arrival.

Measurements

^{1}H NMR and ^{13}C NMR spectra were recorded on Unity+ 300MHz and VXR 300MHz superconducting NMR spectrometers or 500MHz and 500MHz superconducting NMR spectrometers. Infrared spectra were recorded on a Mattson 6021 FT-IR spectrometer with DTGS and MCT detectors. Analytical elemental analysis was provided by Canadian Microanalytical Services Ltd. Molecular weight determinations were carried out with Viscotek Modular GPC apparatus equipped with ViscoGEL^{TM} I-series columns (H + L) and Model 270 dual detector comprised of Refractive Index and Light Scattering detector. TGA and DSC measurements were performed with SDT Q600 V7.0 Build 84.

Synthesis of Salen Ligands

The corresponding salen ligands were synthesized according to literature procedure.[36]

Synthesis of Tridentate Schiff Base Ligands

3,5-di-*tert*-butyl-2-hydroxybenzaldehyde,[12] and tridentate Schiff base ligands[10,11] were synthesized according to literature procedure. 3,5-*tert*-Bu_2-2-$(OH)C_6H_2CH{=}NCH_2CH_2NEt_2$ was synthesized as for 3,5-*tert*-Bu_2-2-$(OH)C_6H_2CH{=}NCH_2CH_2NMe_2$ but with *N*,*N*-Diethylethylenediamine instead of *N*,*N*-Dimethylethylenediamine. 3,5-di-*tert*-butyl-2-hydroxybenzaldehyde (5.0309 g, 21.5 mmol) in methanol (100 ml) was added to *N*,*N*-Diethylethylenediamine (3.0 ml, 21.5

mmol). The solutions was heated a reflux overnight and dried over magnesium sulfate followed by filtration. The volatile component was removed *in vacuo* and repeated washing with pentane at -78°C yielded yellow oily product (5.7507 g, 80.6 % yield). ^{1}H NMR ($CDCl_3$, 300 MHz): δ 13.85 (s, 1H, O*H*), 8.37 (s, 1H, C*H*=N), 7.38 (d, 1H, C_6H_2), 7.09 (d, 1H, C_6H_2), 3.70 (t, 2H, CH_2CH_2), 2.81 (t, 2H, CH_2CH_2), 2.64 (q, 4H, $N(CH_2CH_3)_2$), 1.45 (s, 9H, $C(CH_3)_3$), 1.32 (s, 9H, $C(CH_3)_3$), 1.08 (q, 6H, $N(CH_2CH_3)_2$).

5-*tert*-Bu-2-(OH)C_6H_2CH=$NCH_2CH_2NMe_2$ was synthesized as for 3,5-*tert*-Bu_2-2-(OH)C_6H_2CH=$NCH_2CH_2NMe_2$ but with 5-tert-butyl-2-hydroxybenzaldehyde instead of 3,5-di-tert-butyl-2-hydroxybenzaldehyde. 5-tert-butyl-2-hydroxybenzaldehyde (2.000 g, 11.22 mmol) in methanol (250 ml) was added to *N,N*-Diethylethylenediamine (1.182 g, 13.46 mmol). The solutions was heated a reflux overnight and dried over magnesium sulfate followed by filtration. The volatile component was removed *in vacuo* and repeated washing with pentane at -78°C yielded yellow oily product (1.170 g, 42.1 % yield). ^{1}H NMR ($CDCl_3$, 300 MHz): δ 13.24 (s, 1H, O*H*), 8.36 (s, 1H, C*H*=N), 7.35 (d, 1H, C_6H_3), 7.22 (d, 1H, C_6H_3), 6.90 (d, 1H, C_6H_3), 3.70 (t, 2H, NCH_2CH_2), 2.62 (t, 2H, NCH_2CH_2), 2.29 (s, 6H, $N(CH_3)_2$), 1.29 (s, 9H, $C(CH_3)_3$).

Synthesis of Metal Salen Complexes

The corresponding salen ligands were synthesized according to literature procedure.[13] The synthesis of magnesium and zinc salens have been previously described in literature.[37] The methodology used for the synthesis of {N,N-bis(3,5-di-*tert*-butyl-salicylidene)-ethylene diimine}Al(III)Et was also adapted from the literature.[38] Cr(III)(salen) complexes synthesized according to literature procedure.[13]

Synthesis of Calcium(II) Salen Complexes

General Synthesis of Ca(II)(salen) Complexes

H_2Salen (1.0 eq.) and NaH (5 eq.) were dissolved in THF. After stirring at room temperature overnight, excess NaH was removed by filtration and the sodium salt was transferred *via* cannula through a medium porosity frit packed with Celite to a Schlenk flask containing CaI_2 (1.1 eq.). The reaction mixture became clear and was stirred at ambient temperature overnight. THF was removed under reduced pressure and dichloromethane was added to the reaction mixture subsequent to filtration to remove NaI. The desired complex was isolated following the removal of dichloromethane and was dried in *vacuo*. In general these complexes were obtained with two molecules of THF as solvates.

Synthesis of {N,N'-bis(3,5-di-*tert*-butyl-salicylidene)-1,2-ethylene diimine} Ca(II) (2-1)

Using the general method, 0.492 g of N,N'-*bis*(3,5-di-*tert*-butylsalicylidene)-1,2-ethylenediimine (1.0 mmol) and 0.322 g of CaI_2 (1.1 mol) were dissolved in 30 ml of THF. The final product was a pale yellow solid (0.522 g, 98 % yield). ^{1}H NMR ($CDCl_3$, 300 MHz); δ 8.20(s, CH=N, 2H), 7.26(d, C_6H_2, 2H), 6.94(d, C_6H_2, 2H), 3.81(s, $C{=}NCH_2$, 4H), 1.56(s, 18H, $C(CH_3)_3$), 1.35(s, 18H, $C(CH_3)_3$).

Synthesis of {N,N'-bis(salicylidene)-1,2-phenylene diimine} Ca(II) (2-2)

Using the general method, 0.158 g of N,N'-*bis*(salicylidene)-1,2-phenylenediimine (0.5 mmol) and 0.150 g of CaI_2 (0.52 mmol) were dissolved in 30 ml of THF. The final product was a yellow solid (0.18g, 92 % yield). ^{1}H NMR ($CDCl_3$,

300 MHz); δ 8.37(s, CH=N, 2H), 7.17(d, 2H), 7.08 (d, 2H), 6.90 (d, 2H), 6.63 (d, 2H), 6.60 (d, 2H), 6.38 (d, 2H).

Synthesis of {N,N'-bis(5-*tert*-butylsalicylidene)-1,2-phenylene diimine} Ca(II) (2-3)

Using the general method, 0.216 g of N,N'-*bis*(5-*tert*-butylsalicylidene)-1,2-phenylenediimine (0.5 mmol) and 0.150 g of CaI_2 (0.52 mmol) were dissolved in 30 ml of THF. The final product was a yellow solid (0.207 g, 88 % yield). ^{1}H NMR ($CDCl_3$, 300 MHz); δ 8.32 (s, CH=N, 2H), 7.41 (d, 2H), 7.36 (d, 2H), 7.23 (d, 2H), 6.49 (d, 2H), 6.43 (d, 2H), 1.43 (s, 18H, $C(CH_3)_3$).

Synthesis of {N,N'-bis(3,5-di-*tert*-butylsalicylidene)-1,2-phenylene diimine} Ca(II) (2-4)

Using the general method, 0.275 g of N,N'-*bis*(3,5-di-*tert*-butylsalicylidene)-1,2-phenylenediimine (0.50 mmol) and 0.162 g of CaI_2 (0.55 mol) were dissolved in 20 ml of THF. The final product was a yellow solid (0.272 g, 94 % yield). ^{1}H NMR ($CDCl_3$, 300 MHz); δ 8.64 (s, CH=N, 2H), 6.94-7.27(m, 8H), 1.43 (s, 18H, $C(CH_3)_3$), 1.25 (s, 18H, $C(CH_3)_3$).

Synthesis of {N,N'-bis(3,5-di-chlorosalicylidene)-1,2-phenylene diimine} Ca(II) (2-5)

Using the general method, 0.227 g of N,N'-*bis*(3,5-di-chlorosalicylidene)-1,2-phenylenediimine (0.50 mmol) and 0.162 g of CaI_2 (0.55 mol) were dissolved in 20 ml of THF. The final product was a dark yellow solid (0.167 g, 68 % yield). ^{1}H NMR (DMSO, 300 MHz); δ 8.30 (s, CH=N, 2H), 7.40 (s, 2H), 7.30 (m, 4H), 7.05 (s, 2H).

Synthesis of {N,N'-bis(3-methoxy-5-*tert*-butylsalicylidene)-1,2-phenylenediimine} Ca(II) (2-6)

Using the general method, 0.245 g of N,N'-*bis*(3-methoxy-5-*tert*-butylsalicylidene)-1,2-phenylenediimine (0.50 mmol) and 0.162 g of CaI_2 (0.55 mol) were dissolved in 20 ml of THF. The final product was a orange brown solid (0.227 g, 86 % yield). ^{1}H NMR ($CDCl_3$, 300 MHz,); δ 8.63 (s, CH=N, 2H), 7.35 (m, 4H), 7.04 (s, 2H), 6.73 (s, 2H), 3.79 (s, 6H), 1.42 (s, 18H).

Synthesis of {N,N'-bis(3,5-di-*tert*-butylsalicylidene)-1,2-napthylenediimine} Ca(II) (2-7)

Using the general method, 0.304 g of N,N'-*bis*(3,5-di-*tert*-butylsalicylidene)-1,2-naphthylenediimine (0.50 mmol) and 0.162 g of CaI_2 (0.55 mol) were dissolved in 20 ml of THF. The final product was a brown solid (0.292 g, 93 % yield). ^{1}H NMR ($CDCl_3$, 300 MHz); δ 8.73(s, CH=N, 2H), 7.08-7.92(m, 10H), 1.45(s, 18H, , $C(CH_3)_3$), 1.35 (s, 18H, $C(CH_3)_3$).

Synthesis of {N,N'-bis(3,5-di-*tert*-butyl-salicylidene)-1,2-cyclohexene diimine} Ca(II) (2-8)

Using the general method, 0.283 g of N,N'-*bis*(3,5-di-*tert*-butylsalicylidene)-1,2-cyclohexene diimine (0.52 mmol) and 0.167 g of CaI_2 (1.1 eq.) were dissolved in 30 ml of THF. The final product was a green-yellow solid (0.182 g, 44 % yield). ^{1}H NMR ($CDCl_3$, 300 MHz); δ 8.00(s, CH=N, 2H), 7.02(d, C_6H_2, 2H), 6.82(d, C_6H_2, 2H), 3.60(m, 4H, $O(CH_2CH_2)_2$), 3.34 (m, $(CHCH_2H_2)_2$, 4H), 2.50 (m, $(CHCH_2H_2)_2$ 4H), 1.76(m, 4H, $O(CH_2CH_2)_2$), 1.56(s, 18H, $C(CH_3)_3$), 1.35(s, 18H, $C(CH_3)_3$).

General Synthesis of Tridentate Schiff Base Ca(II) Complexes

Tridentate Schiff base ligands (1.0 eq.) and $NaN(SiMe_3)_2$ (2.0 eq.) were dissolved in THF. After stirring at room temperature for 5 h, it was added to CaI_2 in THF and stirred overnight. Then, the volatile components were removed in *vacuo* and dissolved in dichloromethane followed by filtration. The desired complex was isolated following the removal of dichloromethane and dried in *vacuo*. In general, these complexes were obtained with two or three molecules of THF as solvates.

Synthesis of {3,5-tert-Bu_2-2-$(OH)C_6H_2CH=NCH_2CH_2NMe_2$}Ca(II)$N(SiMe_3)_2$ (2-9)

Using the general method, 3,5-*tert*-Bu_2-2-$(OH)C_6H_2CH=NCH_2CH_2NMe_2$ (0.9140 g, 3.0 mmol) and $NaN(SiMe_3)_2$ (1.1000 g, 6.0 mmol) were dissolved in THF (10 mL). After stirring at room temperature for 5 h, it was added to CaI_2 (0.882 g , 3.0 mmol) in THF (20 mL) and stirred overnight. The final product was a dark yellow solid (1.87 g, 86.2 % yield). ^{1}H NMR ($CDCl_3$, 300 MHz): δ 8.16(s, 1H, C*H*=N), 7.24(d, 1H, C_6H_2), 6.81 (d, 1H, C_6H_2), 3.69 (m, 4H, $O(CH_2CH_2)_2$), 3.55 (t, 2H, CH_2CH_2), 2.53 (t, 2H, CH_2CH_2), 2.02 (s, 6H, $N(CH_3)_2$), 1.70 (m, 4H, $O(CH_2CH_2)_2$), 1.34 (s, 9H, $C(CH_3)_3$), 1.27 (s, 9H, $C(CH_3)_3$), 0.07 (s, 18H, $Si(CH_3)_3$). ^{13}C NMR ($CDCl_3$, 500 MHz) δ 170.29(*C*=N), 168.21 (*C*O in Ar), 140.02, 131.93, 129.40, 128.02, 120.04 (Ar), 68.18 (OCH_2 in THF) 60.39 (C=NCH_2), 56.72 ($CH_2N(CH_3)_2$), 45.80 ($N(CH_3)_2$), 35.38 ($^pC(CH_3)_3$), 33.83 ($^oC(CH_3)_3$), 31.60 ($^pC(CH_3)_3$), 29.61 ($^oC(CH_3)_3$), 25.50 ((OCH_2CH_2 in THF), 2.51 ($Si(CH_3)_3$).

Synthesis of {3,5-tert-Bu_2-2-(OH)C_6H_2CH=N$CH_2CH_2NEt_2$}Ca(II)N($SiMe_3$)$_2$ (2-10).

Using the general method, 3,5-*tert*-Bu_2-2-(OH)C_6H_2CH=N$CH_2CH_2NEt_2$ (1.4107 g, 4.24 mmol) and NaN($SiMe_3$)$_2$ (1.5550 g, 8.48 mmol) were dissolved in THF (10 mL). After stirring at room temperature for 5 h, it was added to CaI_2 (1.2468 g, 4.24 mmol) in THF (20 mL) and stirred overnight. The final product was a dark yellow solid (3.098 g, 97.6 % yield). ^{1}H NMR ($CDCl_3$, 300 MHz): δ 8.13 (s, 1H, C*H*=N), 7.29 (d, 1H, C_6H_2), 6.91 (d, 1H, C_6H_2), 3.77 (m, 4H, O(CH_2CH_2)$_2$), 3.68 (t, 2H, CH_2CH_2), 3.02 (t, 2H, CH_2CH_2), 2.86 (q, 4H, N(CH_2CH_3)$_2$), 1.79 (m, 4H, O(CH_2CH_2)$_2$), 1.37 (s, 9H, C(CH_3)$_3$), 1.22 (s, 9H, C(CH_3)$_3$), 1.10 (q, 6H, N(CH_2CH_3)$_2$), 0.14 (s, 18H, Si(CH_3)$_3$). ^{13}C NMR ($CDCl_3$, 500 MHz) δ 170.22(*C*=N), 167.97 (*C*O in Ar), 139.38, 131.18, 129.25, 127.60, 120.47 (Ar), 68.17 (O*C*H_2 in THF) 56.21 (C=N*C*H_2), 52.75 (*C*H_2N(CH_2CH_3)$_2$), 43.38 (N(*C*H_2CH_3)$_2$), 35.12 (^{p}*C*(CH_3)$_3$), 33.61 (^{o}*C*(CH_3)$_3$), 31.62 (^{p}C(*C*H_3)$_3$), 29.53 (^{o}C(*C*H_3)$_3$), 25.49 ((OCH_2*C*H_2 in THF), 7.98 (N(CH_2*C*H_3)$_2$), 2.47 (Si(*C*H_3)$_3$).

Synthesis of {3,5-tert-Bu_2-2-(OH)C_6H_2CH=N-2-$CH_2C_5H_4N$}Ca(II)N($SiMe_3$)$_2$ (2-11)

Using the general method, 3,5-*tert*-Bu_2-2-(OH)C_6H_2CH= N-2-$CH_2C_5H_4N$ (1.0346 g, 3.2 mmol) and NaN($SiMe_3$)$_2$ (1.1736 g, 6.4 mmol) were dissolved in THF (10 mL). After stirring at room temperature for 5 h, it was added to CaI_2 (0.9371 g, 3.2 mmol) in THF (20 mL) and stirred overnight. The final product was a yellow-brown solid (1.5280 g, 47.9 % yield). ^{1}H NMR ($CDCl_3$, 300 MHz): δ 8.56 (s, 1H, C*H*=N), 6.65-7.62 (m, 6H, C_6H_2 and C_5H_4N), 3.71 (m, 4H, O(CH_2CH_2)$_2$), 1.81 (m, 4H, O(CH_2CH_2)$_2$), 1.30 (s, 9H, C(CH_3)$_3$), 1.21 (s, 9H, C(CH_3)$_3$), 0.05 (s, 18H, Si(CH_3)$_3$). ^{13}C NMR ($CDCl_3$, 500 MHz) δ 174.55 (*C*=N), 170.13, 157.33, 149.22, 147.78, 138.10,

136.25, 129.21, 128.73, 127.12, 122.30, 120.99 (Ar), 68.20 (O*C*H_2 in THF) 65.98 (C=N*C*H_2), 35.15 ($^{p}C(CH_3)_3$), 34.55 ($^{o}C(CH_3)_3$), 31.48 ($^{p}C(CH_3)_3$), 29.37 ($^{o}C(CH_3)_3$), 25.52 ((OCH_2CH_2 in THF), 1.93 (Si(CH_3)$_3$).

Synthesis of {3,5-tert-Bu_2-2-(OH)C_6H_2CH=N-8-C_9H_6N}Ca(II)N($SiMe_3$)$_2$ (2-12)

Using the general method, 3,5-*tert*-Bu_2-2-(OH)C_6H_2CH=N-8-C_9H_6N (0.3600 g, 1.0 mmol) and NaN($SiMe_3$)$_2$ (0.3670 g, 2.0 mmol) were dissolved in THF (5 mL). After stirring at room temperature for 5 h, it was added to CaI_2 (0.2940 g , 1.0 mmol) in THF (10 mL) and stirred overnight. The final product was a red-brown solid (0.6500 g, 83.8 % yield). ^{1}H NMR ($CDCl_3$, 300 MHz): δ 8.85 (m, 1H, C_9H_6N), 8.80 (s, 1H, C*H*=N), 8.18 (d, 1H, C_9H_6N), 7.19-7.72 (m, 6H, C_9H_6N and C_6H_2), 3.80 (m, 4H, O(CH_2CH_2)$_2$), 1.82 (m, 4H, O(CH_2CH_2)$_2$), 1.37 (s, 9H, C(CH_3)$_3$), 1.19 (s, 9H, C(CH_3)$_3$), 0.09 (s, 18H, Si(CH_3)$_3$).

Synthesis of {5-tert-Bu-2-(OH)C_6H_3CH=N$CH_2CH_2NMe_2$}Ca(II)N($SiMe_3$)$_2$ (2-13)

Using the general method, 5-*tert*-Bu-2-(OH)C_6H_3CH=N$CH_2CH_2NMe_2$ (0.4043 g, 1.628 mmol) and NaN($SiMe_3$)$_2$ (0.597 g, 3.256 mmol) were dissolved in THF (15 mL). After stirring at room temperature for 5 h, it was added to CaI_2 (0.479 g , 1.629 mmol) in THF (10 mL) and stirred overnight. The final product was a dark yellow solid (0.449 g, 41.6 % yield). ^{1}H NMR ($CDCl_3$, 300 MHz): δ 7.82(s, 1H, C*H*=N), 7.24(d, 1H, C_6H_3), 7.05 (d, 1H, C_6H_3), 6.62 (d, 1H, C_6H_3), 3.64 (m, 4H, O(CH_2CH_2)$_2$), 2.62 (t, 2H, NCH_2CH_2), 2.43 (t, 2H, NCH_2CH_2), 2.16 (s, 6H, N(CH_3)$_2$), 1.76 (m, 4H, O(CH_2CH_2)$_2$), 1.21 (s, 9H, C(CH_3)$_3$).

Synthesis of {3,5-tert-Bu_2-2-(OH)C_6H_2CH=N$CH_2CH_2NMe_2$}Ca(II)OMe (2-14)

Methanol (15 ml) was added to the solution of **{3,5-tert-Bu_2-2-(OH)C_6H_2CH=N$CH_2CH_2NMe_2$}Ca(II)N$(SiMe_3)_2$ (2-9)** in THF (15 mL). After stirring at room temperature for 2 h, the volatile component was removed in *vacuo.* The final product was a dark brown solid (0.3530 g, 94.2 % yield). ^{1}H NMR ($CDCl_3$, 300 MHz): δ 8.39 (s, 1H, C*H*=N), 7.37 (d, 1H, C_6H_2), 7.02 (d, 1H, C_6H_2), 3.74 (t, 2H, CH_2CH_2), 3.39 (s, 3H, OCH_3) 2.73 (t, 2H, CH_2CH_2), 2.36 (s, 6H, $N(CH_3)_2$), 1.38 (s, 9H, $C(CH_3)_3$), 1.25 (s, 9H, $C(CH_3)_3$).

Zinc(II) Complexes

Synthesis of {3,5-tert-Bu_2-2-(OH)C_6H_2CH=N$CH_2CH_2NMe_2$}Zn(II)N$(SiMe_3)_2$ (2-15)

3,5-*tert*-Bu_2-2-(OH)C_6H_2CH=N$CH_2CH_2NMe_2$ (0.457 g, 1.5 mmol) and $Zn[N(SiMe_3)_2]_2$ (0.578 g, 1.5 mmol) were dissolved in THF (10 mL). After stirring at room temperature for 2 h, THF was removed under reduced pressure. The final product was a yellow solid after recrystallization in pentane (0.730 g, 92.6 % yield). ^{1}H NMR ($CDCl_3$, 300 MHz): δ 8.28 (s, 1H, C*H*=N), 7.34 (d, 1H, C_6H_2), 6.84 (d, 1H, C_6H_2), 3.55 (t, 2H, CH_2CH_2), 2.53 (t, 2H, CH_2CH_2), 2.32 (s, 6H, $N(CH_3)_2$), 1.38 (s, 9H, $C(CH_3)_3$), 1.27 (s, 9H, $C(CH_3)_3$), 0.07 (s, 18H, $Si(CH_3)_3$). ^{13}C NMR ($CDCl_3$, 500 MHz) δ 171.72 (*C*=N), 169.26 (*C*O in Ar), 141.31, 134.02, 129.10, 129.00, 117.06 (Ar), 59.54 (C=NCH_2), 57.68 ($CH_2N(CH_3)_2$), 45.53 ($N(CH_3)_2$), 35.45 ($^pC(CH_3)_3$), 33.76 ($^oC(CH_3)_3$), 31.43 ($^pC(CH_3)_3$), 29.47 ($^oC(CH_3)_3$), 1.00 ($Si(CH_3)_3$).

X-ray Structure Study

Suitable crystals for X-ray analysis were obtained by slow diffusion. A Bausch and Lomb 10x microscope was used to identify a suitable crystal from a representative sample of crystals of the same habit. Each crystal was coated with a cryogenic protectant (i.e, paratone) and mounted on a glass fiber, which in turn was fashioned to a copper mounting. The crystal was placed in a cold nitrogen stream (Oxford) maintained at 110 K on a Bruker SMART 1000 three circle goniometer. The X-ray data were obtained on a Broker CCD diffractomoter and covered more than a hemisphere of reciprocal space by a combination of three sets of exposures; each exposure set had a different angle φ for the crystal orientation and each exposure covered 0.3° in ω. The crystal-to-detector distance was 5.0 cm. Crystal decay was monitored by repeating the data collection of 50 initial frames at the end of the data set and analyzing the duplicate reflections; crystal decay was negligible. The space group was determined based on systematic absences and intensity statistics.[39] The structures were solved by direct methods and refined by full-matrix least squares on F2. All non-hydrogen atoms were refined with anisotropic displacement parameters. All H atoms were placed at idealized positions and refined with fixed isotropic displacement parameters equal to 1.2 (1.5 for methyl protons) times the equivalent isotropic displacement parameters of the atoms to which they were attached.

The following are the programs that were used: data collection and cell refinement, SMART;[39] data reduction, SAINTPLUS (Bruker[40]); program used to solve structures, SHELXS-86 (Sheldrick[41]); program used to refine structures, SHELXL-97

(Scheldrick [42]); molecular graphics and preparation of material for publication, SHELXTL-Plus version 5.0 (Bruker[43]).

Crystal Structure of salen ligand with naphthylene backbone is shown in Figure 2-11 and crystal data are listed in Table 2-1. Details of data collection are listed in Appendix A.

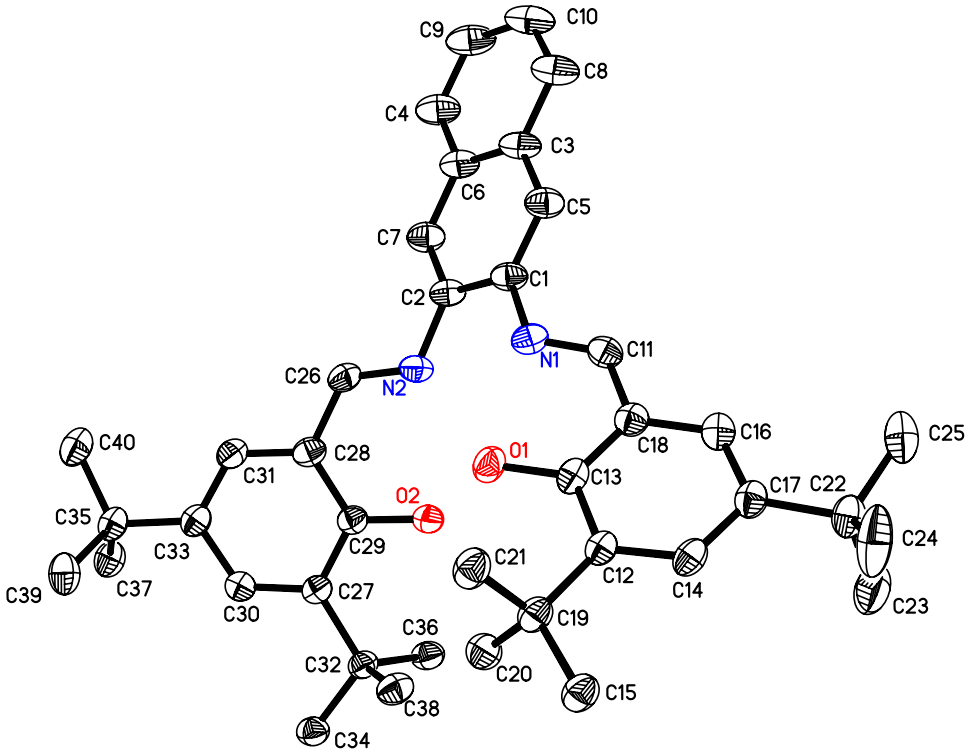

Figure 2-11. Thermal ellipsoid drawing of salen ligand with naphthylene backbone (salen-naph) along with partial atomic numbering scheme.

Table 2-1. Crystal data and structure refinement for salen-naph.

Empirical formula	$C_{40}\ H_{50}\ Cl\ N_2\ O_2$
Formula weight	626.27 g/mol
Temperature	273(2) K
Wavelength	0.71073 Å
Crystal system	Triclinic
Space group	P-1
Unit cell dimensions	a = 9.9055(17) Å
	b = 11.802(2) Å
	c = 18.635(3) Å
	α = 82.598(3)°
	β = 83.107(3)°
	γ = 66.793(3)°
Cell volume	1979.7(6) $Å^3$
Z	2
Density (calculated)	1.051 g/cm^3
Absorption coefficient	0.129 mm^{-1}
F(000)	674
Theta range for data collection	1.11 to 28.43 °
Index ranges	-13<=h<=13, -15<=k<=15, -24<=l<=24
Reflections collected	22597
Independent reflections	9037 [R(int) = 0.0814]
Completeness to theta = 28.43	90.7 %
Absorption correction	None
Refinement method	Full-matrix least-squares on F^2
Data / restraints / parameters	9037 / 0 / 438
Goodness-of-fit on F^2	1.175
Final R indices [I>2sigma(I)]	R1 = 0.1185, wR2 = 0.3223
R indices (all data)	R1 = 0.1686, wR2 = 0.3632
Largest diff. peak and hole	2.431 and -0.753 $e.A^{-3}$

Polymerization Runs

A typical melt polymerization run consisted of adding a 1g of the monomer to a previously flame dried Schlenk flask. The monomer : initiator : coinitiator ratio was maintained at 350:1:1 or The monomer : initiator ratio was maintained at 350:1. The reaction was carried on at 86ºC for 15 minutes under an argon atmosphere for the ring-opening polymerization of trimethylene carbonates and 110ºC for 15 minutes under an argon atmosphere for the ring-opening polymerization of lactide. The resulting polymer was purified by precipitation from dichloromethane, 5% HCl and methanol and then dried *in vacuo*. Turnover frequencies (mol of TMC consumed / mol of the catalyst-hr) were calculated following weighing of the vacuum dried polymer.

Kinetic Studies

Monomer, catalyst (and the cocatalyst if needed) were weighed out in the desired monomer : initiator : coinitiator ratio followed by the addition of dry solvent. The reaction vessel was placed into a preheated oil bath. The percent conversion of the monomer with time was monitored by ^{1}H NMR.

Copolymerization

For random copolymerization, both trimethylene carbonate and *L*-lactide monomers were simultaneously added to the solution of catalyst. For block copolymerization, trimethylene carbonate was added to the solution of catalyst. After completion of polymerization of trimethylene carbonate at room temperature monitoring by ^{1}H NMR, the solution of *L*-lactide monomer (1 eq.) solution was added to the

solution of poly(trimethylene carbonate). Both random and block copolymers were purified by precipitation from 5% HCl and methanol and then dried in *vacuo*.

RESULTS AND DISCUSSION

Ring-Opening Polymerization of Cyclic Monomers Catalyzed by Biometal Salen Complexes

The first priority in this area was to examine the relative effectiveness of the various biometal complexes shown in Figure 2-8 for polymerizing trimethylene carbonate (TMC) to poly(TMC). The common salen ligand employed in this investigation was H_2salen = *N,N'-bis*-(di-*tert*-butylsalicylidene)-1,2-ethylenediimine. For this purpose, melt studies have been carried out at a monomer : catalyst : initiator ratio of 350:1:1 at 86ºC for 15 minutes under an argon atmosphere. The results of this inquiry are summarized in Table 2-2, where the TOFs (mol. of TMC consumed / mol. of catalyst-hr) were determined by precipitating the polymer from dichloromethane, 5% HCl, and methanol, following by drying *in vacuo* and weighing. As revealed by ^{1}H NMR spectra, which exhibit a triplet at 4.23 ppm and a quintet at 2.04 ppm of intensity ratio 2:1, respectively, all polymers showed a complete absence of ether linkages (Figure 2-12). That is, the lack of proton resonance at 1.8 and 3.4 ppm indicates that the poly(TMC)s obtained are free of polyoxetane arising from CO_2 elimination.[44] Included in Table 2-2 is a version of our most effective catalyst reported to date, Al(III) salen.[19] In this instance it was necessary to utilize an Al(III) salen derivative where the internal axial ligand is not involved in the catalytic process, thereby requiring an exterior initiator

or cocatalyst as is needed in the other M(II) cases. Previous studies have shown that the Al-C_2H_5 unit does not participate in the polymerization process.[38] As is readily apparent from Table 2-2, calcium(II) is the most active salen derivative, displaying a catalytic activity in the presence of *n*-$Bu_4N^+Cl^-$ of about twice that of its magnesium or aluminum analogs.

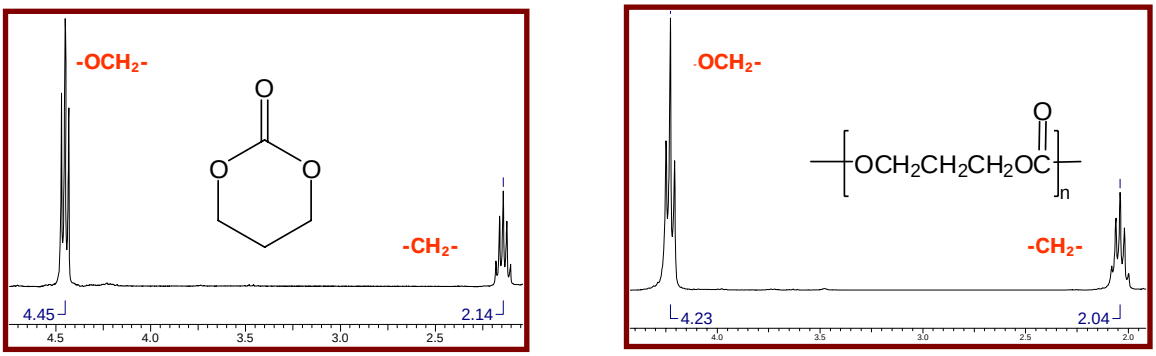

Figure 2-12. ^1H NMR spectra of trimethylene carbonate monomer and poly(trimethylene carbonate) in $CDCl_3$.

Table 2-2. Polymerization of TMC as catalyzed by (salen)M (M = Zn, C_2H_5Al, Mg and Ca) complexes in the presence of one equivalent of *n*-$Bu_4N^+Cl^-$.[a]

M	TOF[b]
Zn	250
C_2H_5Al	485
Mg	541
Ca	1123

[a] Salen ligand contains an ethylene backbone and *t*-butyl groups in the 3,5-positions of the phenolate rings.

Subsequent investigations have been carried out to optimize the catalytic activity of the calcium(II) salen complex by changing the nature of the diimine backbone and substituents on the phenolate rings of the salen ligands. Retaining the salen ligand with the phenylene backbone while changing the substituents in the 3,5-positions of the phenolate rings (Table 2-3) reveal the Ca(II) salen derivative containing the bulky di-*tert*-butyl groups to be the most active. This is consistent with our previously reported observations employing aluminum salen catalysts.[19] The effect of altering the diimine backbone of the Ca(II) salen derivative was also examined while maintaining the di-*tert*-butyl substituents in the 3,5-positions of the phenolate rings. These results are summarized in Table 2-4, and indicate that an electron-withdrawing, rigid and planar backbone leads to enhanced catalytic activity. Nevertheless, as is evident in Table 2-4, changes in the diimine backbone do not significantly effect catalytic activity, where only an 8% increase is noted in proceeding from ethylene to naphthylene.

Table 2-3. Polymerization results on varying the substituents in the 3,5-positions of the phenolate rings for (salen)Ca(II) complexes containing a phenylene backbone.[a]

entry	R^1	R^2	TOF[b]
1	H	H	416
2	H	*t*-butyl	961
3	OMe	*t*-butyl	1132
4	*t*-butyl	*t*-butyl	1175
5	Cl	Cl	756

[a] Each reaction was performed in melt maintaining a monomer : initiator : *n*-$[Bu_4N]^+Cl^-$ ratio as 350:1:1 at 86°C for 15 minutes. [b] The TOF was determined by weighing the polymer after precipitating in 5% HCl and MeOH, and drying in a vacuum oven and is reported as mol of TMC / mol Ca-h.

Table 2-4. Polymerization results for varying the backbone for (salen)Ca(II) complexes where the substituents in the 3,5-positions of the phenolate ring are *t*-butyl groups.[a]

entry	R	TOF[b]
1	Cyclohexylene	1111
2	Ethylene	1123
3	Phenylene	1175
4	Naphthylene	1270

[a] Each reaction was performed in melt maintaining a monomer : initiator : *n*-$[Bu_4N]^+Cl^-$ ratio as 350:1:1at 86°C for 15 minutes. [b] The TOF was determined by weighing the polymer after precipitating in 5% HCl and MeOH, and drying in a vacuum oven and is reported as mol of TMC / mol Ca-h.

The final examination of this melt polymerization process was to probe the influence of the external anionic cocatalyst (X) on the initiation step of the reaction (eq. 2-3).[23b] Studies were conducted with salts of both the very bulky, weakly interacting cation, PPN^+, and the less expensive, slightly more interacting *n*-Bu_4N^+ cation. Importantly, these latter *tetra*-alkylammonium salts have the added advantage over their PPN^+ counterparts in that they are readily soluble in a large variety of organic solvents. Table 2-5 lists our findings, where the PPN^+ salts were found to be only about 10% more active than their *n*-Bu_4N^+ analogs, and azide was only 5% more active than chloride. It should be noted here that two control ROP experiments (15 min melt runs at 88 C°) were performed employing $CaCl_2$ or $CaCl_2$ with n-Bu_4NCl as catalysts resulting in 2.5% conversion and 12.2% conversion (TOF) = 167 h^{-1}, respectively. On the other hand, as

might be anticipated based on other ring-opening processes, the bromide anion is significantly less effective at the initiation step.[45]

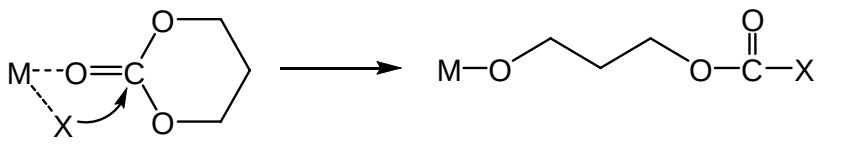

2-3

Table 2-5. Polymerization results on varying the cocatalyst in (salen)Ca(II) complexes containing an ethylene backbone and tert-butyl groups in the 3,5-positions of the phenolate ring.[a]

entry	cocatalyst	TOF[b]
1	$Bu_4N^+Br^-$	766
2	$Bu_4N^+Cl^-$	1123
3	$Bu_4N^+N_3^-$	1183
4	$Bu_4N^+CN^-$	1361
5	PPN^+Cl^-	1221
6	$PPN^+N_3^-$	1286
7	PPN^+CN^-	1375

[a] Each reaction was performed in melt maintaining a monomer : initiator : coinitiator ratio as 350:1:1 at 86°C for 15 mins. [b] The TOF was determined by weighing the polymer after precipitating in 5% HCl and MeOH, and drying in a vacuum oven and is reported as mol of TMC / mol Ca-h.

The molecular weight and polydispersity of poly(trimethylene carbonate) obtained in these studies were measured by gel permeation chromatography (GPC). In general, the melt polymerizations were carried out at 88ºC using {N,N'-bis(3,5-di-*tert*-butylsalicylidene)-1,2-phenylene diimine} Ca(II) (**2-4**) in the presence of one equivalent

of $PPN^+N_3^-$. As indicated in Table 2-6, the molecular weights experimentally determined by GPC closely parallel the theoretical molecular weights. Figure 2-13 illustrates the linear increase in M_n observed with conversion and the low polydispersity indices (PDI, M_w / M_n) of the product polymers. This clearly demonstrates that the level of polymerization control is high.

Table 2-6. The dependence of molecular weights of PTMC on M/I ratios.[a]

entry	M/I	$M_n \times 10^{-4}$		PDI
		GPC	theoretical[b]	
1	275	3.0	2.8	1.76
2	350	3.7	3.4	1.76
3	500	5.6	5.0	1.61
4[c]	700	6.3	6.7	1.48

[a] Reactions conducted at 88°C for 30 minutes using (*N,N'-bis*(3,5-di-*tert*-butylsalicylidene) phenylene diimine)Ca(II) as catalyst and 1eq of $PPNN_3$ as cocatalyst. [b] M(theoretical) = M/I × mol.wt.TMC × % conversion. [c] Entry 4 run for 45 minutes.

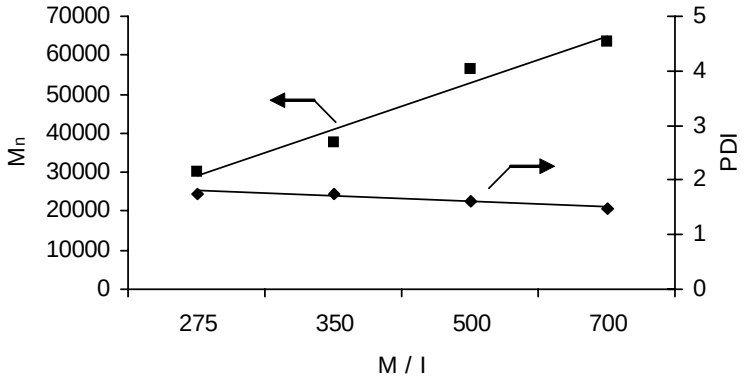

Figure 2-13. Plot of the dependence of molecular weight of PTMC on M/I ratios.

Kinetic measurements of the ring-opening polymerization of trimethylene carbonate in solution in the presence of the (salen)Ca(II) / *n*-$Bu_4N^+X^-$ catalyst system have been initiated. These studies were conducted employing {3,5-di-*tert*-butyl(salicylidene)-1,2-ethylenediimine}Ca(II) (**2-1**) with one equivalent of *n*-$Bu_4N^+Cl^-$ as cocatalyst in 1,1,2,2-tetrachloroethane(TCE). As we previously reported for the ROP of TMC utilizing (salen)AlCl as catalyst, the rate of polymerization in a weakly polar solvent like toluene (dielectric constant = 2.4) was found to be faster than in the more polar TCE solvent (dielectric constant = 10.8). This observation is characteristic of a coordination-insertion mechanism. Although, the polymerization reaction is slower in TCE, it was found to be advantageous to use a high boiling chlorinated solvent for these kinetic studies because of the high solubility of both monomer and polymer in this solvent. The reactions were monitored by ^{1}H NMR spectroscopy.

Figure 2-14a displays a typical monomer consumption *vs.* time plot, whereas, the semi-logarithmic plot of $-\ln[\text{monomer}]_t$ *vs*. time is illustrated in Figure 2-14b. Hence, as might be expected the polymerization reaction is found to be first-order in monomer (TMC) concentration.

Table 2-7 summarizes the determined rate constants for the ROP of TMC as a function of the [catalyst], [cocatalyst], and temperature. Figures 2-15 and 2-16 depict the log-log plots of rate constants *vs*. [catalyst] or [cocatalyst], respectively. These latter plots reveal relationships between ln k_{obsd} *vs.* ln[catalyst] or ln[cocatalyst] with slopes close to unity, thereby, indicative of the polymerization reaction being first-order in [catalyst] or [cocatalyst]. Of course, at concentration of cocatalyst much greater than

one equivalent the polymerization rate eventually should become independent of [cocatalyst] (*vide infra*).

(a)

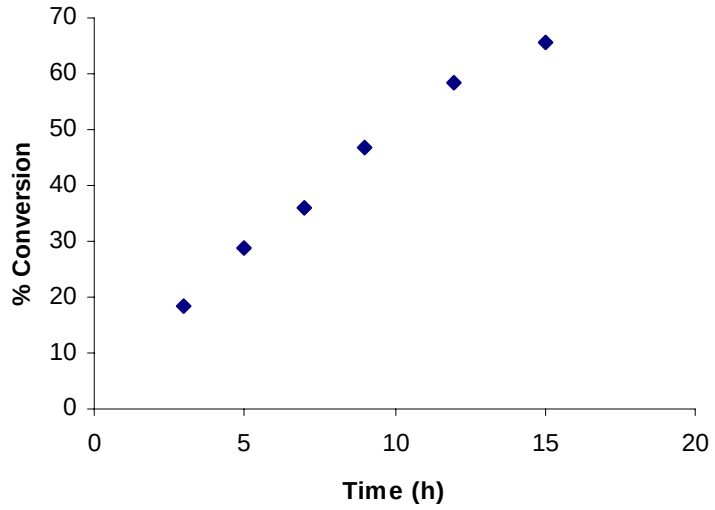

(b)

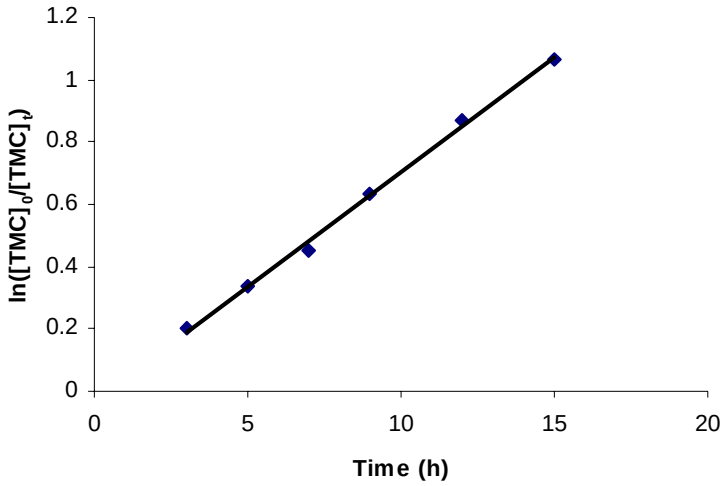

Figure 2-14. (a) Plot of monomer conversion *vs*. time. (b) Semi-logarithmic plot depicting a reaction order of unity with respect to monomer concentration.

Table 2-7. Rate constant dependence on the concentrations of the catalyst, cocatalyst, and temperature.[a]

entry	[Ca](mol/L)	eq. of *n*-$[Bu_4N]^+Cl^-$	temperature (°C)	k_{obsd} (h^{-1})
1	0.0028	1.0	110	0.0426
2	0.00356	1.0	110	0.0666
3	0.0049	1.0	110	0.0749
4	0.0056	1.0	110	0.0889
5	0.0049	1.0	102	0.0625
6	0.0049	1.0	125	0.0995
7	0.0049	1.0	135	0.1141
8	0.0049	0.7	110	0.0572
9	0.0049	0.5	110	0.0439
10	0.0049	0.28	110	0.0247
11	0.0049	2.0	110	0.1305
12	0.0049	3.0	110	0.1609
13	0.0049	6.0	110	0.1945

[a] Monomer concentration held constant at 0.98 M. Reactions carried out in 1,1,2,2-tetrachloroethane.

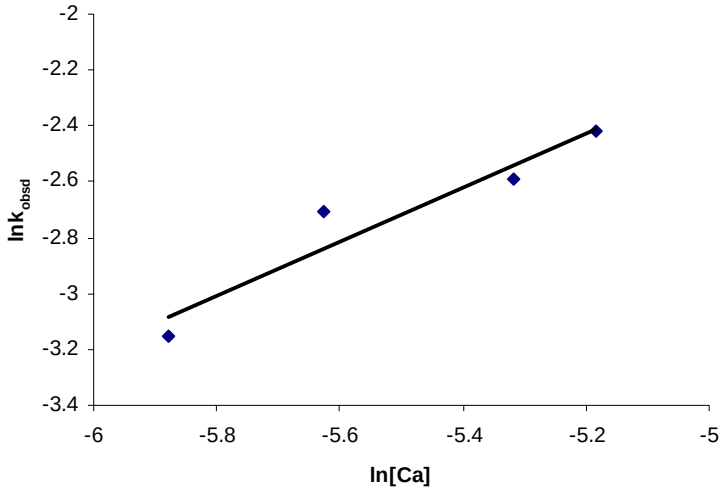

Figure 2-15. Plot of $\ln k_{obsd}$ *vs*. ln[Ca] to determine the order of the polymerization reaction with respect to [catalyst]. Slope = 0.953 with $R^2 = 0.904$.

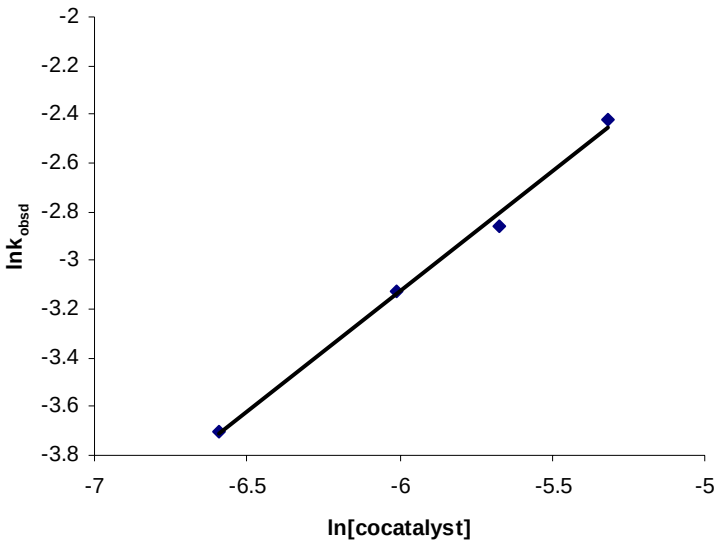

Figure 2-16. Plot of $\ln k_{obsd}$ *vs.* ln[cocatalyst] to determine the order of the polymerization reaction with respect to [cocatalyst] over the range of 0.28-1.0 equivalents. Slope = 0.902 with $R^2 = 0.995$.

Figure 2-17 illustrates the effect of the no. of equivalents of cocatalyst ($Bu_4N^+Cl^-$) on the rate constant of the ROP process. As would be anticipated the initiation process ultimately becomes independent of [cocatalyst], or "saturation" kinetics is observed. A double reciprocal plot of this data reveals a linear relationship with a limiting rate constant of 0.363 ℓ^2-mol^{-2}-h^{-1} (see Figure 2-18).

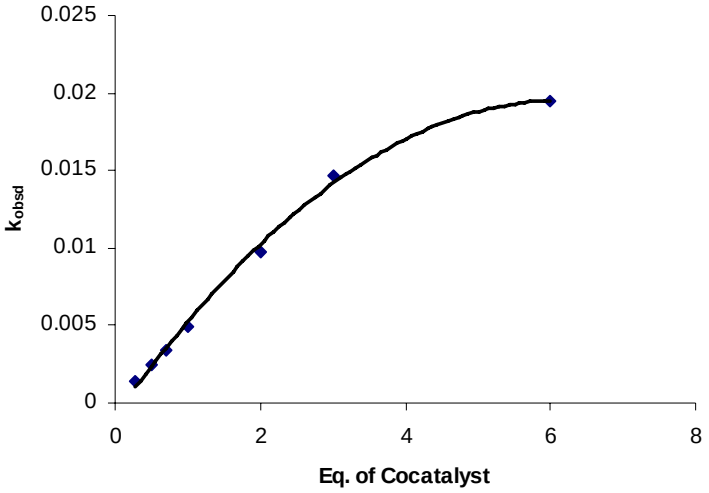

Figure 2-17. Rate constant for production of polymer as a function of the No. of equivalents of *n*-$Bu_4N^+Cl^-$. Data taken from Table 2-7.

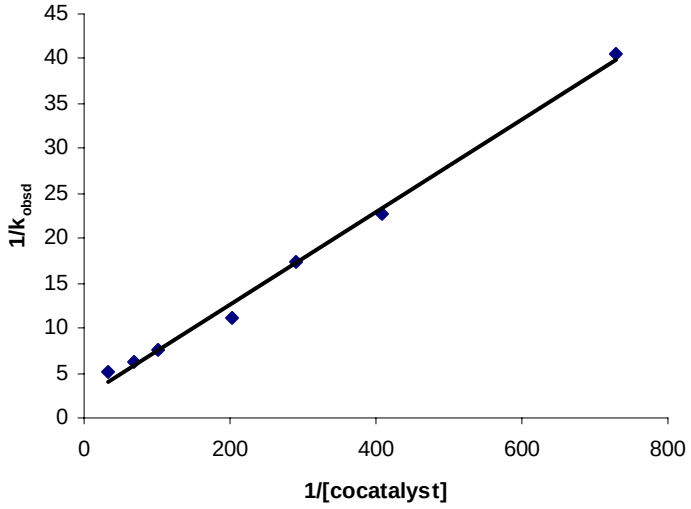

Figure 2-18. Double reciprocal plot of the rate constant dependence of the ROP process with [cocatalyst]. Data taken from Table 2-7. Slope = 0.0511 and intercept = 2.756 with $R^2 = 0.998$.

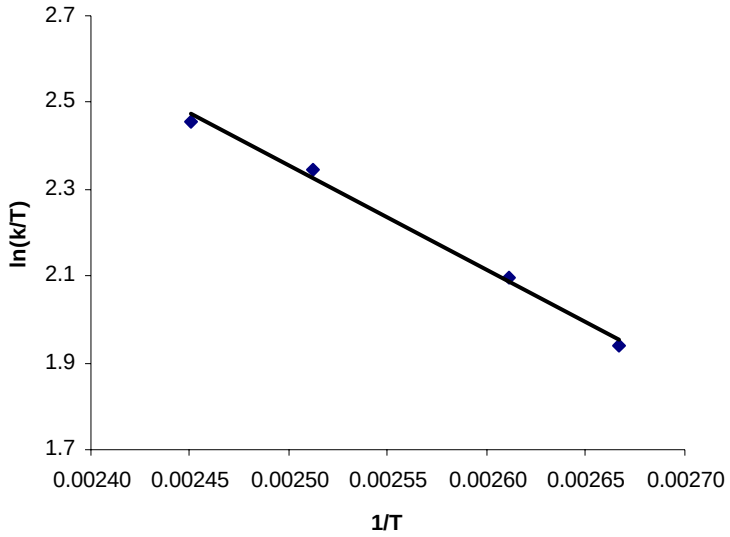

Figure 2-19. Eyring plot of ROP of TMC in the presence (salen)Ca and one equivalent of *n*-$Bu_4N^+Cl^-$ in TCE. Slope = -2.420 with $R^2 = 0.995$.

The activation parameters for the ROP of trimethylene carbonate catalyzed by (salen)Ca(II) and one equivalent of *n*-$Bu_4N^+Cl^-$ in TCE were found to be $\Delta H^{\neq} = 20.1 \pm 1.0$ kJ/mol. and $\Delta S^{\neq} = -128 \pm 3.0$ J/mol-K. These values were calculated from the temperature dependent rate constants listed in Table 2-7 and the Eyring plot (eq. 2-4) depicted in Figure 2-19. The $\Delta G^{\neq}$ value of 58.2 kJ/mol observed for the calcium catalyzed process is 8.5 kJ/mol lower in energy than that which we previously reported for the reaction catalyzed by an aluminum derivative (82.7 kJ/mol).[19] This is consistent with the latter process occurring approximately 15 times slower at similar reaction conditions. In both instances, these activation parameters are in accordance with a

reaction mechanism involving the addition of a nucleophile to a metal-bound cyclic carbonate (*vide infra*).

$$\ln\left(\frac{k}{T}\right) = -\frac{\Delta H^{\neq}}{R}\cdot\frac{1}{T} + \frac{1}{R}\left\{\Delta S^{\neq} + R\cdot\ln\left(\kappa\frac{R}{Nh}\right)\right\} \qquad 2\text{-}4$$

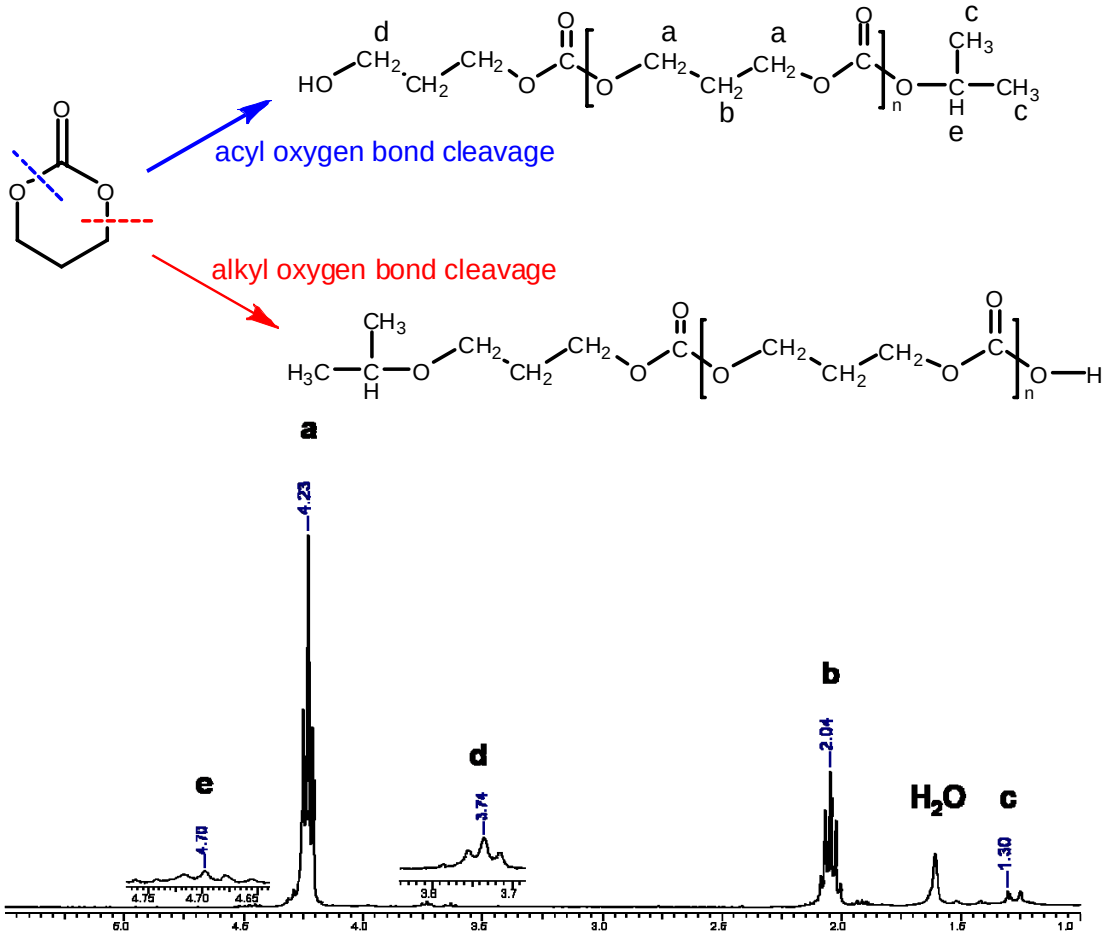

Figure 2-20. ^{1}H NMR spectrum of poly(TMC) terminated by 2-propanol.

Experimental studies were designed to better define the ring-opening process at the molecular level. The mechanism involves an insertion of the monomer into the growing polymer chain by breaking the acyl-oxygen bond instead of the alkyl-oxygen bond (Figure 2-20). This result was obtained by ^{1}H NMR spectroscopy on a low molecular weight polymer derived from chain termination upon reaction with 2-propanol, a procedure employed by Shen and coworkers numerous times.[46] Furthermore, it has also been shown by IR spectroscopy on a low molecular weight polymer derived from a N_3^- initiator that the end group is an azide (Figure 2-21).

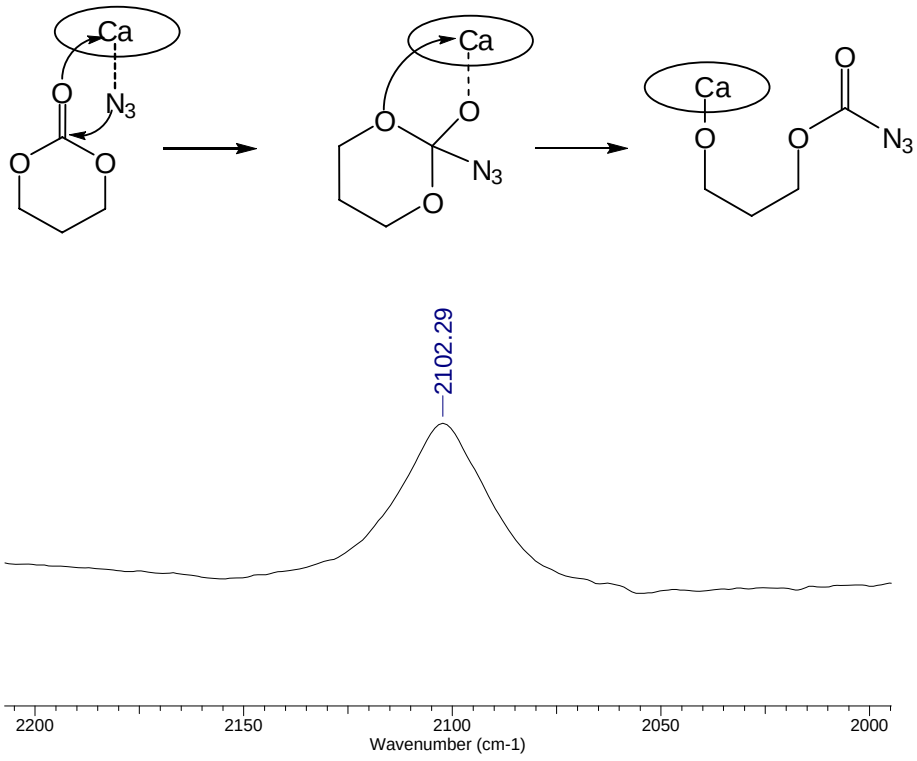

Figure 2-21. Infrared stretch of azide end group in polymer.

Pertinent to the initiation process involving ring-opening of trimethylene carbonate by the anion of the cocatalyst *n*-$Bu_4N^+X^-$, the interaction of (salen)Ca (salen = *N,N'*-bis(3,5-di-*tert*-butylsalicylidene)ethylenediimine) was examined with the azide ion in TCE solution (eq. 2-5).[47] The equilibrium constant for the reaction in eq. 2-5 was determined by monitoring the ν_{N_3} vibrational modes in the metal bound and free species. In this manner K_{eq} at ambient temperature was found to be 79 ± 21 M^{-1}.

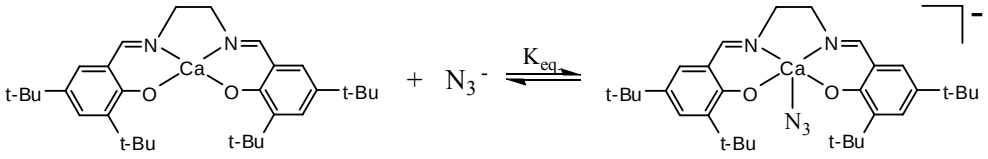

2-5

Although (salen)Ca complexes in the presence of one equivalent of the cocatalyst, *n*-$Bu_4N^+N_3^-$, in tetrachloroethane exist as an equilibrium mixture of (salen)Ca and (salen)CaN_3^-, upon addition of excess trimethylene carbonate all the azide ligand is free in solution. This is best depicted in Figure 2-22 where the calcium bound azide vibration (2059.9 cm^{-1}) is displaced in the presence of only 50 equivalents of trimethylene carbonate. Once the azide nucleophile ring opens the cyclic carbonate its infrared stretching vibrational mode shift to higher frequency, i.e., above 2100 cm^{-1}. This initiation process is fast under catalytic reaction conditions, i.e., the initial ring-opening of the monomer in TCE by azide ion at 110 ºC occurs within 3 minutes. Hence, chain propagation is the slow step in the polymerization process which is consistent with the narrow molecular weight distribution observed for these processes. Because our

kinetic studies were generally carried out in a monomer to initiator ratio of 350 to 1.0, the initiation process most likely involves free or weakly associated azide (or other anion, X^-) at a metal coordinated (activated) trimethylene carbonate monomer (eq. 2-3).

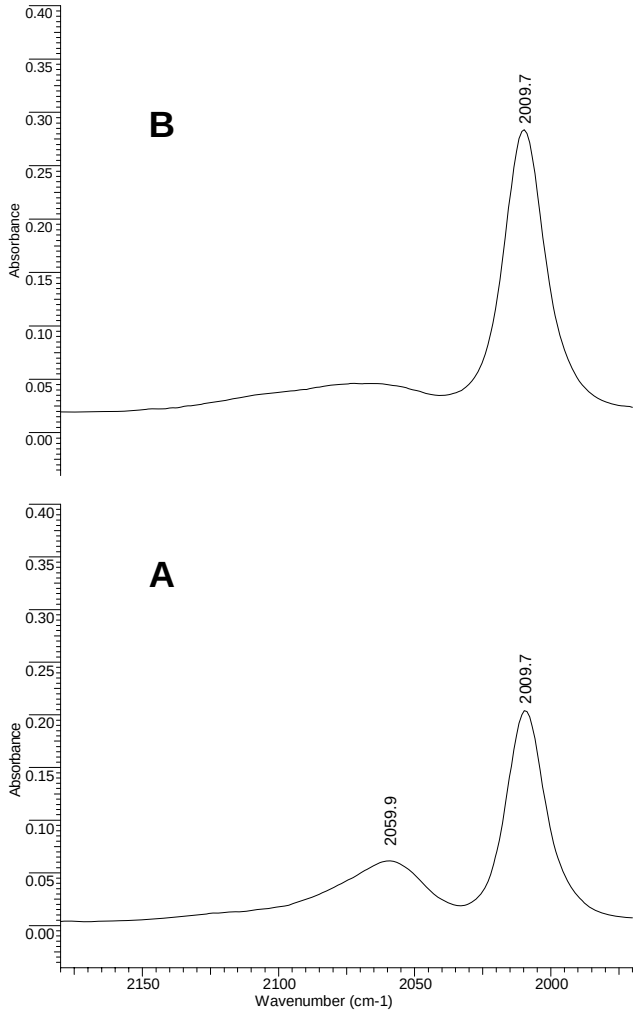

Figure 2-22. Infrared spectra in ν_{N_3} stretching region in tetrachloroethane. **A.** 0.025 M Ca(salen) and one equivalent of *n*-$Bu_4N^+N_3^-$ at ambient temperature, 2009.7 cm^{-1} peak for free N_3^- and 2059.9 cm^{-1} peak for calcium bond N_3^-. **B.** After addition of 50 equivalents of trimethylene carbonate to the solution in **A.** *Note* that free ν_{N_3} absorption has increased.

Ring-opening polymerization of *L*-lactide has been also conducted using a Ca(salen) complexes. Melt polymerizations were carried out at a monomer : catalyst : initiator ratio of 350:1:1 at 110 ºC for 6 h under an argon atmosphere. The results are summarized in Table 2-8, where the TOFs (mol. of *L*-lactide consumed / mol. of catalyst-hr) were determined by precipitating the polymer from dichloromethane, 5% HCl, and methanol, following by drying *in vacuo* and weighing. Characterization of the polymer was done by ^{1}H NMR spectroscopy, which exhibited a quartet at 5.159 ppm (H) and a doublet at 1.555 ppm (CH_3) of intensity ratio 1:3, respectively. For the catalyst optimization, the effect of altering the diimine backbone of the Ca(II) salen derivative has been investigated while maintaining the di-*t*-butyl substituents in the 3,5-positions of the phenolate rings. These results are summarized in Table 2-8, and indicate that an electron-withdrawing, rigid and planar backbone leads to enhanced catalytic activity which is consistent with the results from ROP of TMC.

Table 2-8. Polymerization results for varying the backbone for (salen)Ca(II) complexes where the substituents in the 3,5-positions of the phenolate ring are *t*-butyl groups.[a]

entry	R_1	TOF[b]
1	Ethylene	18.2
2	Phenylene	19.0
3	Naphthylene	22.3

[a] Each reaction was performed in melt maintaining a monomer : initiator : $[PPN]^+N_3^-$ ratio as 350:1:1at 110°C for 6 h. [b] The TOF was determined by weighing the polymer after precipitating in 5% HCl and MeOH, and drying in a vacuum oven and is reported as mol of *L*-LA / mol Ca-h.

The influence of the external anionic cocatalyst (X) on the initiation step of the ring-opening polymerization of lactide was also examined with PPN^+ and *n*-Bu_4N^+ salts. Table 2-9 lists our findings, where the PPN^+ salts were a little more active than their *n*-Bu_4N^+ analogs, and azide was more active than chloride.

Table 2-9. Polymerization results on varying the cocatalyst in Ca(II)(salen) complexes containing an ethylene backbone and tert-butyl groups in the 3,5–positions of the phenolate ring.[a]

entry	cocatalyst	TOF[b]
1	$Bu_4N^+Cl^-$	6.3
2	$Bu_4N^+N_3^-$	17.8
3	PPN^+Cl^-	12.6
4	$PPN^+N_3^-$	18.2

[a] Each reaction was performed in melt maintaining a monomer : initiator : coinitiator ratio as 350:1:1 at 110°C for 6 h. [b] The TOF was determined by weighing the polymer after precipitating in 5% HCl and MeOH, and drying in a vacuum oven and is reported as mol of *L*-LA / mol Ca-h.

Copolymerization results under various polymerization conditions are summarized in Table 2-10. This system has shown rather low catalytic activity for the ring-opening polymerization of lactides. Therefore, a new catalytic system for the ring-opening polymerization of lactides has been developed. Herein, it was noticed that the rates of growing individual polymer chains depend on the reaction conditions, and conversion of lactide to poly(lactide) is faster than that of TMC to poly(trimethylene carbonate) in random copolymerization reactions. Conversion of PLA in

copolymerization is faster than that in homopolymerization while conversion of PTMC in copolymerization is slower than that in homopolymerization.

Table 2-10. Copolymerization results under various copolymerization conditions using (salen)Ca(II) complexes with $[PPN]N_3$.

polymer	feed ratio (mol/mol)[a]	composition (mol/mol)[b]	TOF[c]	copolymerization conditions[d]
TMC-*ran*-*L*-LA	50/50	38/62	47.8	melt at 110°C for 5h
TMC-*ran*-*L*-LA	50/50	21/79	11.4	in toluene at 80°C 22h
L-LA-*block*-TMC[e]	50/50	92/8	3.2	in TCE at 110°C for 102h
TMC-*block*-*L*-LA[f]	50/50	95/5	0.9	in TCE at 110°C for 316h
Poly(TMC)	100/0	100/0	95.3	in TCE at 110°C for 3h
Poly(*L*-LA)	0/100	0/100	0.5	in TCE at 110°C for 96h

[a] Mol TMC / mol *L*-LA added. [b] Based on NMR after precipitating with 5% HCl in MeOH, and drying in a vacuum oven. [c] TOF = mol of each monomer consumed / (mol of catalyst · h). [d] $[PPN]N_3$ used as a cocatalyst and [M] = 0.69 M in solution. [e] TMC monomer added to poly(*L*-LA) block. [f] *L*-LA monomer added to poly(TMC) block.

Ring-Opening Polymerization of Cyclic Monomers Catalyzed by Tridentate Schiff Base Biometal Complexes

Calcium salen complexes in the presence of anionic initiators exhibit a high activity for the ring-opening polymerization of trimethylene carbonates. However, this system has shown rather low catalytic activity for the ring-opening polymerization of lactides. Herein, calcium complexes with tridentate Schiff base ligands has been synthesized for the effective polymerization of both lactides and trimethylene carbonate. The general structure of the calcium complexes employed in these studies is depicted in Figure 2-23, where modifications of the Schiff base ligands are readily achieved by

variations of the aldehyde and diamine starting reagents.[10-12] The most part *bis*(trimethylsilyl)amide has been utilized as an initiator, which is very air and moisture sensitive. These calcium derivatives were found to contain two or three bound molecules of THF by ^{1}H NMR measurements.

Initially, the effectiveness of the calcium complexes was examined for the ring-opening polymerization of *L*-lactide or *D*-lactide. Melt polymerizations were performed at a monomer : catalyst ratio of 350:1 at 110°C for 15 minutes under an argon atmosphere. The results of these melt polymerization runs are summarized in Table 2-11, where TOFs mol of *L*-lactide consumed / (mol of catalyst · hour) were determined by precipitating the polymers from dichloromethane, 5% hydrochloric acid, and methanol followed by drying *in vacuo* and weighing. As indicated in Table 2-11, a calcium salen catalyst with *bis*(phosphoranylidene)ammonium azide ([PPN]N_3) as a cocatalyst is much less active than calcium with tridentate Schiff base ligands. Furthermore, the analogous zinc complex (**2-15**) is also less active than calcium complex (**2-9**). Changing the initiator to methoxy displayed similar activity to *bis*(trimethylsilyl)amide. Less hindered and less donating hydrogen substituent on R^2 (**2-13**) resulted in similar activity to bulky t-butyl group and less stereoselectivity. However, more significant changes in TOFs were noted upon altering the nature of the imine backbone. The calcium complex containing the more donating and less bulky dimethyl imine backbone resulted in the most active catalyst (**2-9**), which is 2.2 times more active than that containing the more electron withdrawing and bulky aminoquinoline imine backbone.

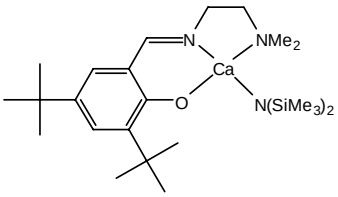

2-9

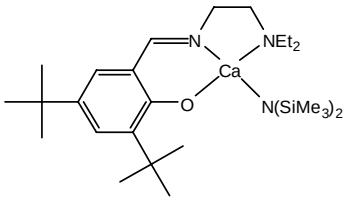

2-10

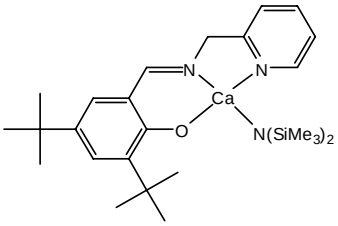

2-11

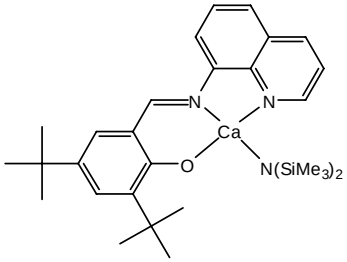

2-12

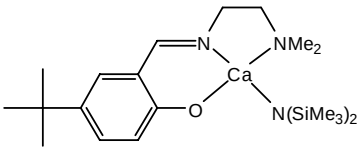

2-13

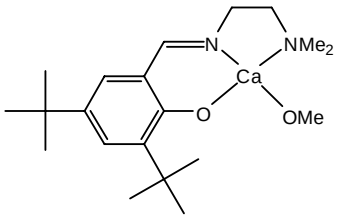

2-14

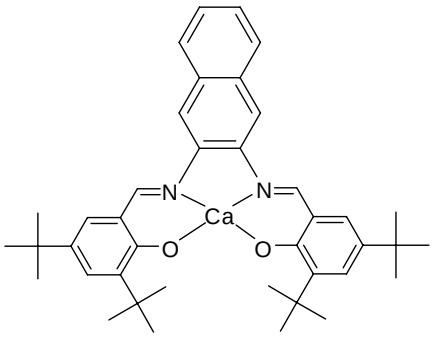

2-7

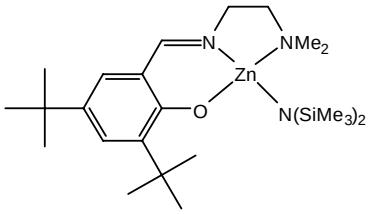

2-15

Figure 2-23. Structures of calcium complexes with tridentate Schiff base ligands.

Table 2-11. Polymerization of *L*-lactide catalyzed by calcium complexes with tridentate Schiff base ligands[a]

entry	catalyst	conversion (%)[b]	TOF[c]
1	**2-9**	80	1124
2	Ca(salen) (**2-15**)	35[d]	22.3
3	**2-10**	54	753
4	**2-11**	41	519
5	**2-12**	39	502
6	**2-13**	64	891
7	**2-14**	59	826

[a] Each reaction was performed in melt maintaining a nomomer:initiator ratio as 350:1 at 110°C for 15 minutes. [b] Obtained from ^{1}H NMR. [c] The TOFs were determined by weighing the polymer after precipitating in 5% HCl and MeOH and drying in a vacuum oven and is reported as mol of *L*-LA consumed / (mol of Ca·h). [d] For 6 h.

The molecular weight and polydispersity of poly(*L*-lactide) obtained in these studies were measured by Gel Permeation Chromatography (GPC). The melt polymerizations were carried out at 110 °C using catalyst **2-9** depending on M/I ratios. As indicated in Table 2-12, the molecular weights increase with increasing M/I ratios maintaining narrow polydispersity indices (PDI, M_w / M_n), thus demonstrating that the level of polymerization control is high (Figure 2-24).

Table 2-12. Dependence of poly(lactide) molecular weight on M/I.[a]

		M_n		
entry	M/I	theoretical[b]	GPC	PDI
1	350	40,481	65,005	1.022
2	450	45,360	82,362	1.048
3	500	50,400	94,529	1.035
4	700	69,552	110,624	1.039

[a] Each reaction was performed in melt at 110°C for 30 minutes using catalyst **2-9**. [b] Theoretical M_n = (M/I) × (% Conversion) × (M_w of lactide)

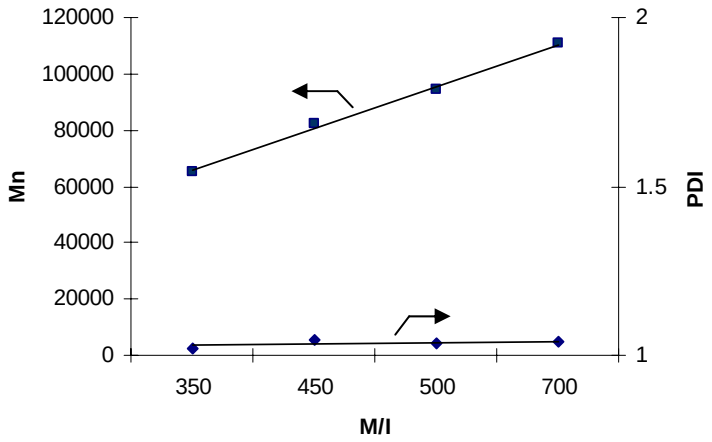

Figure 2-24. Plot of the dependence of molecular weight of poly(*L*-lactide) on M/I ratios.

Kinetic measurements of the ring-opening polymerization of *L*-lactide in solution have been initiated in the presence of catalyst **2-9**. The kinetic studies were conducted in $CDCl_3$ and monitored by ^1H NMR spectroscopy. The polymerization reaction was found to be first order in monomer (*L*-lactide) concentration (Figure 2-25) and catalyst with $k = 19.9\ M^{-1}h^{-1}$ at ambient temperature (Figure 2-26). Table 2-13 summarizes the determined rate constants (k_{obsd}) for the ring-opening polymerization of *L*-lactide as a function of the catalyst concentration and temperature. The rate of polymerization in the coordinating solvent tetrahydrofuran was found to be much faster than in the chlorinated solvent, since the complexation of calcium ion by coordinating solvents enhances the nucleophilicity of the initiator.[22] The polymerization rates have been observed changing the amount of THF in $CDCl_3$ solution in the presence of catalyst **2-13** (Table 2-14). It was found that the polymerization is faster with increasing amount of THF (Figure 2-27).

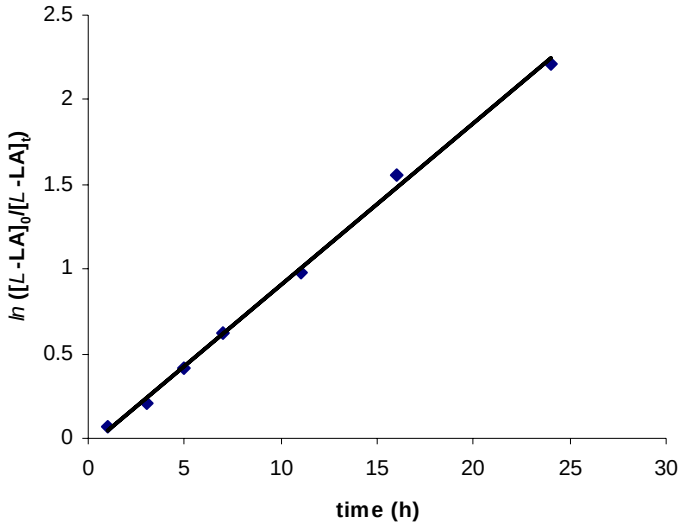

Figure 2-25. ln([*L*-LA]$_0$/[*L*-LA]$_t$) *vs*. time plot depicting a reaction order of unity with respect to monomer concentration ($R^2 = 0.997$).

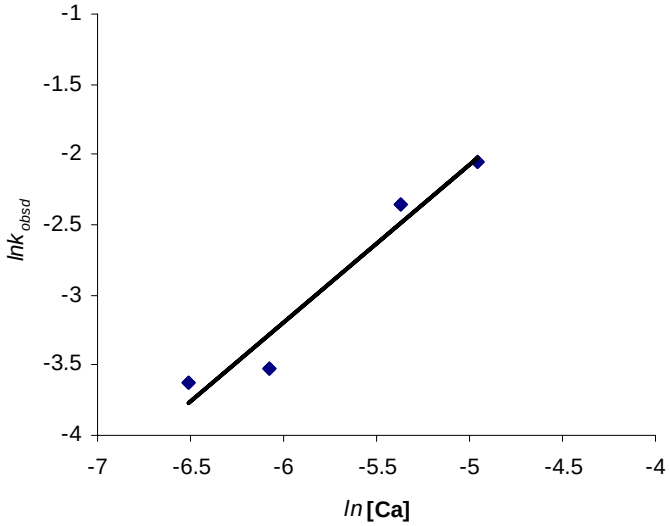

Figure 2-26. Plot of $\ln k_{obsd}$ *vs*. ln[Ca] to determine the order of the polymerization reaction with respect to the concentration of catalyst. Slope = 1.12 with $R^2 = 0.949$.

Table 2-13. Rate constants dependence on the concentration of the catalyst and temperature.

entry	[Ca] (mM)	temp. (°C)	k_{obsd} (h^{-1})
1	1.49	25	0.0266
2	2.30	25	0.0295
3	4.66	25	0.0955
4	7.03	25	0.1277
5	4.66	0	0.0047
6	4.66	41	0.4731
7	4.66	51	0.8083

Monomer concentration held constant at 0.69 M and reactions carried out in $CDCl_3$.

Table 2-14. Rate constants dependence on the amount of THF in $CDCl_3$.

entry	$CDCl_3$ (mol %)	THF (mol %)	k_{obsd} (h^{-1})
1	100	0	0.0074
2	80~90	10~20	0.0158
3	0	100	0.0239

Monomer concentration held constant at 0.69 M and [cat] = 2.30 mM. Reactions carried out at room temperature

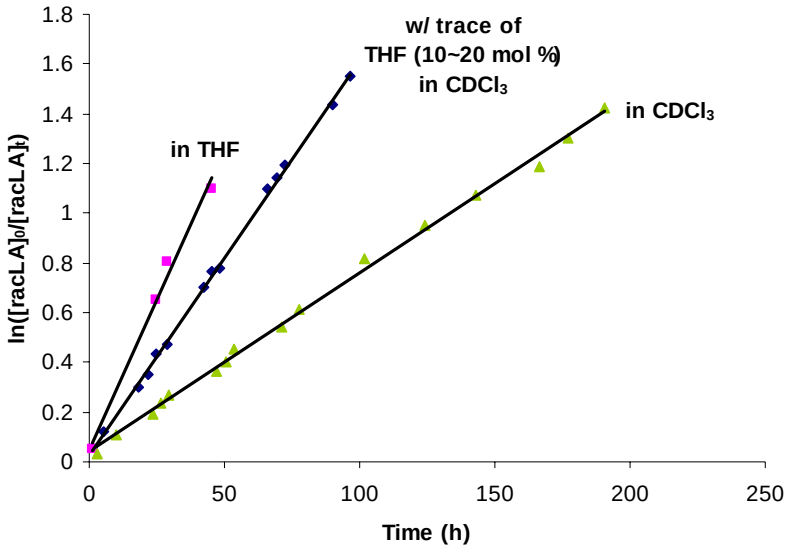

Figure 2-27. First-order kinetic plots for *rac*-lactide polymerizations in different solvent mixture.

The activation parameters for the ring-opening polymerization of *L*-lactide catalyzed by **2-9** in $CDCl_3$ were found to be $\Delta H^{\neq}$ = 73.5 ± 3.8 kJ/mol and $\Delta S^{\neq}$ = -42.5 ± 12.6 J/(mol·K). These values were calculated from the temperature-dependent rate constants listed in Table 2-13 and Eyring plot in Figure 2-28. A $\Delta G^{\neq}$ value of 86.1 kJ/mol was calculated for the ring opening polymerization of *L*-lactide catalyzed by calcium catalyst (**2-9**) at 25ºC.

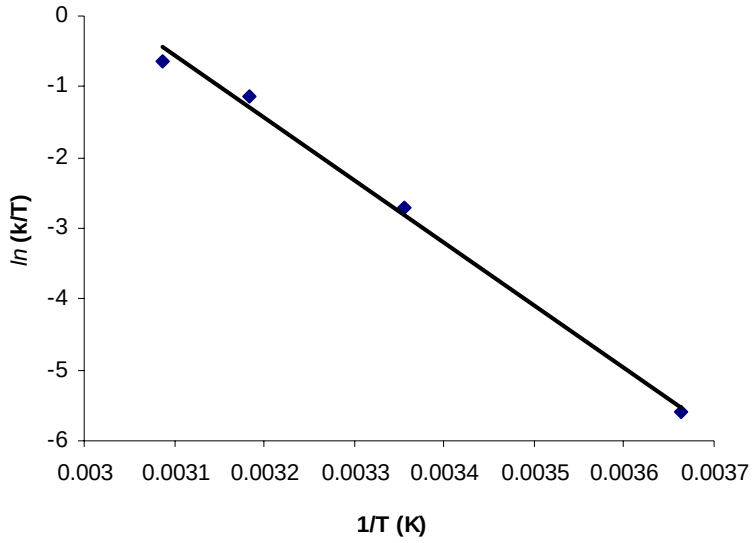

Figure 2-28. Eyring plot of ROP of *L*-lactide in the presence of catalyst **2-9** in $CDCl_3$. Slope = -8836 with R^2 = 0.995.

The control of stereoregularity in polymers by catalysts is an important feature for applications since polymer tacticity caused different polymer properties. Selectivities toward different lactide isomers have been studied using catalyst **2-9** which has more hindered tert-butyl group on R^2 positions, and **2-13** which has less hindered H on R^2 under various polymerization conditions. The tacticity of the polymer was

assigned using the methine proton signals with homonuclear decoupling as described by Hillmyer and coworkers.[48] Pr values were calculated by (area of isi and sis) / (total area in methine proton region) from decoupled ^{1}H NMR spectra (Figure 2-29 and 2-30). It is observed that **2-9** with more bulky t-butyl group has better stereoselectivity than **2-13** with less hindered H group. It is also observed that the polymerization at lower temperature resulted in clearer heterotactic polylactide and selectivity increases in $CDCl_3$ than in THF. Catalyst **2-9** produced isotactic polylactide from *L*-lactide and predominantly produces heterotactic polylactide from *rac*-lactide.

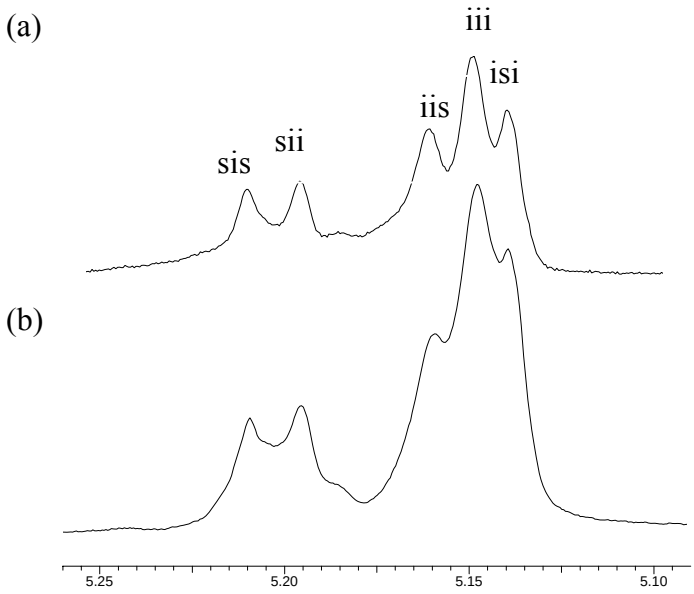

Figure 2-29. Homonuclear decoupled ^{1}H NMR ($CDCl_3$, 500 MHz) spectra of the methine region of poly(lactide) prepared from *rac*-lactide with **2-13** (a) in THF at room temperature (Pr = 0.48), (b) in $CDCl_3$ at room temperature (Pr = 0.54).

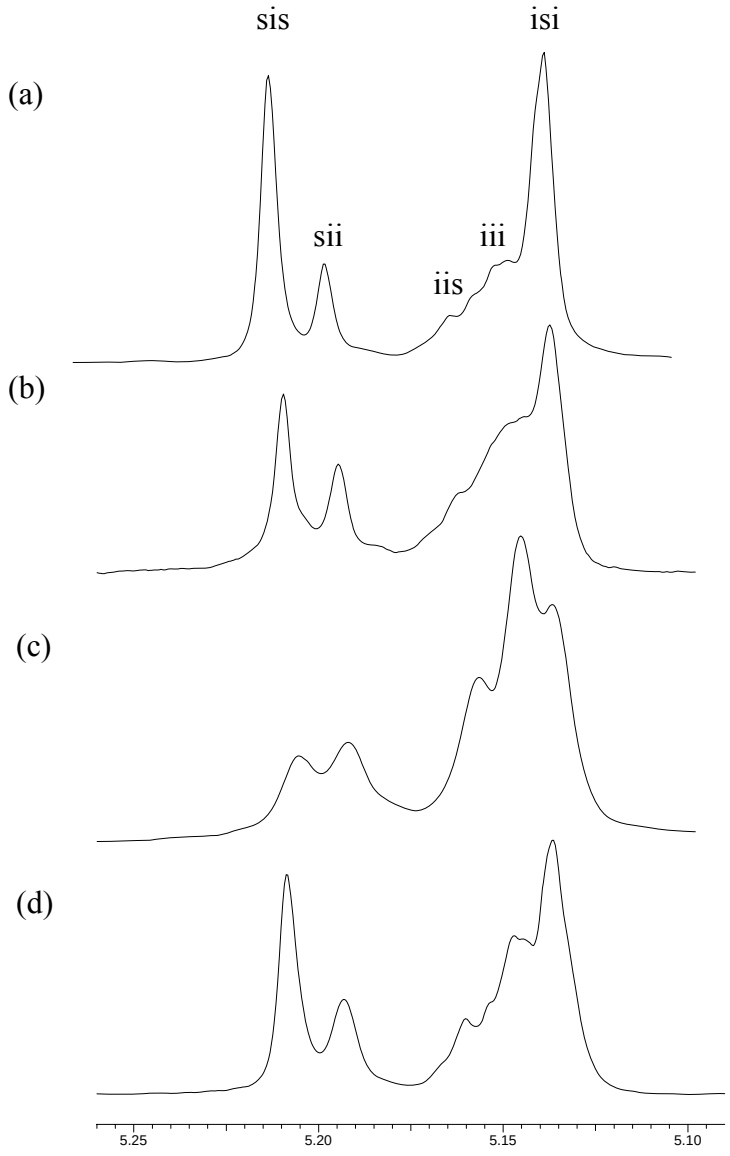

Figure 2-30. Homonuclear decoupled ^{1}H NMR ($CDCl_3$, 500 MHz) spectra of the methine region of poly(lactide) prepared from *rac*-lactide with **2-9** (a) in THF at -33°C (Pr = 0.73), (b) in THF at 0°C (Pr = 0.57) (c) in THF at room temperature (Pr = 0.52), (d) in $CDCl_3$ at room temperature (Pr = 0.66).

It was similarly observed that the ring-opening polymerization of trimethylene carbonate catalyzed by complex **2-9** in $CDCl_3$ is first order in monomer (Figure 2-31) and catalyst concentrations (Figure 2-32). Table 2-15 summarizes the determined rate constants (k_{obsd}) for the ring-opening polymerization of trimethylene carbonate as a function of the catalyst concentration and temperature. In this instance, the rate is much faster than that for *L*-lactide with a rate constant at ambient temperature determined to be 500 $M^{-1}h^{-1}$. As previously reported for calcium salen complexes initiated by an external nucleophile, the ring-opening polymerization of trimethylene carbonate by complex **2-9** was found to have a high level of polymerization control.[23a] That is, the product polymers exhibited a linear increase in M_n with conversion and possessed low polydispersity indices.

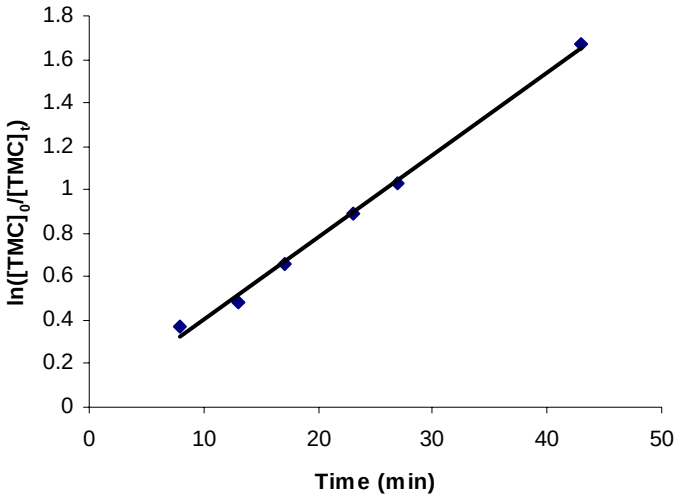

Figure 2-31. $\ln([TMC]_0/[TMC]_t)$ *vs*. time plot depicting a reaction order of unity with respect to monomer concentration ($R^2 = 0.996$).

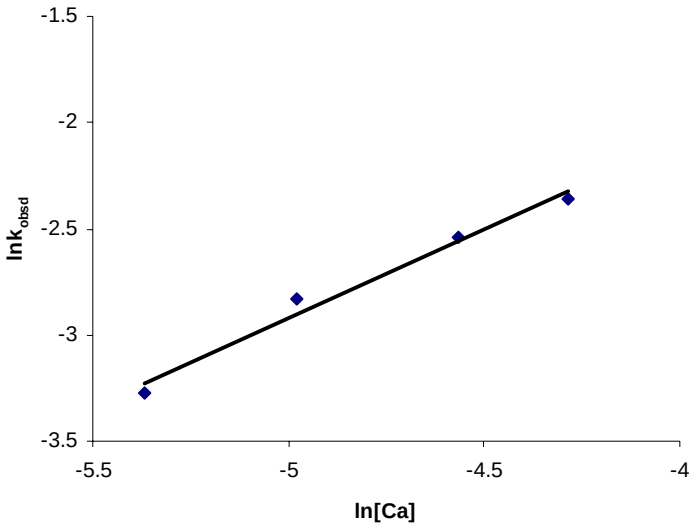

Figure 2-32. Plot of $\ln k_{obsd}$ *vs.* ln[Ca] to determine the order of the polymerization reaction with respect to the concentration of catalyst. Slope = 0.83 with $R^2 = 0.984$.

Table 2-15. Rate constants dependence on the concentration of the catalyst and temperature for ROP of TMC.

entry	[Ca] (mM)	temp. (°C)	k_{obsd} (min^{-1})
1	4.66	22	0.0379
2	6.90	22	0.0588
3	10.4	22	0.0787
4	13.8	22	0.0948
5	6.90	0	0.0101
6	6.90	6	0.0146
7	6.90	-33	0.001124

Monomer concentration held constant at 0.69 M and reactions carried out in $CDCl_3$.

Activation parameters have been determined from Eyring plot (Figure 2-33) and these are comparable with activation parameters for the ring-opening polymerization of TMC catalyzed by **2-9** in $CDCl_3$ ($\Delta H^{\neq}$ = 37.9 ± 3.1 kJ/mol, $\Delta S^{\neq}$ = -135.1 ± 11.4 J/(mol·K) and $\Delta G^{\neq}$ = 78.2 kJ/mol at 25ºC which proves ring-opening polymerization of TMC is a less energy process than that of lactide.

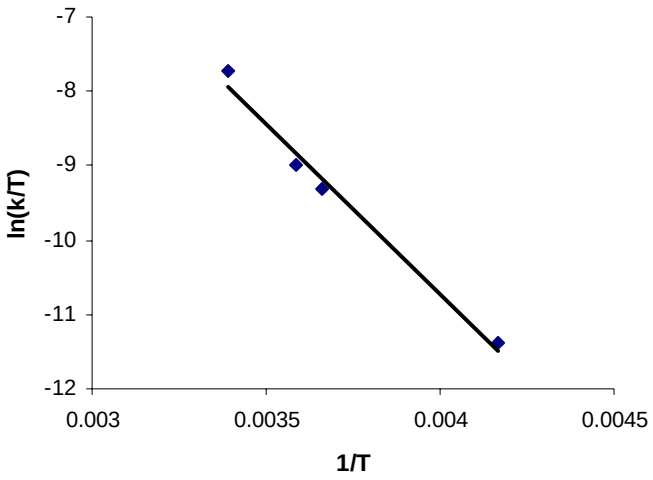

Figure 2-33. Eyring plot of ROP of TMC in the presence of catalyst **2-9** in $CDCl_3$. Slope = -4557 with R^2 = 0.987.

Catalyst **2-9** efficiently produces both random and block copolymers from lactides and trimethylene carbonate. For random copolymerization, both trimethylene carbonate and *L*-lactide monomers were simultaneously added to the solution of catalyst **2-9** in $CDCl_3$ at room temperature. For block copolymerization, trimethylene carbonate was added to the solution of catalyst **2-9** in $CDCl_3$. After completion of polymerization of trimethylene carbonate at room temperature monitoring by ^1H NMR, the solution of

L-lactide monomer (1 eq.) in $CDCl_3$ was added to the solution of poly(trimethylene carbonate). Polymerization was stopped when % conversion of TMC to PTMC was 75 %. Both random and block copolymers were purified by precipitation from 5% HCl and methanol and then dried in *vacuo*. Diblock copolymer has composition = 55:45 (mol PLLA : mol PTMC) by ^1H NMR after purification. Molecular weight of diblock copolymer was determined by GPC to M_n = 18,083, PDI = 1.734 (theoretical M_n = 11,025). The block copolymer produced by **2-9** is stable up to 250°C with T_m = 150°C (Figure 2-34).

Kinetic study for the random copolymerization reaction catalyzed by **2-9** has been investigated monitoring the rate of enchainment of trimethylene carbonates as well as that of lactide during copolymerization. Interestingly, it was observed that the rate of enchainment of trimethylene carbonate monomer is much slower than that of lactide during the copolymerization reactions, which has been also observed with Ca(II)(salen) catalyst system. It is also noticed that the rate of enchainment of trimethylene carbonate is increased after ROP of lactide is consumed which means that the two reactions of ring-opening polymerization of cyclic monomers compete with each other and influence the other reaction. In order to investigate the kinetics in detail, the concentration of catalyst and feed ratio of trimethylene carbonate and lactide have been changed.

(a)

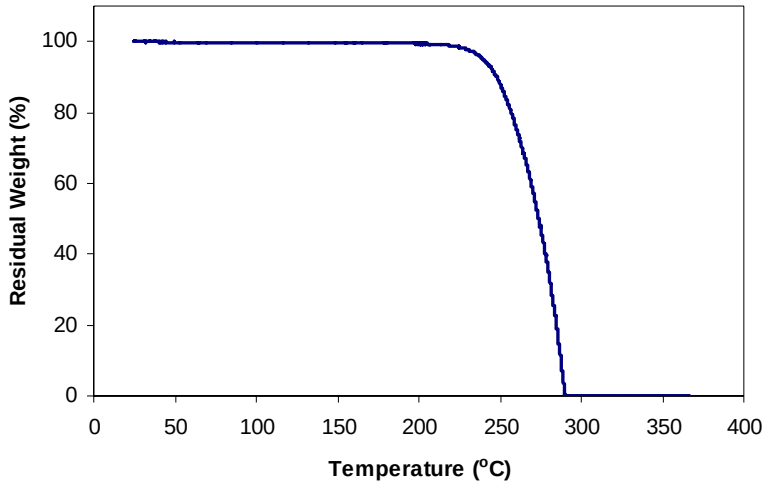

(b)

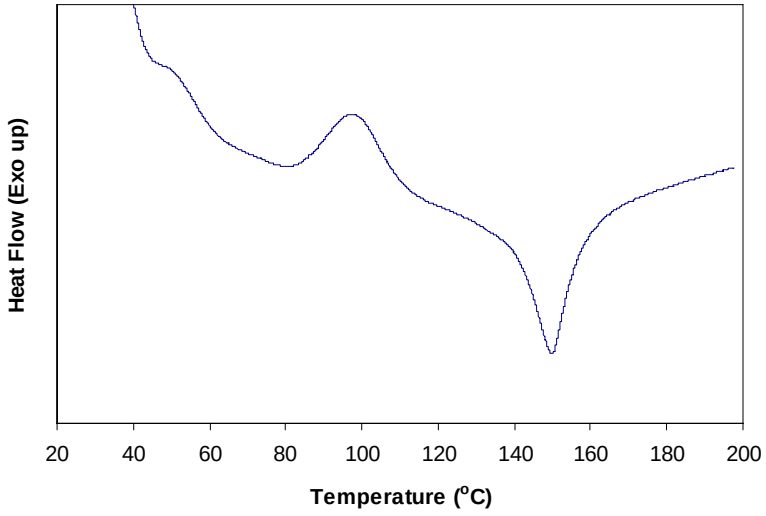

Figure 2-34. (a) TGA and (b) DSC curves (second heating run) of TMC-*block*-LLA copolymer (composition = 55:45 (mol:mol) by ^{1}H NMR after purification).

The polymerization reaction was found to be first order in each monomer (trimethylene carbonates and *L*-lactide) concentration (Figure 2-35) and catalyst (Figure 2-36). Table 2-16 summarizes the determined rate constants (k_{obsd}) for random

copolymerization of trimethylene carbonate and *L*-lactide as a function of the catalyst concentration and temperature when the feed ratio is 50 : 50 (mol : mol).

Table 2-16. Rate constants dependence on the concentration of the catalyst and temperature in random copolymerization.

entry	[cat] (mM)	temp.(°C)	k_{obsd} (lactide) (h^{-1})	k_{obsd} (TMC) (h^{-1})
1	13.8	25	0.0997	0.0078
2	20.7	25	0.1847	0.0113
3	27.6	25	0.2108	0.0175
4	34.5	25	0.2677	0.0180
5	13.8	0	0.0125	0.00106
6	13.8	41	0.8732	0.0672
7	13.8	51	n.d.*	0.0918

Each monomer concentration held constant at 0.69 M and reactions carried out in $CDCl_3$. * n.d. = not detected because of fast reaction.

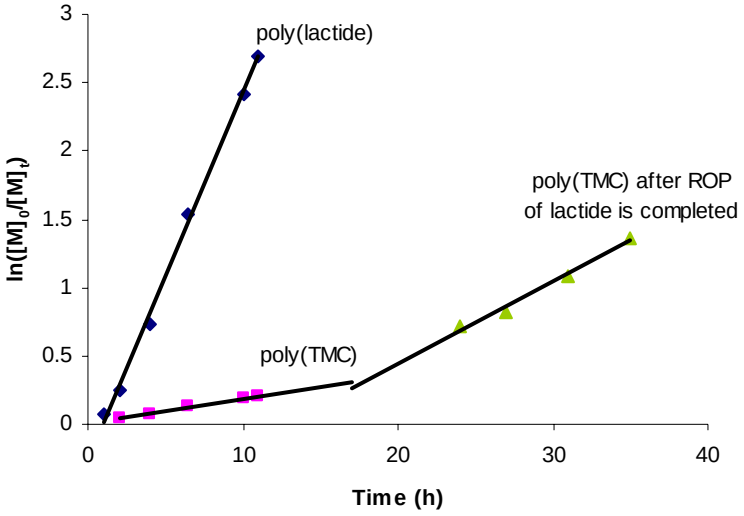

Figure 2-35. $\ln([M]_0/[M]_t)$ *vs*. time plot depicting a reaction order of unity with respect to each monomer concentration (R^2 = 0.997 for poly(lactide) and R^2 = 0.993 for poly(TMC)).

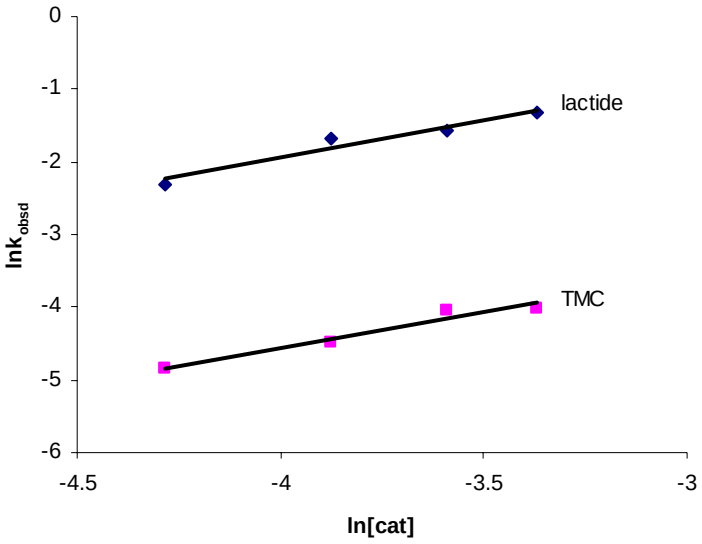

Figure 2-36. Plot of $\ln k_{obsd}$ *vs*. ln[Ca] to determine the order of the polymerization reaction with respect to the concentration of catalyst. Slope = 1.04 with $R^2 = 0.956$ for lactide. Slope = 0.983 with $R^2 = 0.956$ for TMC.

Based on kinetic results, the copolymerization rate can be expressed in eq. 2-6 and activation parameters have been determined from Eyring plot (Figure 2-37 and 2-38) and these are compared with activation parameters for homopolymerization of lactide or trimethylene carbonate (Table 2-17). $\Delta H^{\neq}$ for ROP of lactide in random copolymerization is lower than that in homopolymerization while $\Delta H^{\neq}$ for ROP of TMC in random copolymerization is higher than that of its homopolymerization. From these kinetic parameters for ROP of LA and TMC, it was observed that LA has a higher $\Delta H^{\neq}$ than that of TMC and less negative $\Delta S^{\neq}$ than that of TMC in both homopolymerization and random copolymerization process.

$$\text{rate} = [\text{cat}](k_{LA}[LA] + k_{TMC}[TMC]) \qquad 2\text{-}6$$

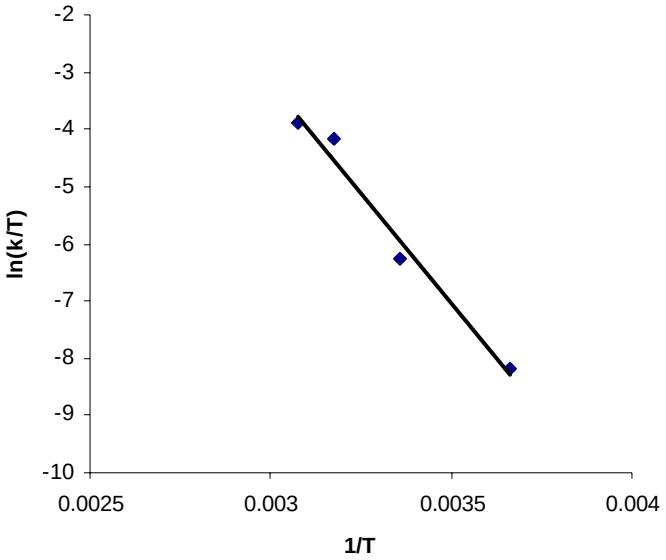

Figure 2-37. Eyring plot of ROP of TMC in the presence of catalyst **2-9** in $CDCl_3$ during random copolymerization with lactide. Slope = -7691 with $R^2 = 0.977$.

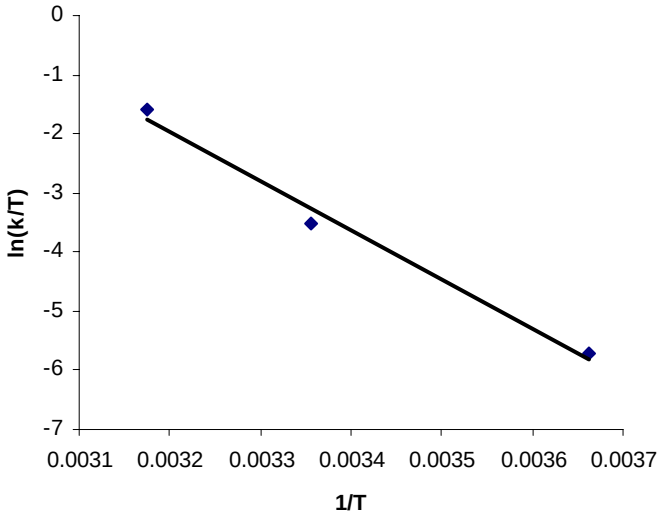

Figure 2-38. Eyring plot of ROP of lactide in the presence of catalyst **2-9** in $CDCl_3$ during random copolymerization with TMC. Slope = -8270 with $R^2 = 0.989$.

Table 2-17. Comparison of activation parameters in homopolymerization and random copolymerization.

	homopolymerization		random copolymerization	
	lactide	TMC	lactide	TMC
$\Delta H^{\neq}$ (kJ/mol)	73.5 ± 3.8	37.9 ± 3.1	68.8 ± 8.3	63.9 ± 6.7
$\Delta S^{\neq}$ (J/(mol·K))	-42.5 ± 12.6	-135.1 ± 11.4	-62.0 ± 28.3	-100.3 ± 22.4
$\Delta G^{\neq}$ (kJ/mol) at RT	86.1	78.2	87.3	93.8

Pertinent to $\Delta S^{\neq}$ values for ROP of lactide and TMC, binding studies between these monomer and the metal complex have been investigated using (salen)Ca complex and *n*-$Bu_4N^+N_3^-$ in tetrachloroethane which exist as an equilibrium mixture of (salen)Ca and (salen)CaN_3^- (eq. 2-7). As mentioned for ROP of TMC, upon addition of excess trimethylene carbonate all the azide ligand is free in solution. The infrared spectra showed the free ν_{N_3} absorption was not increased much with the addition of lactide (Figure 2-39) compared to that with addition of TMC (Figure 2-22). The better binding ability of TMC to Ca(II) metal is consistent with the larger negative $\Delta S^{\neq}$ value for ROP of TMC.

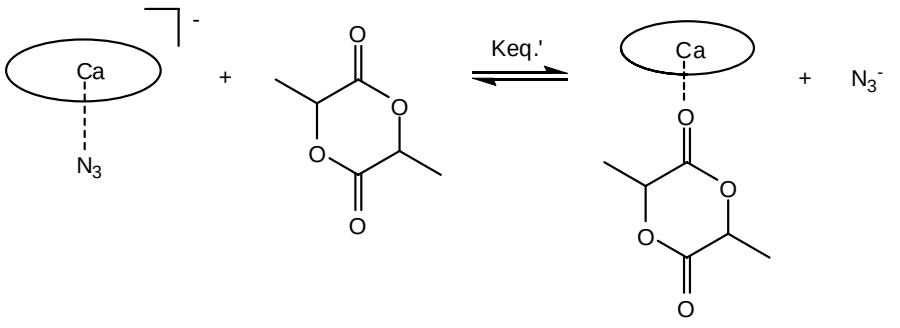

2-7

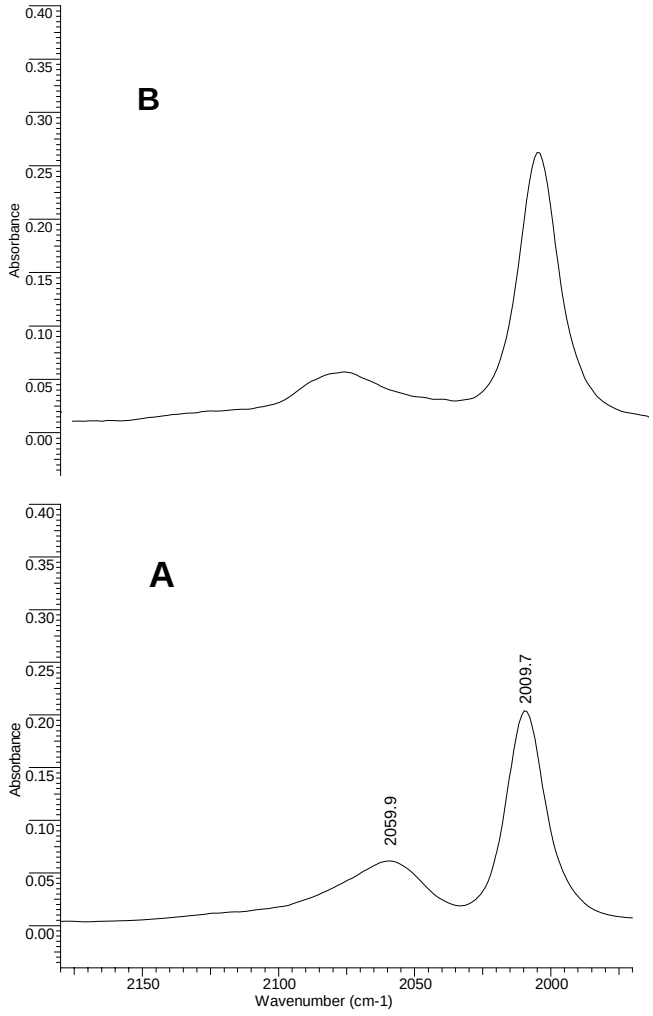

Figure 2-39. Infrared spectra in ν_{N_3} stretching region in tetrachloroethane. **A.** 0.025 M Ca(salen) and one equivalent of *n*-$Bu_4N^+N_3^-$ at ambient temperature, 2009.7 cm^{-1} peak for free N_3^- and 2059.9 cm^{-1} peak for calcium bond N_3^-. **B.** After addition of 50 equivalents of lactide to the solution in **A.** *Note* that free ν_{N_3} absorption has increased less with addition of lactide than that with TMC (see Figure 2-22).

The feed ratios were also changed in order to investigate the influence of the other monomer and Table 2-18 lists the determined rate constants (k_{obsd}) for the various feed ratios. Rate constants for *L*-lactide polymerization or TMC polymerization in a random copolymerization process have been plotted depending on the fraction of the other monomers (Figure 2-40). According to these results, the rate to grow poly(lactide) is increased with increasing amounts of TMC, while the rate to grow poly(TMC) is decreased with increasing amounts of lactide. Rate constants were found to change significantly between 0 and 0.1 of monomer fraction and little between 0.25 and 0.75, and the rate drops more dramatically in TMC polymerization even with very little amounts of lactide.

Table 2-18. Rate constants dependence on the monomer feed ratio in random copolymerization.

entry	LA : TMC (mol : mol)	k_{obsd} (lactide) (h^{-1})	k_{obsd} (TMC) (h^{-1})	k_{obsd} (TMC)[a] (h^{-1})
1	1 : 99	n.d.[b]	0.2115	0.6450
2	5 : 95	0.3453	0.0620	0.5270
3	25 : 75	0.1971	0.0150	0.0158
4	50 : 50	0.1847	0.0113	0.0465
5	75 : 25	0.1722	0.0101	0.0360
6	95 : 5	0.1685	n.d.	0.0029
7	99 : 1	0.1540	n.d.	n.d.

Reactions carried out in $CDCl_3$ at room temperature. [cat] = 0.0207 mM.
[a] Determined rate constant after lactide polymerization is completed. [b] n.d. = not detected because of too little amount of monomer.

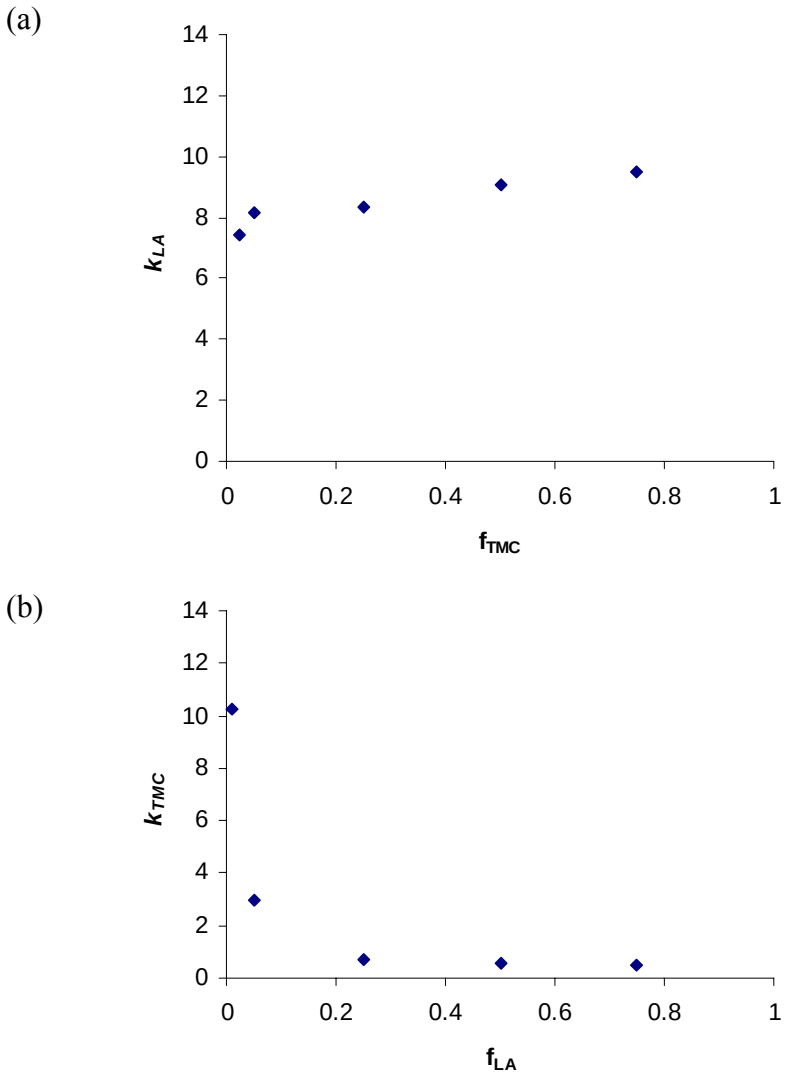

Figure 2-40. Rate constants as a function of fraction of monomers in random copolymerization of lactide and TMC (a) rate constant for lactide polymerization *vs*. fraction of TMC and (b) rate constant for TMC polymerization *vs*. fraction of lactide.

The average copolymerization rate is expressed in eq. 2-8 and is plotted as a function of the fraction of TMC (Figure 2-41), where the average rate was calculated from eq. 2-9 and $\bar{k}$ is an average rate constant for copolymerization.[49] The average rate

constant for copolymerization is decreased with the fraction of TMC between 0 and 0.75 and increased very dramatically between 0.95 and 1. It is noticed that the copolymerization rate depends on the feed ratio.

$$\text{rate} = \bar{k}[\text{cat}]([\text{LA}]+[\text{TMC}]) \qquad 2\text{-}8$$

$$\text{total \% conversion} = \frac{\%\ \text{conv(LA)} \times \text{g of LA} + \%\ \text{conv(TMC)} \times \text{g of TMC}}{\text{g of LA} + \text{g of TMC}} \qquad 2\text{-}9$$

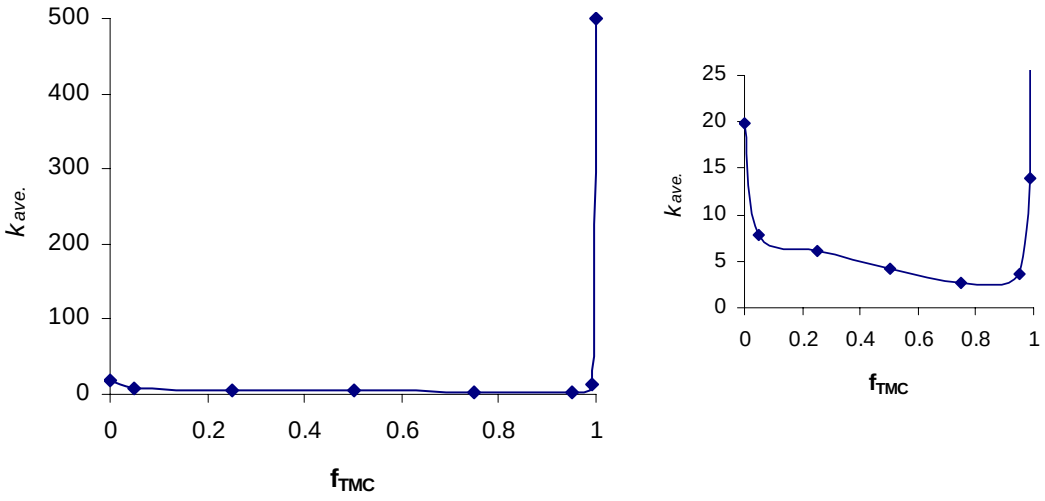

Figure 2-41. Average rate constants as a function of fraction of TMC monomers in random copolymerization of lactide and TMC.

Degradation studies have been performed with poly(trimethylene carbonate), poly(*L*-lactide), and the copolymers from trimethylene carbonate and *L*-lactide by Angela Jones, a TAMU undergraduate researcher in our laboratory. The data for these studies are listed in Appendix B.

Ring-Opening Polymerization of Lactides Catalyzed by (cyclohexylsalen)*CrCl

Ring-opening polymerization reactions of lactides have been performed using {(R,R)-cyclohexylsalen}CrCl and *n*-Bu_4NN_3 (Figure 2-42) to investigate the stereoselectivity toward *L*-lactide and *D*-lactide. An enantiomorphic site control mechanism is possible since (cyclohexylsalen)*CrCl has a chiral center on the cyclohexyl backbone similar to {(R,R)-cyclohexylsalen}AlO^iPr. Ring-opening polymerization of both *L*-lactide and *D*-lactide were carried out in toluene at 100 °C. Figure 2-43 indicates *D*-lactide polymerization is about 3 times faster than *L*-lactide polymerization.

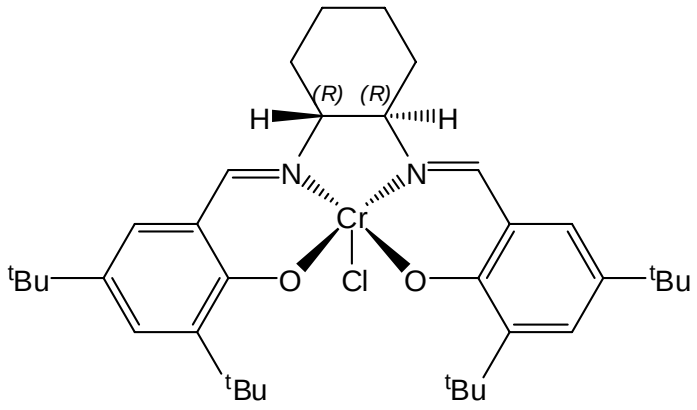

Figure 2-42. Structure of {(R,R)-cyclohexylsalen}CrCl.

Other catalyst systems with chiral center are under investigation for selectivity toward *L*-lactide, *D*-lactide and *meso*-lactide polymerization. The stereoelectivity has been studied from various combinations of the chirality of the ligand bound to the metal, the chirality of the end group of the growing polymer chain, and solvent for *L*-lactide and *D*-lactide polymerization by Chisholm, and it was reported all these factors play a complex and unpredictable role in the preference for *L*-lactide or *D*-lactide in *rac*-lactide polymerization.[50]

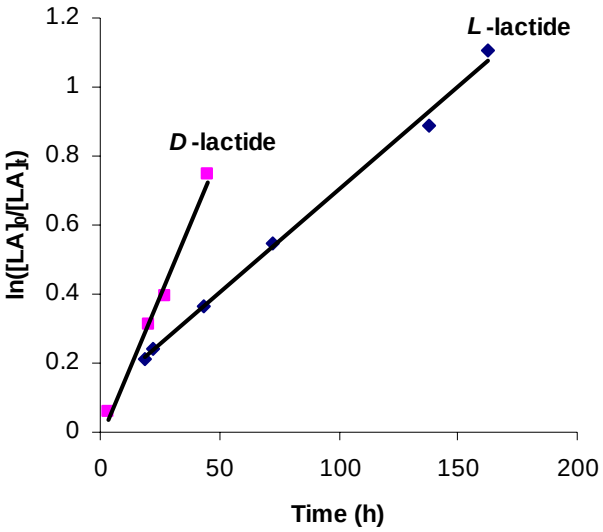

Figure 2-43. First-order kinetic plots for *L*-lactide and *D*-lactide polymerization in toluene at 100°C with $[M]_0/[I]_0$ = 200 and $[M]_0$ = 0.98 M. Slope = 0.0163 with R^2 = 0.991 for *D*-lactide polymerization and slope = 0.00600 with R^2 = 0.996 for *L*-lactide polymerization.

CONCLUSIONS

Herein it has been reported on the use of biometal Schiff base derivatives as catalysts for the ring-opening polymerization of trimethylene carbonate and lactides. The catalytic activity varied with metal in the order $Ca^{+2} > Mg^{+2} \approx C_2H_5Al^{+2} > Zn^{+2}$. Optimization of the calcium(II) system was achieved by changing backbone, substituents in the 3,5-positions of the phenolate rings and initiators. These calcium systems have shown excellent catalytic activity for ring-opening polymerization of trimethylene carbonate or lactide to produce high molecular weight polymers with narrow polydispersities. In addition these catalysts effectively copolymerize these two monomers. Solution kinetic studies revealed the polymerization reaction to be first-order in [monomer], [catalyst], and [cocatalyst] (in case of the catalytic system of (salen)Ca and an external initiator). The polymerization reaction was shown to be *quasi-living* as illustrated by a linear relationship between M_n and % conversion and a low polydispersity index, clearly demonstrating that the level of polymerization control was high.

For stereoselectivity studies of lactide polymerization, the polymer products under various polymerization conditions have been investigated and it was found that catalyst **2-9** predominantly produced heterotactic poly(lactide) from *rac*-lactide.

Activation parameters for trimethylene carbonate and lactides homopolymerization have been obtained and it was found that ROP of TMC has a lower $\Delta G^{\neq}$ than that of lactide. Activation parameters for copolymerization of lactide and trimethylene carbonate have also been determined and compared with those for

homopolymerization. It was observed that the feed ratios influence not only polymer properties and degradation, but also copolymerization rate.

Crystal structures of calcium complexes, stereoselectivity under various polymerization conditions and new catalytic system with chiral center for stereoselectivity are further studies for this research program. Copolymer's properties and biodegradation with various monomer compositions from random and block copolymerization (diblock and triblock copolymer) are also under investigation.

The calcium catalysts can also be applied to ring-opening polymerization of other cyclic monomers such as glycolide, caprolactone, and *p*-dioxanone (Figure 1-5) in order to tailor ideal copolymers as biomaterials.

CHAPTER III

ALTERNATING COPOLYMERIZATION OF OXETANES AND CARBON DIOXIDE*

INTRODUCTION

The alternating copolymerization of CO_2 and epoxides in the presence of heterogeneous metal catalysts to provide polycarbonates, along with cyclic carbonates, was pioneered by Inoue and coworkers in 1969.[51] Since that time the development of discrete metal catalysts for this process has led to greatly enhanced catalytic activity and selectivity, for both *alicyclic* and *aliphatic* epoxides.[52] Nevertheless, the synthesis of polycarbonates from these latter epoxides has been a real challenge due to the propensity of aliphatic epoxides to couple with CO_2 to afford cyclic carbonates, either *via* a direct route or by copolymer degradation.[53] An alternative process for the synthesis of aliphatic polycarbonates is the ring-opening polymerization (ROP) of 6- and 7-membered cyclic carbonates. In previous chapter, it was described upon the use of biometal Schiff base derivatives as effective homogeneous catalysts for the ROP of the six-membered cyclic carbonate, trimethylene carbonate (TMC), eq. 3-1. This process was found to occur with complete retention of carbon dioxide in the polycarbonate, i.e., there were no ether linkages in the copolymer. Aliphatic polycarbonates, such as poly(trimethylene carbonate), can be utilized to modify the properties of the brittle

---

* Reproduced in part with permission from: Darensbourg, D. J.; Ganguly, P.; and Choi, W. *Inorg. Chem.* **2006**, *34*, 3831.

biodegradable polyesters (polylactide or polyglycolide) as mentioned in previous chapter.[54]

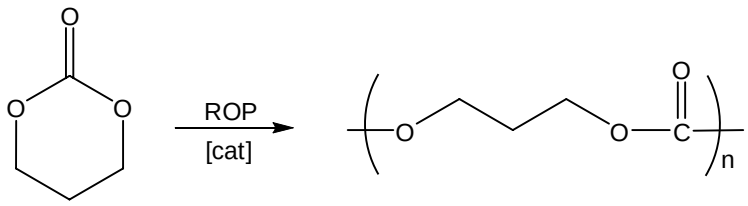

3-1

Since four-membered cyclic ethers have only slightly less ring-strain energy than epoxides, it might be anticipated that active catalysts for the CO_2 / epoxide coupling process, such as (salen)MX complexes in the presence of a cocatalyst, would be effective at coupling CO_2 and oxetanes (eq. 3-2). It was reported that the heat of polymerization of ethylene oxide ($-\Delta H_p$ = 104 kJ/mol) differs from that of oxetane (trimethylene oxide, TMO) by only 23 kJ/mol.[55] Importantly, in this instance the byproduct, cyclic carbonate, unlike that in the epoxide process, can ultimately be transformed into the completely alternating copolymer by way of reaction 3-1. Surprisingly, the reaction in equation 3-2 has received very limited attention.[52] Copolymerization of carbon dioxide and oxetane was initiated with a ternary catalytic system composed of $Al(C_2H_5)_3$ / H_2O / acetylacetone (2:1:1) and this catalytic system has suffered from low conversion of polymer formation and very low selectivity for copolymer formation.[56] The process employing organotin halides or tetraphenylstibonium iodide as catalysts improved selectivity for copolymer formation with reasonable CO_2 linkage.[57] However, it showed low catalytic activity with low TOF.

The mechanism proposed that TMC is a primary product from the reaction of oxetane and CO_2, and then poly(TMC) is produced from TMC (Scheme 3-1). It also revealed the selectivity for poly(TMC) is enhanced at higher temperature.

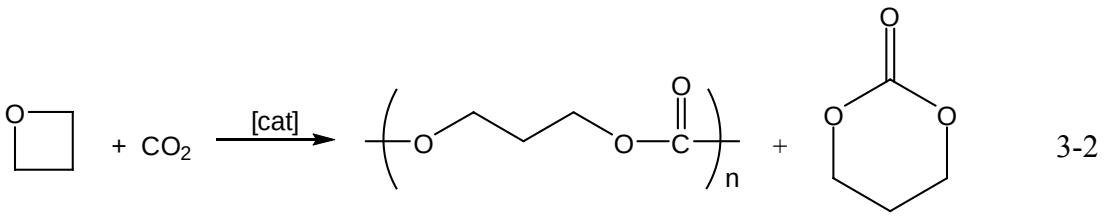

3-2

Scheme 3-1. Proposed mechanism for the reaction of carbon dioxide and oxetane catalyzed by organotin halide complexes.

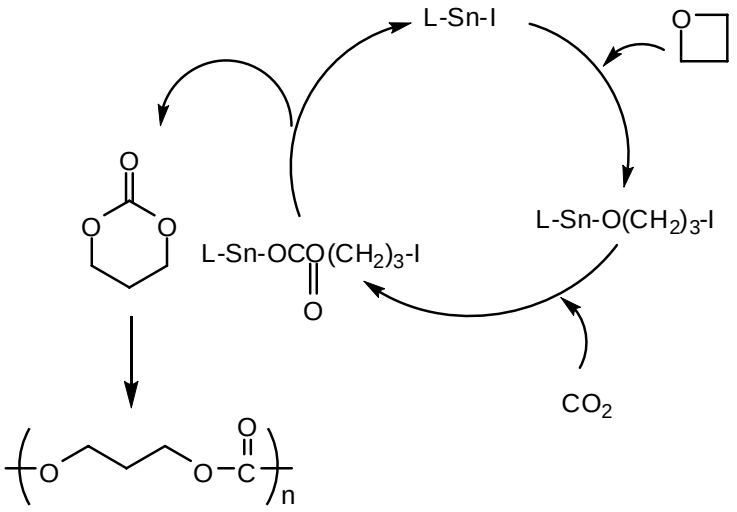

In this chapter, the preliminary findings will be addressed utilizing chromium(III) and aluminum(III) salen derivatives as catalysts for the coupling of oxetane (trimethylene oxide) and carbon dioxide to provide completely alternating copolymer and trimethylene carbonate.

EXPERIMENTAL

Methods and Materials

All syntheses were carried out under an argon atmosphere using standard Schlenk and glovebox techniques. Toluene was freshly distilled from sodium / benzophenone prior to use. Tetra-*n*-butylammonium chloride was purchased from Aldrich and recrystallized from acetone / ether twice before use. Both CH_2Cl_2 and 1,1,2,2-tetrachloroethane (TCE) were freshly distilled from CaH_2. Tetra-*n*-butylammonium azide (TCI) was stored in the freezer of the glovebox immediately upon arrival and used as received. Trimethylene oxide (Lancaster) was freshly distilled from CaH_2 before use. Trimethylene carbonate (Boehringer Ingelheim) was recrystallized from THF / ether, dried *in vacuo* overnight and stored in the glovebox. ^1H NMR spectra were recorded on a Unity+ 300 MHz or VXR 300 MHz superconducting NMR spectrometer. Infrared spectra were recorded on a Mattson 6021 FT-IR spectrometer with DTGS and MCT detectors. Molecular weight determinations were carried out at the New Jersey Center for Biomaterials, Rutgers University. MALDI-TOF-MS measurements were carried out at the Laboratory for Biological Mass Spectroscopy at Texas A&M University.

Synthesis of Catalysts

Chromium salen chloride (**3-1** and **3-3**)[13] and aluminum salen chloride catalysts (**3-2**)[38] were synthesized according to literature procedures.

Copolymerization of Trimethylene Oxide and Carbon Dioxide

The catalyst / cocatalyst and 1.15 g of trimethylene oxide were dissolved in 10 mL of toluene. The solution was added *via* an injection port into a 300 mL Parr autoclave maintained at 110°C which had previously been dried *in vacuo* for 8 hours. The autoclave was charged with 35 bar CO_2 pressure and left at 110°C. After a designated period of reaction time, the autoclave was cooled in an ice bath to below 10°C and vented in a fume hood. The % TMC (δ = 4.45 (t, 4H, OCH_2) and 2.14 (quintet, 2H, CH_2) in $CDCl_3$) and % poly(TMC) (δ = 4.23 (t, 4H, OCH_2) and 2.04 (quintet, 2H, CH_2) in $CDCl_3$) were determined by ^{1}H NMR.

For the time-dependence solution studies of poly(TMC) formation, the catalyst / cocatalyst and 1.15 g of trimethylene oxide were dissolved in 3 mL of toluene. The solution was added into the autoclave and the polymerization was carried out in the same conditions as described above. The % conversion of trimethylene oxide (trimethylene oxide shows peaks at δ = 4.68 (t, 4H, OCH_2) and 2.71 (quintet, 2H, CH_2) in $CDCl_3$)), % poly(TMC) formation, % TMC formation, and % CO_2 content of copolymer (poly(TMC) *vs*. poly(trimethylene oxide), where poly(trimethylene oxide) shows peaks at δ = 3.45 (t, 4H, OCH_2) and 1.82 (quintet, 2H, CH_2) in $CDCl_3$) were determined as a function of time by ^{1}H NMR spectroscopy.

For the molecular weight determinations, the catalyst / cocatalyst mixture was dissolved in 4.0 g of trimethylene oxide. The solution was added into the autoclave and the polymerization was carried out at the same reaction conditions as described above. The resulting polymer was purified by precipitation from dichloromethane, 5% hydrochloric acid and methanol, and then dried *in vacuo*. Turnover frequencies (mol of TMO consumed / mol of catalyst · hr) were determined by weighing the vacuum dried copolymer.

Kinetic Studies

For kinetic studies of ROP of TMC, TMC, catalyst, and the cocatalyst were weighed out in a Schlenk flask in the desired monomer : initiator : coinitiator ratio followed by the addition of dry 1,1,2,2-tetrachloroethane (TCE). The reaction vessel was placed into a preheated oil bath. The percent conversion of the monomer with time was calculated by manually sampling a small aliquot of the solution, quenching it and analyzing it by ^{1}H NMR.

RESULTS AND DISCUSSION

The initial examining at the copolymerization reaction of oxetanes and carbon dioxide involved the utilization of the metal salen derivatives shown in Figure 3-1 as catalysts. These particular metal complexes, along with anions as cocatalysts, were previously determined to be among the most active for selective coupling of cyclohexene oxide and CO_2 to poly(cyclohexylene)carbonate.[13,55,56] Copolymerizations of trimethylene oxide and CO_2 in the absence of organic solvent, i.e., in CO_2-expanded

TMO have been performed using complexes **3-1** and **3-2**. These results are listed in Table 3-1, where both complexes **3-1** and **3-2** were employed as catalysts in the presence of anionic cocatalysts where highly purified alkylammonium salts instead of the hydrophobic PPN (*bis*(triphenylphosphine)iminium) salts were employed as cocatalysts because these latter salts are only sparingly soluble in toluene. As is apparent from the data in Table 3-1, the chromium salen derivative is much more effective than its aluminum analog. This is consistent with observations for the epoxide / CO_2 copolymerization process.[38]

Furthermore, the coupling of CO_2 and TMO occurs at a reduced rate compared to propylene oxide or cyclohexene oxide and CO_2. This latter observation is not unanticipated based on the fact that ring-opening of three-membered cyclic ethers is energetically favored by approximately 20 kJ/mol over their four-membered counterparts. These results show that the selectivity for copolymer formation from oxetane and CO_2 is very high (>97%) in all instances, even at 110ºC.

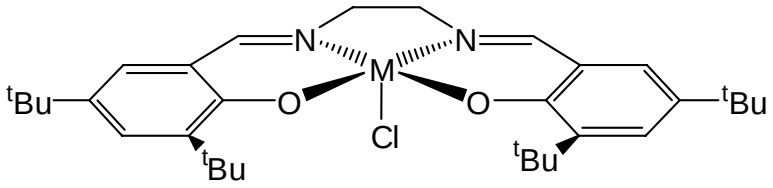

M = Cr (**3-1**) or Al (**3-2**)

Figure 3-1. Structure of metal salen catalysts utilized for the copolymerization reactions in eq. 3-2.

Table 3-1. Copolymerization of trimethylene oxide and CO_2 with (salen)MCl (M = Al, Cr) catalysts in CO_2-expanded oxetane.[a]

catalyst	cocatalyst	% TMC	% poly(TMC)	% CO_2 content	TOF[c]	yield (%)
3-1	*n*-Bu_4NCl	2.9	97.1	96.7	41.2[d]	24.0
3-1	*n*-Bu_4NN_3	1.7	98.3	95.9	38.8[e]	19.5
3-2	*n*-Bu_4NCl	1.7	98.3	94.2	8.59[d]	5.0

[a] Copolymerization conditions: catalyst loading = 0.138 mol %, 4.0 g of TMO, 110ºC, M/I = 1292, 35 bar CO_2. [b] Two equivalents of cocatalyst. [c] Measured in mol TMO consumed / mol of metal•hr. [d] Reaction time = 7.5 hr. [e] Reaction time = 6.5 hr.

Table 3-2 contains data for reaction 3-2 carried out in toluene at 110ºC. As is readily seen from Table 3-2, formation of poly(TMC) is favored using either one or two equivalents of the cocatalysts *n*-Bu_4NCl or *n*-Bu_4NN_3, with the latter salt being more selective towards formation of the copolymer. Indeed, in this instance the utilization of two equivalents of *n*Bu_4NN_3 afforded 100% copolymer under these conditions.

Table 3-2. Copolymerization of trimethylene oxide and carbon dioxide in the presence of complex **3-1**.[a]

entry	cocatalyst	% TMC[b]	% poly (TMC)[b]
1	*n*-Bu_4NCl (1 eq.)	22.4	77.6
2	*n*-Bu_4NCl (2 eq.)	18.4	81.6
3	*n*-Bu_4NN_3 (1 eq.)	6.6	93.4
4	*n*-Bu_4NN_3 (2 eq.)	0	100

[a] Copolymerization conditions: 17 mg of catalyst **3-1** (0.15 mol %), M/I = 675:1, 10 mL of toluene, 35 bar CO_2, 110ºC, 24 hr reaction time. [b] Based on ^{1}H NMR measurements at ~100% conversion.

For technical reactions, copolymerization of oxetane and carbon dioxide has not been able to be monitored by *in situ* infrared spectroscopy since 6-membered cyclic

carbonate (TMC) and poly(TMC) show carbonyl stretching in very close region. Therefore, several bulk polymerization reactions were carried out under identical reaction conditions for time-dependence copolymerization. Table 3-3 and Figure 3-2 contain the results of this study, where it is apparent that the high selectivity of reaction 3-2 for poly(TMC) formation (98.5%) catalyzed by complex **3-1** in the presence of 2 eq. of *n*-Bu_4NCl is independent of time. In an effort to ascertain whether the copolymer was formed directly via reaction 3-2 or originated from subsequent ROP of the first formed TMC, the rate of this latter process has been examined under identical reaction conditions. For ROP of TMC by complex **3-1**, cocatalyst is not necessary. However, this process takes place much faster in the presence of 2 eq. of n-Bu_4NCl than in complex **3-1** alone. Consequently, the ROP of TMC in toluene was found to proceed to completion in less than 4 h (Figure 3-2), or on a much shorter time scale than the formation of poly(TMC) from oxetane and carbon dioxide. Hence, from these preliminary products from the coupling of oxetane and carbon dioxide, with a concomitant backbiting process providing trace quantities if TMC, or a secondary product from a facile ROP process involving preformed TMC. That is, the copolymerization reaction in eq. 3-2 proceeds in part (Figure 3-3(a)) or exclusively by way of the intermediate formation of TMC (eq. 3-3 and Figure 3-3(b)).

Table 3-3. Time-dependent copolymerization runs of trimethylene oxide and CO_2 catalyzed by complex **3-1** in the presence of 2 eq. of *n*-Bu_4NCl.[a]

entry	time (h)	% conversion	% TMC[b]	% poly(TMC)[b]	% CO_2 content of copolymer
1	4	20.4 (21.4)[c]	1.5 (4.9)[c]	98.4 (95.1)[c]	90.3 (82.4)[c]
2	10.5	42.3	1.6	98.4	89.5
3	18	57.3	1.4	98.6	91.4
4	24	72.7	1.2	98.6	91.8

[a] Copolymerization conditions: 17 mg of **3-1**, M/I = 675, 3 mL of toluene, 35 bar CO_2, 110ºC. [b] Respective average values with standard deviations for the five entries are 1.5 ± 0.2, 98.5 ± 0.2, and 90.8 ± 1.1. [c] Reaction temperature elevated to 130ºC.

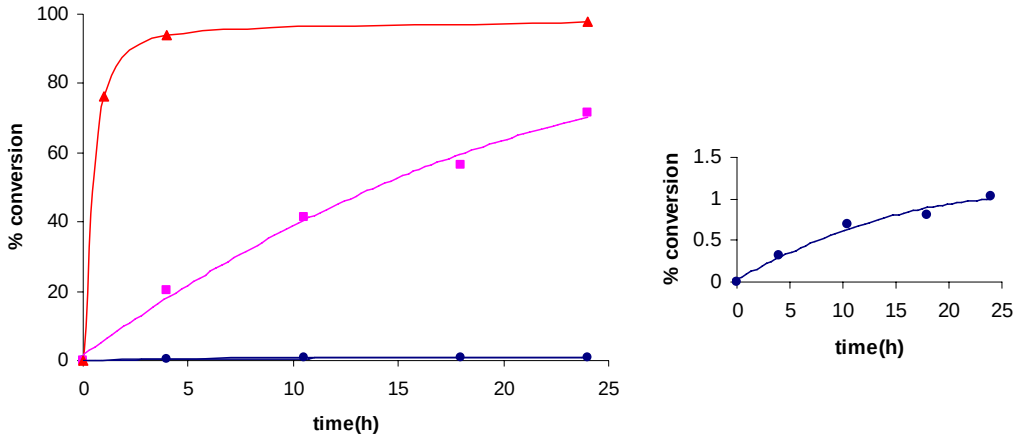

Figure 3-2. Time dependence of poly(TMC) formation: (■) poly(TMC) and (●) trace TMC produced by way of CO_2 and oxetane (shown as well in the inset); (▲) poly(TMC) produced from the ROP of TMC. Reaction conditions are described in Table 3-2.

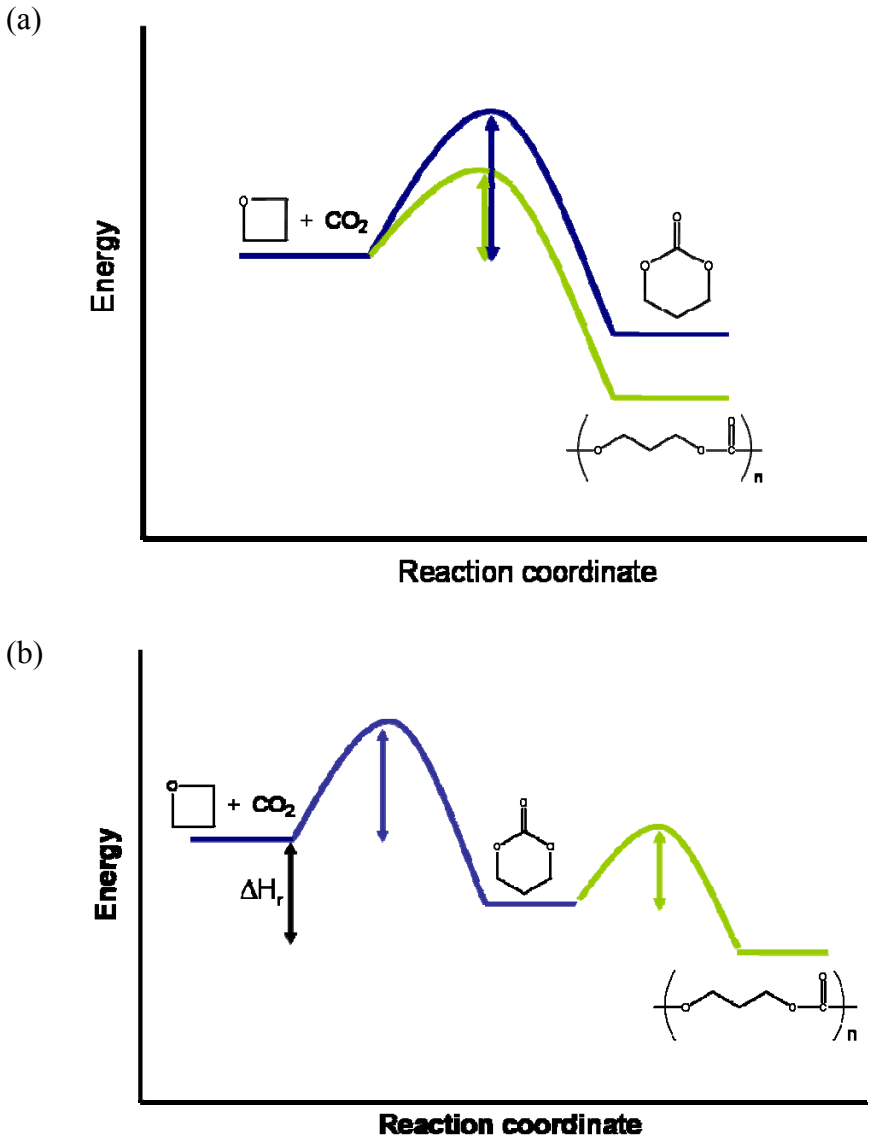

Figure 3-3. Reaction coordinate diagram of copolymerization of oxetane and carbon dioxide. (a) the copolymerization reaction proceeds in part or (b) by way of the intermediate formation of TMC.

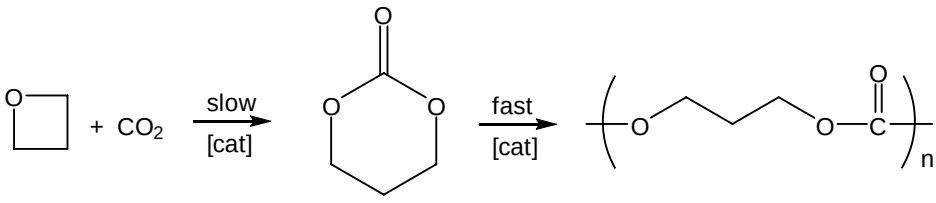

3-3

The molecular weights of the copolymers reported in Table 3-1 produced from catalyst **3-1** in the presence of cocatalysts *n*-Bu_4NCl and *n*-Bu_4NN_3 were determined by GPC to be 10,100 and 7,400 with corresponding PDIs of 1.58 and 1.51, respectively. Furthermore, a low molecular weight copolymer produced from a reaction catalyzed by complex **3-1** and one equivalent of *n*-Bu_4NN_3 revealed an azide end-group by MALDI-TOF-MS. Consistent with this observation this copolymer possessed a ν_{N3} vibrational frequencies at 2102 cm^{-1} in CH_2Cl_2 which is representative of an organic azide. The initiation step in the presence of ionic cocatalyst has been depicted in Figure 3-4 where X = Cl or N_3, monomer enchainment is occurring on one side of the metal(salen) plane. It has been shown to be first order in both (salen)CrCl and PPNX.

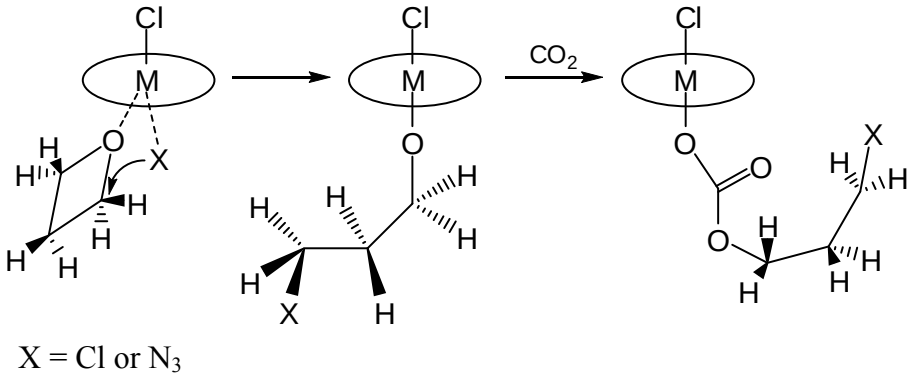

Figure 3-4. Initiation step in the presence of an ionic cocatalyst for copolymerization of oxetane and carbon dioxide.

These latter observations, i.e., azide polymer end groups and molecular weights are much smaller than theoretical molecular weight (about one-third to half) are

earmarks of the copolymerization of epoxide and carbon dioxide catalyzed by (salen)CrCl / $PPNN_3$.[45] By way of contrast, the ROP of TMC employing Ca(salen) catalyst with external cocatalyst has provided completely alternating copolymers with molar weights that track the monomer / initiator (M/I) ratio.[22a] Therefore, the current findings suggest that the copolymer produced in eq. 3-2 results from the direct enchainment of oxetane and CO_2 following the initiation step in Figure 3-4.

In order to understand the copolymer production, kinetic studies and mechanistic studies have been carried out for copolymerization of oxetane* and CO_2 as well as ROP of TMC using same catalytic system. For the ROP of TMC, (salen)CrCl with cyclohexylene backbone ((CyHsalen)CrCl, catalyst **3-3**) and di-*tert*-butyl groups in the 3,5-positions of the phenolate rings has been chosen from the catalyst optimization (Figure 3-5). As a cocatalyst, 2 eq. of *n*-Bu_4NN_3 has been used since it resulted in good selectivity for poly(TMC). Eq. 3-4 shows that catalyst **3-3** and 2 eq. of *n*-Bu_4NN_3 forms diazide species. This structure has been confirmed by IR spectroscopy changing the number of equivalents of cocatalyst,* which is different from Ca(salen) and azide anion (eq. 2-5).

* The optimization of (salen)MX and cocatalyst, kinetic, and mechanistic studies for copolymerization of oxetane and carbon dioxide as well as diazide species confirmed by IR have been done by Adriana I. Moncada in DJD group.

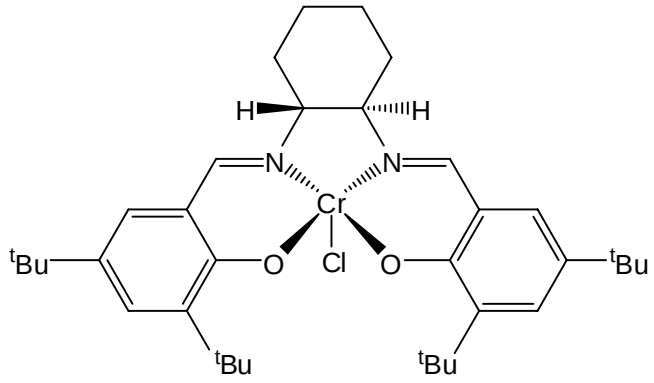

Figure 3-5. Structure of (salen)CrCl with cyclohexylene backbone ((CyHsalen)CrCl).

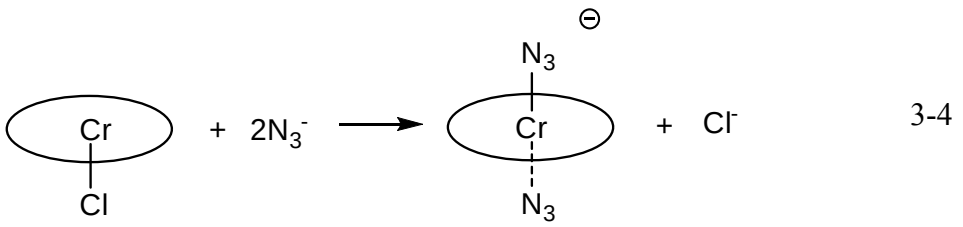

3-4

Kinetic measurements of the ring-opening polymerization of TMC in TCE solution have been initiated in the presence of catalyst **3-3** and 2 eq. of n-Bu_4NN_3. The polymerization reaction was found to be first order in monomer (TMC) concentration (Figure 3-6), catalyst (Figure 3-7) and cocatalyst concentration (Figure 3-8). Table 3-4 summarizes the determined rate constants (k_{obsd}) for the ring-opening polymerization of TMC as a function of the catalyst concentration and temperature. Here, ROP of TMC with only catalyst or cocatalyst have been also performed (entry 7 and 8 in Table 3-4)

and it is noticed that ROP of TMC with only catalyst or cocatalyst is very slow compared to that with catalyst and 2 eq. of cocatalyst.

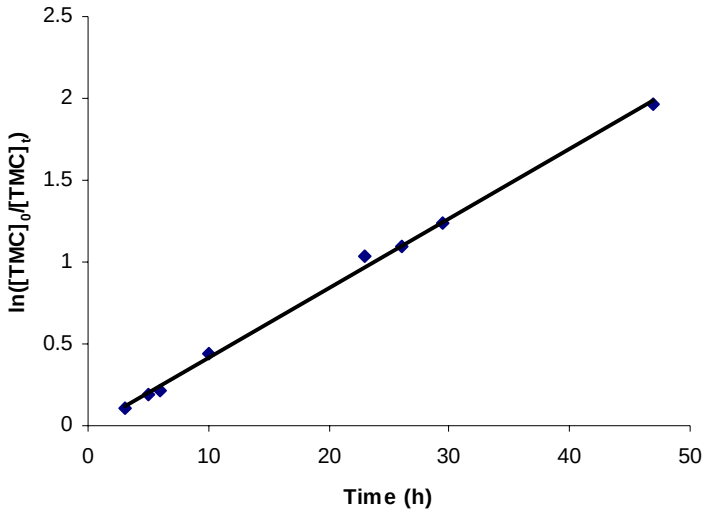

Figure 3-6. $\ln([TMC]_0/[TMC]_t)$ *vs*. time plot depicting a reaction order of unity with respect to monomer concentration ($R^2 = 0.998$).

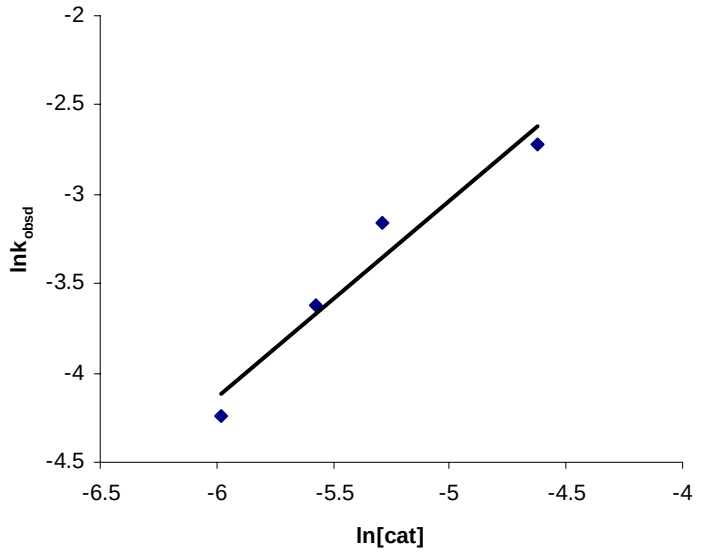

Figure 3-7. Plot of $\ln k_{obsd}$ *vs*. ln[cat] to determine the order of the polymerization reaction with respect to the concentration of catalyst. Slope = 1.11 with $R^2 = 0.948$.

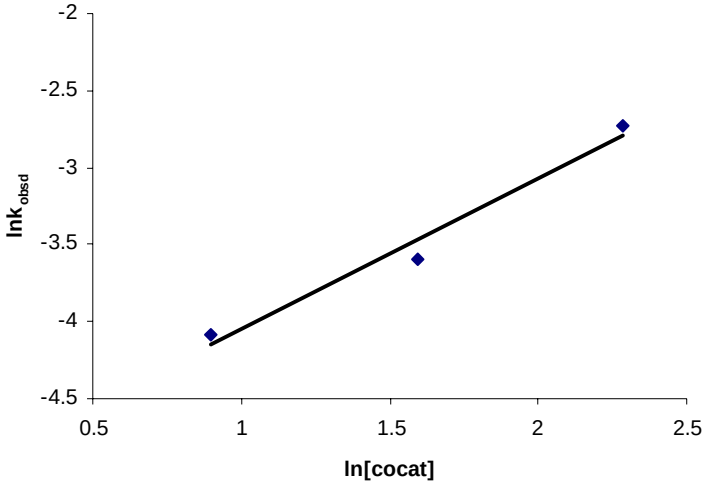

Figure 3-8. Plot of $\ln k_{obsd}$ *vs.* ln[cocat] to determine the order of the polymerization reaction with respect to the concentration of cocatalyst. Slope = 0.982 with $R^2 = 0.975$.

Table 3-4. Rate constant dependence of the copolymerization of trimethylene oxide and CO_2 on the concentrations of the catalyst, cocatalyst, and temperature.[a]

entry	[Cr] (mM)	eq. of *n*-$[Bu_4N]^+N_3^-$	temperature (°C)	k_{obsd} (h^{-1})
1	2.53	2.0	120	0.0144
2	3.80	2.0	120	0.0268
3	5.06	2.0	120	0.0424
4	9.81	2.0	120	0.0655
5	5.06	1.0	120	0.0275
6	5.06	0.5	120	0.0168
7	5.06	0.0	120	0.0036[b]
8	0.00	5.06[c]	120	0.0080[d]
9	5.06	2.0	100	0.0062
10	5.06	2.0	110	0.0167
11	5.06	2.0	130	0.0879

[a] Monomer concentration held constant at 0.99 M. Reactions carried out in 1,1,2,2-tetrachloroethane. [b] The determined rate constant from copolymerization without cocatalyst. [c] Concentration of cocatalyst. [d] The determined rate constant from copolymerization without catalyst.

The activation parameters for the ring-opening polymerization of TMC catalyzed by (CyHsalen)CrCl and *n*-Bu_4NN_3 in TCE were found to be $\Delta H^{\neq}$ = 108.0 ± 3.6 kJ/mol and $\Delta S^{\neq}$ = 15.3 ± 9.2 J/(mol·K). These values were calculated from the temperature-dependent rate constants listed in Table 3-4 and Eyring plot in Figure 3-9. A $\Delta G^{\neq}$ value of 103.4 kJ/mol was calculated for the ring opening polymerization of TMC catalyzed by catalyst **3-3** and 2 eq. of *n*-Bu_4NN_3 in TCE at 25ºC, which is much higher than that of (salen)Ca and *n*-Bu_4NCl system (58.2 kJ/mol). The activation parameters for copolymerization of carbon dioxide and oxetane have been also determined by Adriana I. Moncada to be $\Delta H^{\neq}$ = 46 kJ/mol and $\Delta S^{\neq}$ = -162 J/(mol·K). At 110ºC which is the usual experimental temperature for copolymerization of carbon dioxide and oxetane, $\Delta G^{\neq}$ for copolymerization of carbon dioxide and oxetane is 108 kJ/mol while $\Delta G^{\neq}$ for ROP of TMC is 102 kJ/mol which means that the rate for ROP of TMC is 6.6 times faster than that for copolymerization of carbon dioxide and oxetane at 110ºC. The differences of kinetic parameters between ring-opening polymerization of trimethylene carbonate and copolymerization of carbon dioxide and oxetane support that the formation of copolymer does not proceed via the intermediacy of trimethylene carbonate since it was also observed that the process of ring-opening polymerization of trimethylene carbonate to produce poly(trimethylene carbonate) favors high temperature while the selectivity to produce poly(trimethylene carbonate) from copolymerization of carbon dioxide and oxetane is increased at lower reaction temperature (Table 3-3, entry 1).

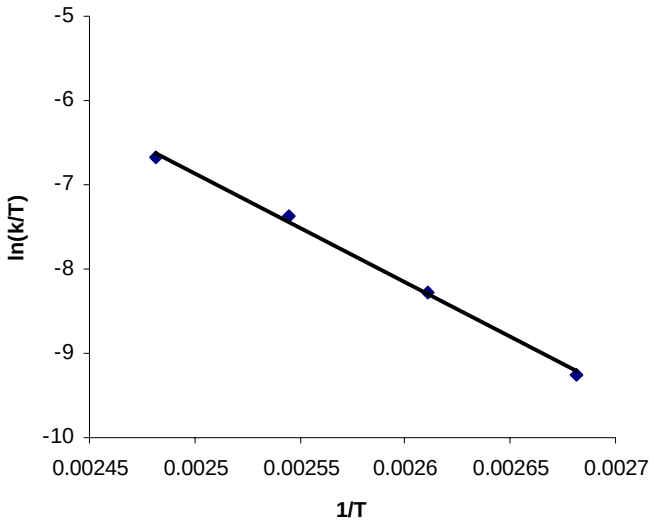

Figure 3-9. Eyring plot of ROP of TMC in the presence of catalyst **3-3** and two equivalents of *n*-Bu_4NN_3 in TCE. Slope = -12986 with $R^2 = 0.998$.

CONCLUSIONS

Metal salen derivatives of chromium and aluminum, along with *n*-Bu_4NX (X = Cl or N_3) salts, have been shown to be effective catalysts for the selective coupling of CO_2 and oxetane (trimethylene oxide) to provide the corresponding polycarbonate with only trace quantities of ether linkages. These results have shown that the selectivity for copolymer formation from oxetane and CO_2 is very high (97 %) in all instances, even at 110°C. This selectivity for copolymer formation might be anticipated because the six-membered cyclic carbonate has greater ring strain than its five-membered analogue.[58] The formation of copolymer is suggested, based on circumstantial evidence, not to proceed via the intermediacy of trimethylene carbonate, which was observed as a minor

product of the coupling reaction. For a reaction catalyzed by (salen)CrCl in the presence of *n*-Bu_4NN_3 as the cocatalyst, both matrix-assisted laser desorption ionization time-of – flight mass spectroscopy and infrared spectroscopy revealed an azide end group in the copolymer.

Studies to further address these issues, as well as investigations into the mechanistic aspects of the oxetane and CO_2 coupling reaction and ring-opening polymerization of TMC are underway in our laboratories.

CHAPTER IV

ALTERNATING COPOLYMERIZATION OF EPOXIDES AND CARBON DIOXIDE

INTRODUCTION

The industrial method for producing the most useful polycarbonate, Lexon, is to synthesize it from Bisphenol A and phosgene by a polycondensation (Figure 4-1). However, this process involves highly toxic and hazardous starting materials as well as the high cost of chlorinated solvents. Moreover, the process is limited to affording aromatic polycarbonates of high molecular weights.[3] Aliphatic or alicyclic polycarbonates with high molecular weight cannot be obtained by a polycondensation process. All these factors have given impetus to research in the formation of polycarbonates by alternative routes.

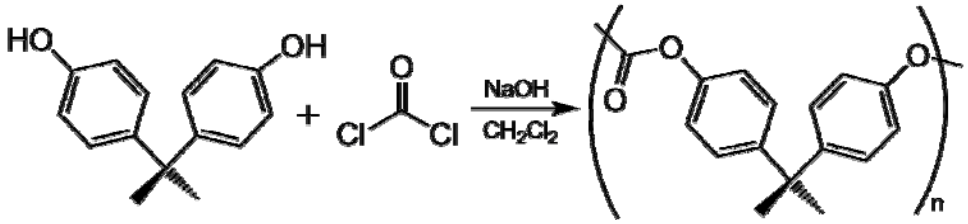

Figure 4-1. Industrial method to production of polycarbonate.

An alternative route to produce polycarbonates is copolymerization of carbon dioxide and epoxides in the presence of an organometallic catalyst (Figure 4-2). Carbon

dioxide is an abundant, inexpensive and environmentally friendly non-toxic material. However, the thermodynamically stable nature of carbon dioxide demands effective catalysts to form ideal polycarbonates.

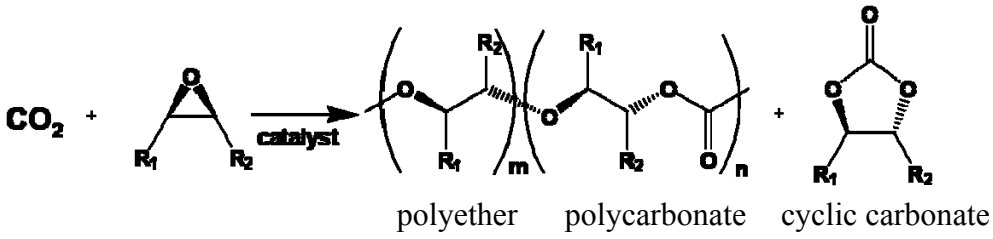

Figure 4-2. Copolymerization of carbon dioxide and epoxides.

The discovery by Inoue and coworkers in 1969 using a heterogeneous catalyst system of $Zn(C_2H_5)_2$: H_2O (1:1) led to an important direction.[3] Inoue and coworkers also reported the first single-site catalyst which is an aluminum complex containing a tetraphenylphorphyrin ligand (Figure 4-3) which was active toward copolymerization of propylene oxide and carbon dioxide affording a copolymer with a narrow PDI but low molecular weight.[59] In the 1990's, Darensbourg developed homogeneous monomeric zinc phenoxide catalysts, which presented 10 times higher TOF (turnover frequencies) up to 10 mol monomer consumed / mol of Zn-hr than Inoue systems (Figure 4-4).[13] In 1998, Coates reported that Zn(II) β-diimine complexes achieved 800 h^{-1} at low temperature and CO_2 pressure although the Zn(II) catalysts are extremely air-sensitive and make ether linkages in polymer chain (Figure 4-5).[60]

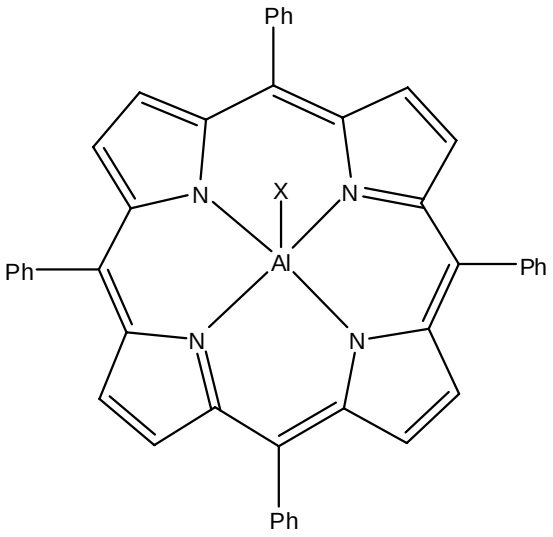

Figure 4-3. Aluminum porphyrin complex.

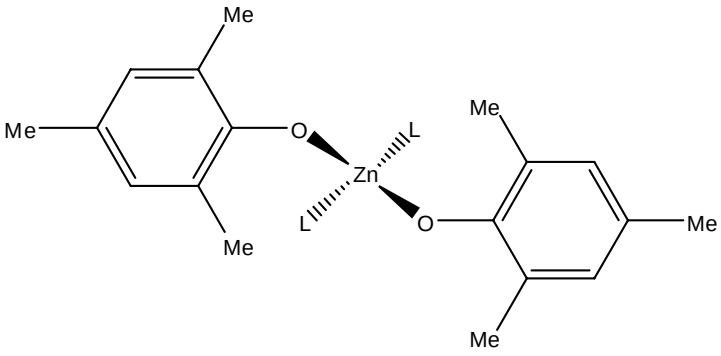

L = solvent (THF or ether)

Figure 4-4. Zinc(bis-phenoxide) complex.

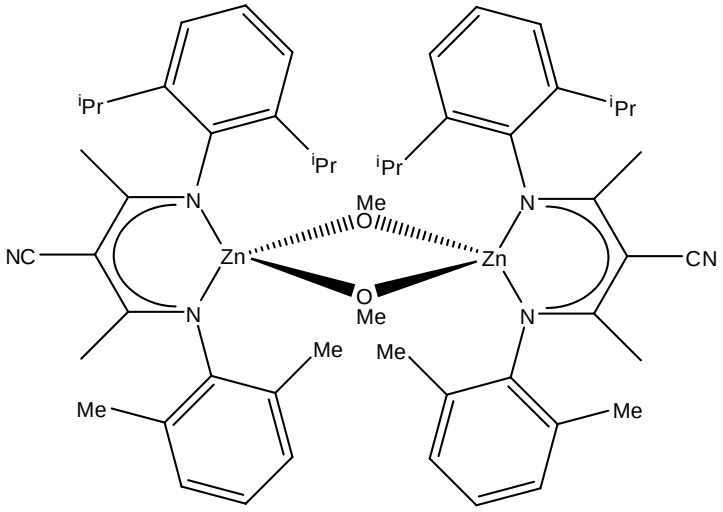

Figure 4-5. Zinc(β-diiminate) complex.

Recently, Cr(III) salen complexes have been studied and showed TOFs as high as 1200 h^{-1} for epoxides such as cyclohexene oxide. For the mechanistic studies of copolymerization of epoxides and carbon dioxide in the presence of Cr(salen)X complexes where X is anion, the energy barrier for cyclic carbonate production is higher than that of polycarbonates.[5] It has been reported that polycarbonates are unmakable from five membered cyclic carbonate compounds without losing CO_2 since they are thermodynamically more stable than polycarbonates.[6] Instead, cyclic carbonates are made from polymer by backbiting.[6] Metal salen complexes are robust and easily synthesized and can be tuned among multiple electronic and steric variations by varying R, R_1, R_2 and X (Figure 4-6). Cocatalysts are required for metal(II) complexes and can be employed to enhance the catalytic activity for metal(III) complexes.

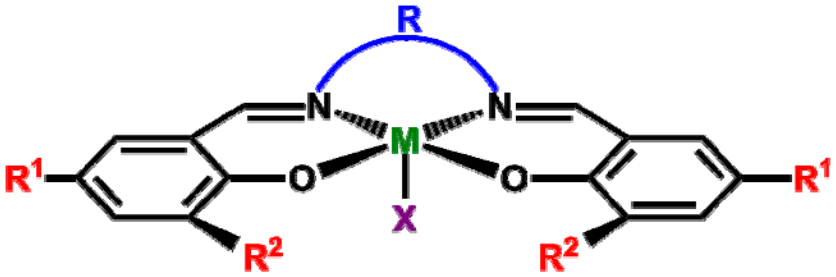

Figure 4-6. Metal salen complex.

Tridentate Schiff base ligands are easily synthesized and have various applications as catalysts for ring-opening polymerization,[9] ethylene polymerization,[10] and atomic transfer radical polymerization.[11] Compared to salen ligands, they are tridentate and have -1 charge with an extra nucleophile while salen ligands are tetradentate and have -2 charge. Modifications of these Schiff base ligands are readily achieved by variations of the aldehyde (variations of R^1 and R^2) and diamine (variation of R) starting reagents.[9,12] The structure of metal salen and tridentate Schiff base metal complexes are well determined (Figure 4-7).[10,11]

Figure 4-7. Tridentate Schiff base metal complex.

In our group, the study of the copolymerization of cyclohexene oxide and CO_2 has been thoroughly investigated. Further investigations of the copolymerization of carbon dioxide and other available epoxides such as propylene oxide, limonene oxide and [2-(3,4-epoxycyclohexyl)ethyl]trimethoxysilane (TMSO) have been performed (Figure 4-8). Propylene oxide has already shown excellent reactivity and industrial applications including binders, lost foam casting, and coatings.[61] However, the kinetic parameters for copolymerization of carbon dioxide and propylene oxide are different from those for copolymerization of carbon dioxide and cyclohexene oxide. Activation energy toward the formation of cyclic carbonate in propylene oxide is much greater than that in cyclohexene oxide (133 kJ/mol *vs*. 100.5 kJ/mol with Cr(salen)Cl.[5] Therefore, the formation of cyclic carbonate is more facile and more temperature-dependent in copolymerization of carbon dioxide and propylene oxide than that in copolymerization of carbon dioxide and cyclohexene oxide.

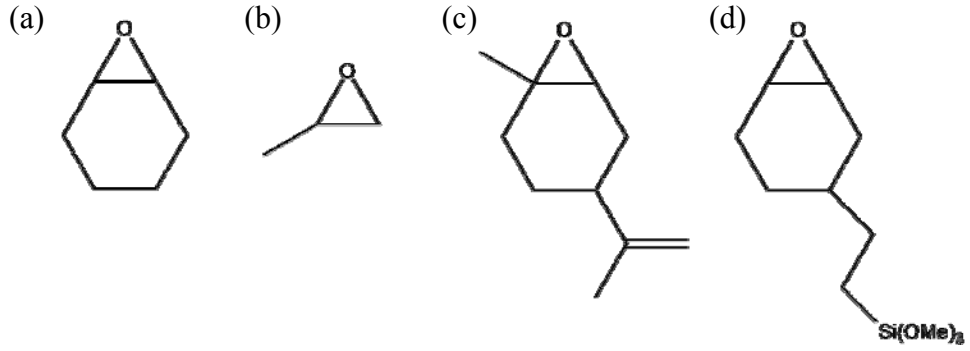

Figure 4-8. Alternative epoxides for copolymerization (a) cyclohexene oxide, (b) propylene oxide, (c) limonene oxide, and (d) [2-(3,4-epoxycyclohexyl)ethyl] trimethoxysilane (TMSO).

Limonene oxide is a biorenewable epoxide monomer which is the most common terpene produced by more than 300 plants.[62] It is commercially available with low cost and abundance. It is structurally similar to cyclohexene oxide but is a challenge to copolymerize with carbon dioxide because it is more difficult to ring open than cyclohexene oxide.

The epoxy-functionalized silane, [2-(3,4-epoxycyclohexyl)ethyl]trimethoxy silane (TMSO) is designed as cross-linkers for coating formulations.[63] It has shown similar reactivity with Cr(salen)Cl to cyclohexene oxide and enhanced the properties of polymer after crosslinking (Figure 4-9).[64]

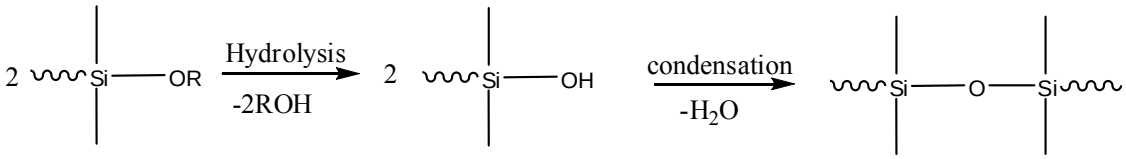

Figure 4-9. Mechanism of crosslinking for [2-(3,4-epoxycyclohexyl)ethyl]trimethoxy silane (TMSO).

In this chapter, copolymerization from epoxides and carbon dioxide using tridentate Schiff base metal complexes will be addressed changing metal, ligand, and cocatalysts.

EXPERIMENTAL

Methods and Materials

Unless otherwise specified, all manipulations were performed using a double manifold Schlenk vacuum line under an atmosphere of argon or an argon filled glovebox. Dichloromethane, tetrahydrofuran and methanol were freshly distilled from CaH_2, sodium / benzophenone and magnesium, respectively. Deutrated chloroform from Aldrich was stored in the glovebox and used as received. Salicylaldehyde, ethylenediamine, 1,2-phenylenediamine and 1,2-napthylenediamine were purchased from Aldrich and used as received. *N,N'*-bis(3,5-di-*tert*-butylsalicylidene)-1,2-cyclohexene diimine was purchased from Strem and used without further purification. *N,N*-dimethylethylenediamine, *N,N*-diethylethylenediamine, 2-(aminomethyl)pyridine, and 8-aminoquinoline were purchased from Acros and used as received. Cyclohexene oxide was purchased from Lancaster or TCI and freshly distilled from CaH_2. 2-(3,4-Epoxycyclohexyl)-ethyltrimethoxysilane (TMSO) was purchased from Gelest and vacuum distilled from CaH_2. Bone dry carbon dioxide supplied in a high pressure cylinder equipped with a liquid dip-tube was purchased from Scott Specialty Gases. PPN^+Cl^- ($PPN^+ = (Ph_3P)_2N^+$) were purchased from Aldrich and recrystallized from dichloromethane / ether before use, and $PPN^+N_3^-$ was synthesized according to published procedure.[16] Tetra-*n*-butylammonium halides (Aldrich) were recrystallized from acetone / ether twice before use. Tetra-*n*-butylammonium azide (TCI) was stored in the freezer of the glovebox immediately upon arrival. Tricyclohexylphosphine from Aldrich was

recrystallized from ethanol. *N*-Methylimidazole was purchased from Aldrich and distilled over sodium metal prior to use.

Measurements

^{1}H NMR and ^{13}C NMR spectra were recorded on Unity+ 300MHz and VXR 300MHz superconducting NMR spectrometers. Infrared spectra were recorded on a Mattson 6021 FT-IR spectrometer with DTGS and MCT detectors.

Synthesis of Tridentate Schiff Base Ligands

3,5-di-*tert*-butyl-2-hydroxybenzaldehyde,[12b] and tridentate Schiff base ligands[10,11] were synthesized according to literature procedure or have been previously described in this dissertation.

Synthesis of Tridentate Schiff Base Metal Complexes.

{3,5-tert-Bu_2-2-$(OH)C_6H_2CH{=}NCH_2CH_2NMe_2$}Fe(II)Cl (**4-10**) and {(1S,2R)-1-[(2-Hydroxy-3,5-di-tert-butyl-benzylidene)-amino]-indan-2-ol}Cr(III)Cl (**4-11**) were synthesized according to literature procedure.[10,65]

General Synthesis of Tridentate Schiff Base Chromium Complexes.

Method I

Tridentate Schiff base ligands (1.0 eq.) and NaH (5.0 eq.) were dissolved in THF. After stirring at room temperature overnight followed by filtration of excess amount of NaH, the filtrate was added to $Cr(III)Cl_3(THF)_3$ in THF and stirred overnight. Then the volatile components were removed in *vacuo* and dissolved in dichloromethane followed by filtration. The desired complex was isolated following the removal of dichloromethane and dried in *vacuo*.

Method II

Tridentate Schiff base ligands (1.0 eq.), Cr(III)$Cl_3(THF)_3$ (1.0 eq.), and triethylamine were dissolved in toluene and refluxed for 6 h. After cooling down to room temperature, NEt_3·HCl salt was filtered off and the desired complex was isolated following the removal of toluene and dried in *vacuo*.

Synthesis of {3,5-tert-Bu_2-2-(OH)C_6H_2CH=N$CH_2CH_2NMe_2$}Cr(III)Cl_2 (4-1)

Using the general method I, 3,5-*tert*-Bu_2-2-(OH)C_6H_2CH=N$CH_2CH_2NMe_2$ (1.200 g, 4.0 mmol) and NaH (5 eq.) were dissolved in THF (20 mL). After stirring at room temperature overnight followed by filtration of excess amount of NaH, the filtrate was added to Cr(III)$Cl_3(THF)_3$ (1.5094 g, 4.0 mmol) in THF (20 mL) and stirred overnight. The final product was a dark brown solid (1.70 g, 99 % yield).

Synthesis of {3,5-tert-Bu_2-2-(OH)C_6H_2CH=N$CH_2CH_2NEt_2$}Cr(III)NCl_2 (4-2)

Using the general method I, 3,5-*tert*-Bu_2-2-(OH)C_6H_2CH=N$CH_2CH_2NEt_2$ (1.011 g, 3.0 mmol) and NaH (5 eq.) were dissolved in THF (10 mL). After stirring at room temperature overnight followed by filtration of excess amount of NaH, the filtrate was added to Cr(III)$Cl_3(THF)_3$ (1.124 g, 3.0 mmol) in THF (20 mL) and stirred overnight. The final product was a dark green-brown solid (1.043 g, 75.7 % yield).

Synthesis of {3,5-tert-Bu_2-2-(OH)C_6H_2CH=N-2-$CH_2C_5H_4$N}Cr(III)Cl_2 (4-3)

Using the general method II, 3,5-*tert*-Bu_2-2-(OH)C_6H_2CH= N-2-$CH_2C_5H_4$N (0.975 g, 3.0 mmol), Cr(III)$Cl_3(THF)_3$ (1.124 g, 3.0 mmol) and NEt_3 (0.4048 g) were dissolved in toluene (20 mL). After refluxing for 6 h, a dark brown product was obtained. (1.200 g, 89 % yield).

Synthesis of {3,5-tert-Bu_2-2-(OH)C_6H_2CH=N-8-C_9H_6N}Cr(III)Cl_2 (4-4)

Using the general method I, 3,5-*tert*-Bu_2-2-(OH)C_6H_2CH=N-8-C_9H_6N (0.540 g, 1.5 mmol) and NaH (5 eq.) were dissolved in THF (20 mL). After stirring at room temperature overnight followed by filtration of excess amount of NaH, the filtrate was added to Cr(III)$Cl_3(THF)_3$ (0.562 g , 1.5 mmol) in THF (10 mL) and stirred overnight. The final product was a red-brown solid (0.780 g, 99 % yield).

Synthesis of {3,5-tert-Bu_2-2-(OH)C_6H_2CH=N$CH_2CH_2NMe_2$}Cr(II)Cl (4-5)

Using the general method II, 3,5-*tert*-Bu_2-2-(OH)C_6H_2CH=N$CH_2CH_2NMe_2$ (1.200 g, 4.0 mmol), $CrCl_2$ (0.492 g, 4 mmol) and NEt_3 (0.4048, 4 mmol) were dissolved in toluene (20 mL). After refluxing for 6 h, a dark green product was obtained. (0.87 g, 56 % yield).

Zinc(II) Complexes

Synthesis of {3,5-tert-Bu_2-2-(OH)C_6H_2CH=N$CH_2CH_2NMe_2$}Zn(II)N($SiMe_3$)$_2$ (4-6)

3,5-*tert*-Bu_2-2-(OH)C_6H_2CH=N$CH_2CH_2NMe_2$ (0.457 g, 1.5 mmol) and Zn[N($SiMe_3$)$_2$]$_2$ (0.578 g, 1.5 mmol) were dissolved in THF (10 mL). After stirring at room temperature for 2 h, THF was removed under reduced pressure. The final product was a yellow solid after recrystallization in pentane (0.730 g, 92.6 % yield). ^{1}H NMR ($CDCl_3$, 300 MHz): δ 8.28 (s, 1H, C*H*=N), 7.34 (d, 1H, C_6H_2), 6.84 (d, 1H, C_6H_2), 3.55 (t, 2H, CH_2CH_2), 2.53 (t, 2H, CH_2CH_2), 2.32 (s, 6H, N(CH_3)$_2$), 1.38 (s, 9H, C(CH_3)$_3$), 1.27 (s, 9H, C(CH_3)$_3$), 0.07 (s, 18H, Si(CH_3)$_3$). ^{13}C NMR ($CDCl_3$, 500 MHz) δ 171.72 (*C*=N), 169.26 (*C*O in Ar), 141.31, 134.02, 129.10, 129.00, 117.06 (Ar), 59.54

(C=N*C*H_2), 57.68 (*C*H_2N(CH_3)$_2$), 45.53 (N(*C*H_3)$_2$), 35.45 (^{p}*C*(CH_3)$_3$), 33.76 (^{o}*C*(CH_3)$_3$), 31.43 (^{p}C(*C*H_3)$_3$), 29.47 (^{o}C(*C*H_3)$_3$), 1.00 (Si(*C*H_3)$_3$).

Cobalt(II) Complex

Synthesis of {3,5-tert-Bu$_2$-2-(OH)C$_6$H$_2$CH=NCH$_2$CH$_2$NMe$_2$}Co(II)OAc (4-7)

3,5-*tert*-Bu$_2$-2-(OH)C$_6$H$_2$CH=NCH$_2$CH$_2$NMe$_2$ (0.609 g, 2.0 mmol) and Co(OAc)$_2$ (0.500 g, 2.0 mmol) were dissolved in methanol (30 mL) and refluxed overnight. A dark orange product was isolated after removal of methanol.

Calcium(II) Complexes

Synthesis of {3,5-tert-Bu$_2$-2-(OH)C$_6$H$_2$CH=NCH$_2$CH$_2$NMe$_2$}Ca(II)I (4-8)

3,5-*tert*-Bu$_2$-2-(OH)C$_6$H$_2$CH=NCH$_2$CH$_2$NMe$_2$ (0.609 g, 2.0 mmol) and NaH (0.2 g, 10 mmol) were dissolved in THF (20 mL). After stirring at room temperature overnight followed by filtration of excess amount of NaH, the filtrate was added to CaI_2 (0.5878 g, 2.0 mmol) in THF (20 mL) and stirred overnight. Then the volatile components were removed in *vacuo* and dissolved in dichloromethane followed by filtration. The desired complex was isolated following the removal of dichloromethane and dried in *vacuo*. The final product was a dark yellow solid (1.27 g, 92.6 % yield). ^{1}H NMR ($CDCl_3$, 300 MHz): δ 8.17(s, 1H, C*H*=N), 7.25(d, 1H, C$_6$*H*$_2$), 6.89 (d, 1H, C$_6$*H*$_2$), 3.75 (m, 4H, O(C*H*$_2$CH$_2$)$_2$), 3.55 (t, 2H, C*H*$_2$CH$_2$), 2.47 (t, 2H, CH$_2$C*H*$_2$), 1.71 (m, 4H, O(CH$_2$C*H*$_2$)$_2$), 1.31 (s, 9H, C(C*H*$_3$)$_3$), 1.19 (s, 9H, C(C*H*$_3$)$_3$), 0.76 (s, 6H, N(C*H*$_3$)$_2$).

Synthesis of {3,5-tert-Bu$_2$-2-(OH)C$_6$H$_2$CH=N-2-CH$_2$C$_5$H$_4$N}Ca(II)I (4-9)

3,5-*tert*-Bu$_2$-2-(OH)C$_6$H$_2$CH=N-2-CH$_2$C$_5$H$_4$N (0.967 g, 3.0 mmol) and NaH (0.303 g, 15 mmol) were dissolved in THF (30 mL). After stirring at room temperature

overnight followed by filtration of excess amount of NaH, the filtrate was added to CaI_2 (0.882 g, 3.0 mmol) in THF (30 mL) and stirred overnight. Then the volatile components were removed in *vacuo* and dissolved in dichloromethane followed by filtration. The desired complex was isolated following the removal of dichloromethane and dried in *vacuo*. The final product was an orange-yellow solid (1.27 g, 92.6 % yield).

Synthesis of {(1S,2R)-1-[(2-Hydroxy-3,5-di-tert-butyl-benzylidene)-amino]-indan-2-ol}Ca(II) (4-12)

(1S,2R)-1-[(2-Hydroxy-3,5-di-tert-butyl-benzylidene)-amino]-indan-2-ol ligand was synthesized according to literature procedure.[65] (1S,2R)-1-[(2-Hydroxy-3,5-di-tert-butyl-benzylidene)-amino]-indan-2-ol ligand (0.183 g, 0.5 mmol) and NaH (5 eq.) were dissolved in THF (20 mL). After stirring at room temperature overnight, excess NaH was removed by filtration, and the sodium salt was transferred *via* cannula through a medium porosity frit packed with Celite to a Schlenk flask containing CaI_2 (0.201 g, 0.75 mmol). The reaction mixture became clear and was stirred at ambient temperature overnight. THF was removed under reduced pressure, and dichloromethane was added to the reaction mixture subsequent to filtration to remove NaI. The desired complex, a yellow-green solid was isolated following the removal of dichloromethane and was dried in *vacuo*. ^{1}H NMR ($CDCl_3$, 300 MHz): δ 8.46(s, 1H, C*H*=N), 7.39(d, 1H, C_6H_2), 7.25-712. (m, 5H), 4.76(d, NC*H*, 1H), 3.75 (m, 4H, O(CH_2CH_2)$_2$), 3.18 (m, CH_2, 2H), 1.80 (s, C*H*OCa, 1H), 1.71 (m, 4H, O(CH_2CH_2)$_2$), 1.38 (s, 9H, C(CH_3)$_3$), 1.28 (s, 9H, C(CH_3)$_3$).

Synthesis of Cr(III)(salen) Complexes

Cr(III)(salen) complexes were synthesized according to literature procedure.[13] H_2Salen (1.0 eq.) and NaH (5.0 eq.) were dissolved in THF. After stirring at room temperature overnight, excess NaH was removed by filtration and the sodium salt was transferred *via* cannula through a medium porosity frit packed with Celite to a Schlenk flask containing Cr(III)$Cl_3(THF)_3$ (1.0 eq.). The reaction mixture became dark brown and was stirred at ambient temperature overnight. THF was removed under reduced pressure and dichloromethane was added to the reaction mixture subsequent to filtration to remove NaCl. The desired complex was isolated following the removal of dichloromethane and was dried in *vacuo*.

Synthesis of [N{C_3F_7C(Dipp)N}$_2$]Zn(II) N($SiMe_3$)$_2$ (4-13)

[N{C_3F_7C(Dipp)N}$_2$]H was synthesized according to literature procedure.[66] Fluorinated triazapentadienyl ligand (0.262 g, 0.361 mmol) was dissolved in THF (30 mL) and Zn[N($SiMe_3$)]$_2$ (0.140 g, 0.362 mmol) was added to fluorinated Triazapentadienyl ligand solution. The reaction mixture was stirred for 3 hours at room temperature. THF was removed under reduced pressure and it became white sold from clear solution. Pentane (10 mL) was added and a white solid was obtained followed by filtration. (0.10 g, 29 % Yield).

X-ray Structure Study

Suitable crystals for X-ray analysis were obtained by slow diffusion. A Bausch and Lomb 10x microscope was used to identify a suitable crystal from a representative sample of crystals of the same habit. Each crystal was coated with a cryogenic

protectant (i.e, paratone) and mounted on a glass fiber, which in turn was fashioned to a copper mounting. The crystal was placed in a cold nitrogen stream (Oxford) maintained at 110 K on a Bruker SMART 1000 three circle goniometer. The X-ray data were obtained on a Broker CCD diffractomoter and covered more than a hemisphere of reciprocal space by a combination of three sets of exposures; each exposure set had a different angle φ for the crystal orientation and each exposure covered 0.3° in ω. The crystal-to-detector distance was 5.0 cm. Crystal decay was monitored by repeating the data collection of 50 initial frames at the end of the data set and analyzing the duplicate reflections; crystal decay was negligible. The space group was determined based on systematic absences and intensity statistics.[39] The structures were solved by direct methods and refined by full-matrix least squares on F2. All non-hydrogen atoms were refined with anisotropic displacement parameters. All H atoms were placed at idealized positions and refined with fixed isotropic displacement parameters equal to 1.2 (1.5 for methyl protons) times the equivalent isotropic displacement parameters of the atoms to which they were attached.

The following are the programs that were used: data collection and cell refinement, SMART;[39] data reduction, SAINTPLUS (Bruker[40]); program used to solve structures, SHELXS-86 (Sheldrick[41]); program used to refine structures, SHELXL-97 (Scheldrick[42]); molecular graphics and preparation of material for publication, SHELXTL-Plus version 5.0 (Bruker[43]).

Crystal Structure of **4-4** is shown in Figure 4-10 and crystal data are listed in Table 4-1. Details of data collection are listed in Appendix C.

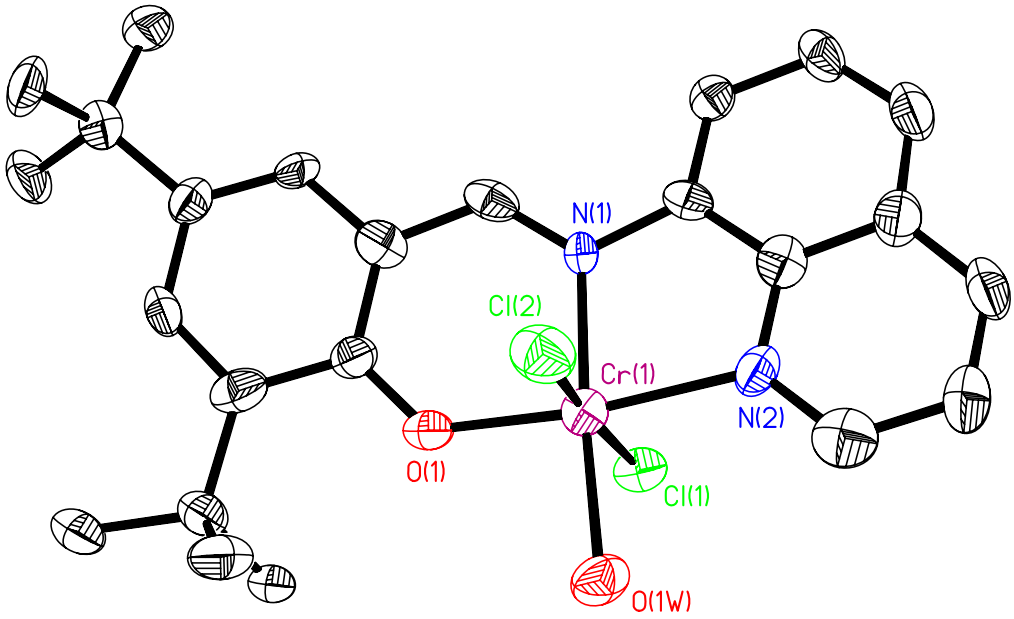

Figure 4-10. Thermal ellipsoid drawing of compound **4-4** along with partial atomic numbering scheme.

Table 4-1. Crystal data and structure refinement for **4-4**.

Identification code	4-4
Empirical formula	C_{31} H_{39} Cl_2 Cr N_2 O_3
Formula weight	610.54 g/mol
Temperature	110(2) K
Wavelength	0.71073 Å
Crystal system	Triclinic
Space group	P-1
Unit cell dimensions	a = 9.639(12) Å
	b = 10.592(13) Å
	c = 16.41(2) Å
	α = 108.70(3)°
	β = 103.89(3)°
	γ = 90.39(3)°
Cell volume	1534(3) $Å^3$
Z	2
Density (calculated)	1.322 g/cm^3
Absorption coefficient	0.581 mm^{-1}
F(000)	642
Crystal size	0.13 x 0.10 x 0.05 mm^3
Theta range for data collection	1.36 to 27.61°
Index ranges	-6<=h<=12, -12<=k<=13, -21<=l<=20
Reflections collected	9488
Independent reflections	6601 [R(int) = 0.1013]
Completeness to theta = 27.61°	92.4 %
Absorption correction	None
Refinement method	Full-matrix least-squares on F^2
Data / restraints / parameters	6601 / 0 / 359
Goodness-of-fit on F^2	0.999
Final R indices [I>2sigma(I)]	R1 = 0.1290, wR2 = 0.3199
R indices (all data)	R1 = 0.3067, wR2 = 0.3902
Largest diff. peak and hole	0.621 and -0.728 e.$Å^{-3}$

Copolymerization of Epoxides and Carbon Dioxide

Catalyst (50 mg) and cocatalyst were dissolved in 20 mL of neat epoxide. The solution was added via injection port into a 300 mL Parr autoclave already at 80°C that was under vacuum for 8 hours previous. The flask was charged with 52 bar CO_2 pressure and left at 80°C. After a designated period of time, the autoclave was cooled down to room temperature and vented in a fume hood. The polymer was extracted with dichloromethane and dried in a vacuum oven. The polycarbonate was weighed to determine turnover frequencies and analyzed by ^1H NMR in order to determine the percent yield of cyclic carbonate, polycarbonate and polyether.

Copolymerization Reactions Monitored by IR Spectroscopy

In a typical experiment, 10 mL of neat cyclohexene oxide was transferred *via* the injection port into a 300 mL stainless steel Parr autoclave reactor which had been dried overnight at 80°C. The reactor is modified with a silico window to allow for the use of and ASI ReactIR 1000 system equipped with a MCT detectors and 30 bounce siCOPM *in situ* probe. In this manner, a single 128-scan background spectrum was collected. The catalyst (in 10 mL of neat cyclohexene oxide) was then injected into the reactor *via* the injection port, resulting 20 mL reaction solution. The reactor was pressurized to 52 bar in CO_2 and heated to the desired temperature as the IR probe began collecting scans. The infrared spectrometer was set up to collect one spectrum every 3 minutes over a 10-hour period. Profiles of the absorbance at 1750 cm^{-1} (polycarbonate) and 1803 cm^{-1} (cyclic carbonate) with time were recorded after baseline correction.

RESULTS AND DISCUSSION

Tridentate Schiff base metal complexes as catalysts for alternative copolymerization of epoxides and carbon dioxide are shown in Figure 4-11 and 4-12. The crystal structure of **4-4** is depicted in Figure 4-10. It is apparent from the thermal ellipsoid drawing that the tridentate Schiff base ligand is located cis to the nucleophiles (two chloride ligands) and the two nucleophiles are located trans to each other. A solvent molecule is located cis to the nucleophiles, thereby, the molecular structure of Cr(III) compound (**4-4**) shows octahedral geometry while similar Al(III) and Fe(III) show trigonal bipyramidal geometry at the metal centers.

First, polymerization results of the copolymerization from cyclohexene oxide and carbon dioxide changing imine backbone on Cr(III) complexes were investigated. The polymerizations have been performed at 80 °C under 35 bar CO_2 pressure for 24 h.

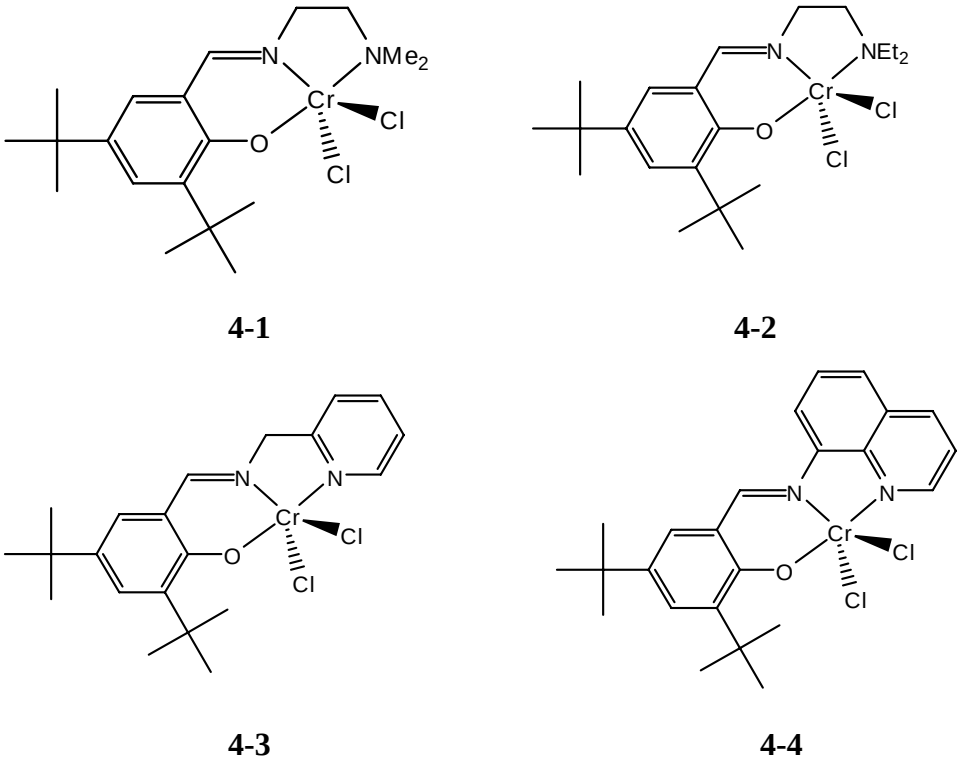

4-1 **4-2**

4-3 **4-4**

Figure 4-11. Structures of tridentate Schiff base metal(III) complexes.

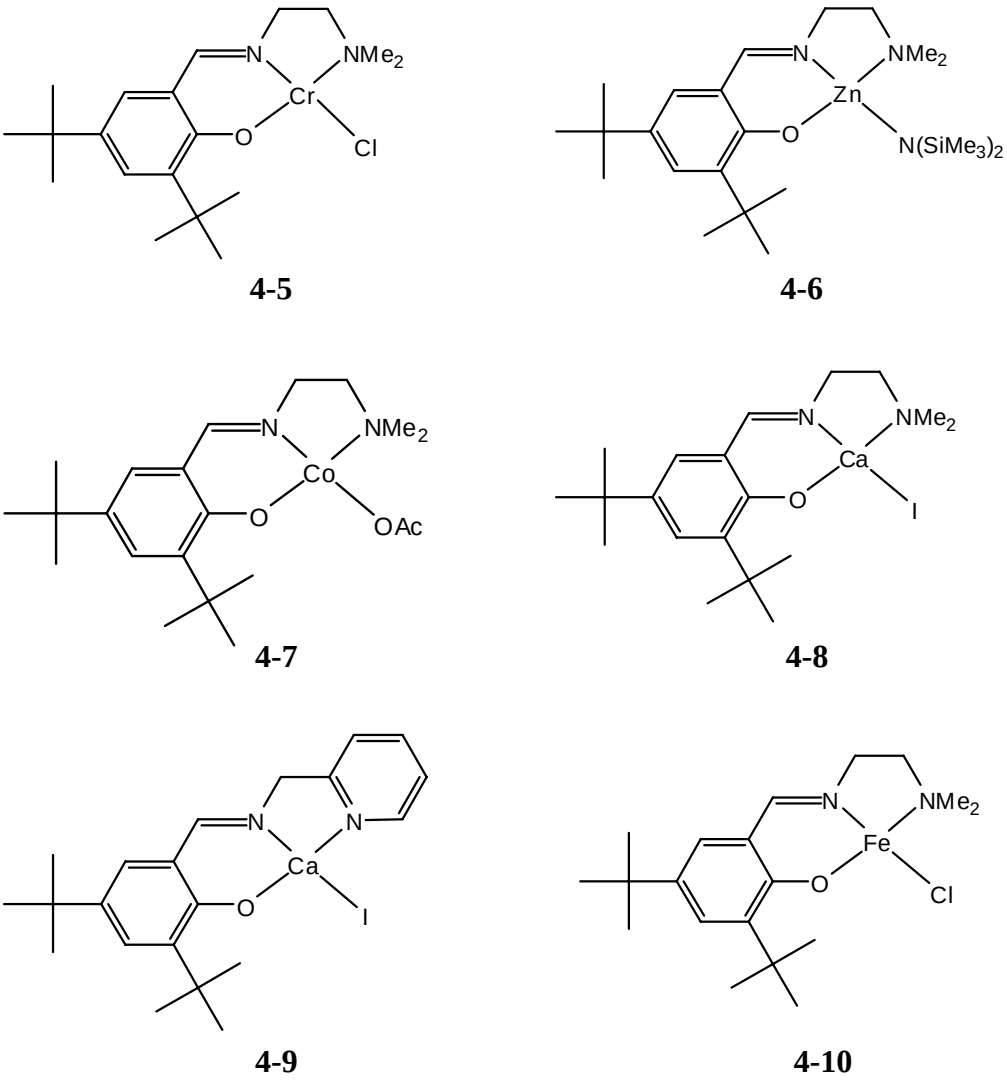

Figure 4-12. Structures of tridentate Schiff base metal(II) complexes.

The collected polycarbonates were analyzed by ^{1}H NMR, where the amount of ether linkage was determined by integrating the peaks corresponding to the methine protons of polyether at ~ 3.5 ppm and polycarbonate at ~ 4.6 ppm. Table 4-2 listed TON (mol epoxide consumed / mol catalyst) and CO_2 content in copolymer *vs*. polyether

linkage using tridentate Schiff base Cr(III) catalysts with different imine backbone. According to copolymerization results in Table 4-2, TON and CO_2 content increase with catalyst containing more donating imine backbone.

Table 4-2. Copolymerization results from CO_2 and cyclohexene oxide.[a]

catalyst	cocatalyst	TON[b]	CO_2 content (%)[c]
4-1	None	66.0	65
4-1	1 eq. PCy_3	54.0	77
4-2	1 eq. PCy_3	77.5	81
4-3	1 eq. PCy_3	63.5	72
4-4	1 eq. PCy_3	27.1	64

[a] Copolymerization was carried out at 80°C, 52 bar CO_2 pressure for 24 hours. [b] TON = mol epoxide consumed / mol catalyst. [c] Detected by ^{1}H NMR.

Further analysis was investigated by infrared spectroscopy to identify monomeric cyclohexyl carbonate with ν(C=O) at 1800 cm^{-1} *vs*. polycarbonate with ν(C=O) at 1750 cm^{-1}. Figure 4-13 though 4-15 displays the IR spectra after polymerization for 24 hours using **4-1** to **4-4** indicating cyclohexyl carbonate with ν(C=O) at ~ 1800 cm^{-1} and polycarbonate with ν(C=O) at ~ 1750 cm^{-1} in dichloromethane.

IR spectra indicated catalyst **4-1** and **4-2** mostly produce polycarbonate and a small amount of cyclic carbonate, where ν(C=O) with a shoulder about 1818 cm^{-1} indicates trans cyclic carbonate while catalyst **4-3** and **4-4** produce both polycarbonate and cyclic carbonate.

(a)

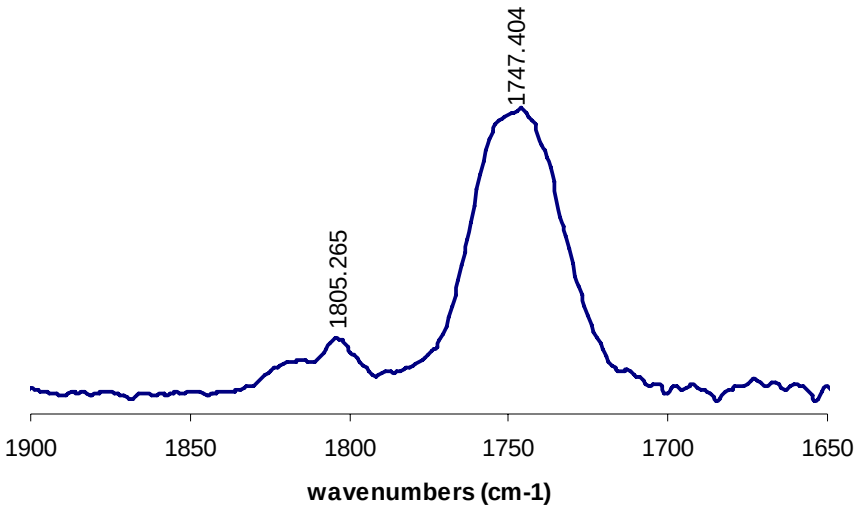

(b)

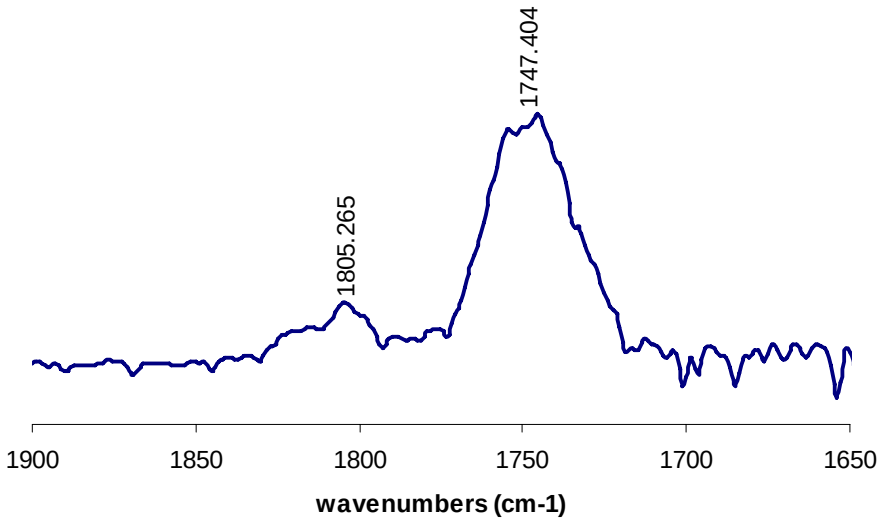

Figure 4-13. IR spectra after copolymerization of cyclohexene oxide and carbon dioxide for 24 hours using **4-1** (a) without any cocatalyst and (b) with 1 eq. of tricyclohexylphosphine (PCy_3) as a cocatalyst.

(a)

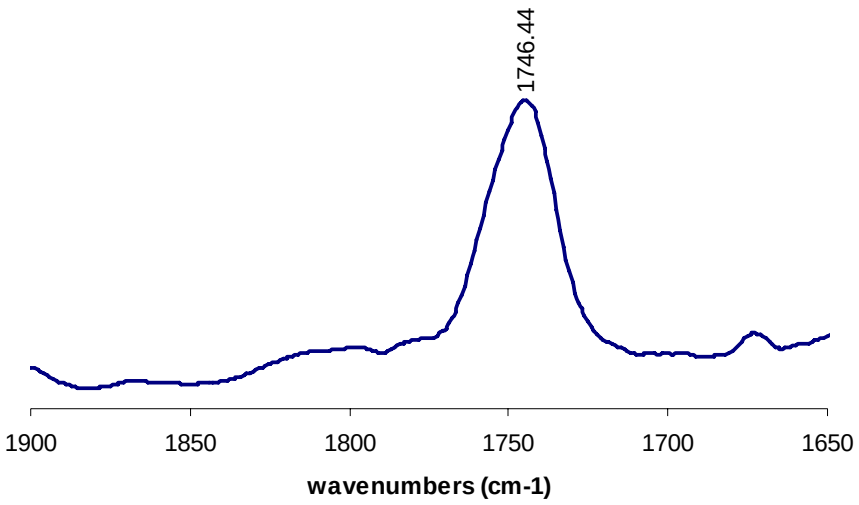

(b)

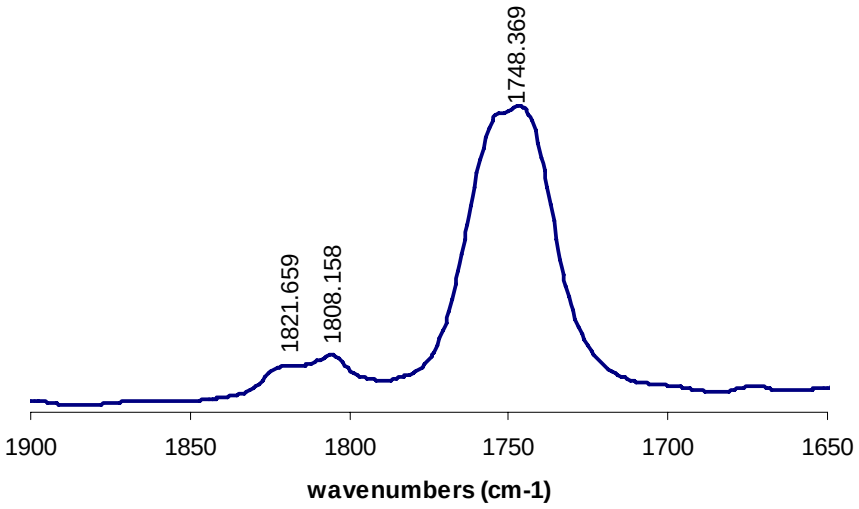

Figure 4-14. IR spectra after copolymerization of cyclohexene oxide and carbon dioxide for 24 hours using **4-2** (a) without any cocatalyst and (b) with 1 eq. of tricyclohexylphosphine (PCy_3) as a cocatalyst.

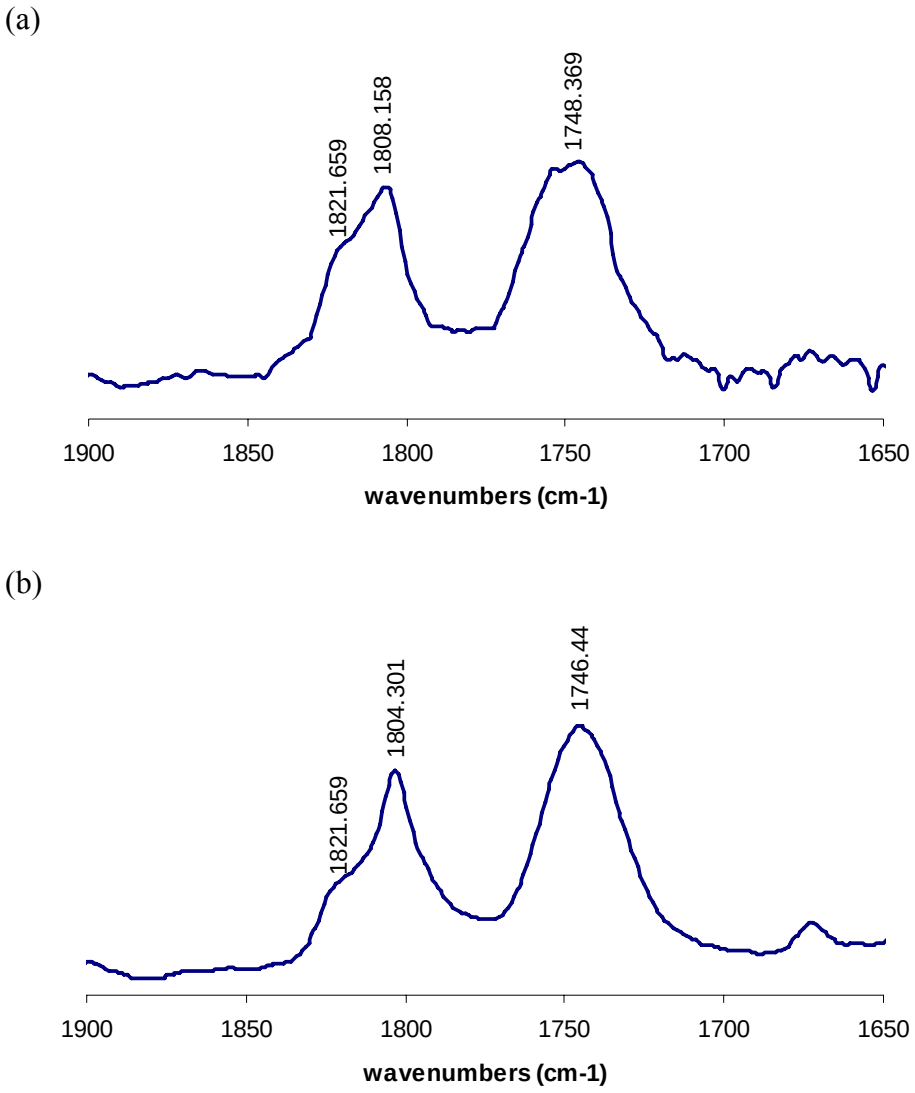

Figure 4-15. IR spectra after copolymerization of cyclohexene oxide and carbon dioxide for 24 hours using (a) **4-3** and (b) **4-4** with 1 eq. of tricyclohexylphosphine (PCy_3) as a cocatalyst.

The next investigation was to change the metal to Cr(II), Zn(II), Ca(II) or Fe(II). Figures 4-16 though 4-19 show IR spectra after each polymerization run from cyclohexene oxide and carbon dioxide for 24 hour. According to the IR spectra, the Cr(III) catalyst is more active for copolymerization of cyclohexene oxide and carbon

dioxide than other metal catalysts with the same ligand. These catalysts produced trace amounts of copolymers. Therefore, TONs of these isolated copolymers were difficult to determine.

(a)

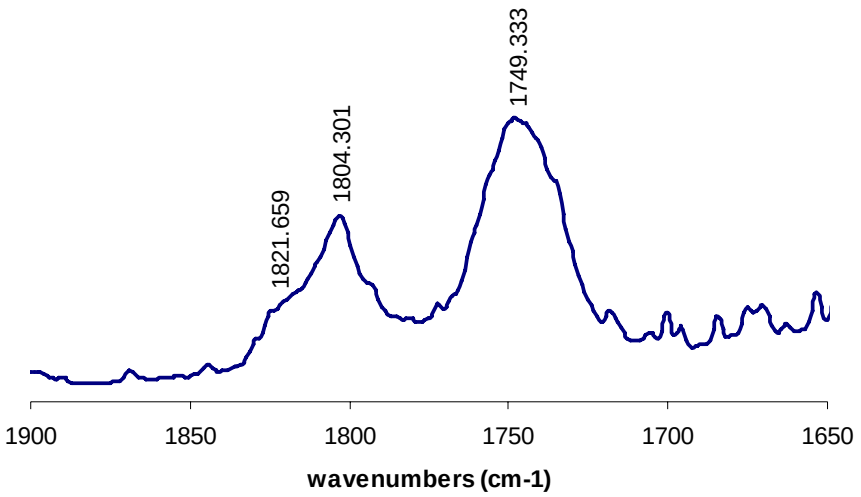

(b)

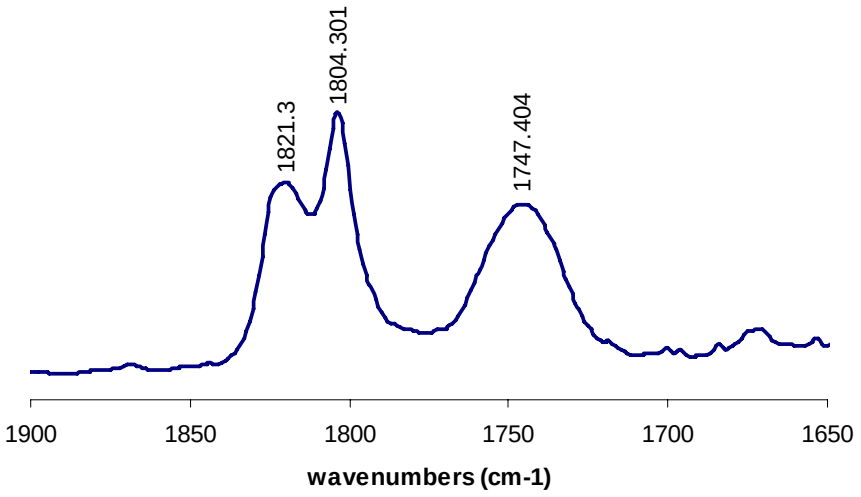

Figure 4-16. IR spectra after copolymerization of cyclohexene oxide and carbon dioxide for 24 hours using **4-5** (a) with 1 eq. of tricyclohexylphosphine (PCy_3) as a cocatalyst and (b) with 1 eq. of N-methylimidazole (NMeI) as a cocatalyst.

(a)

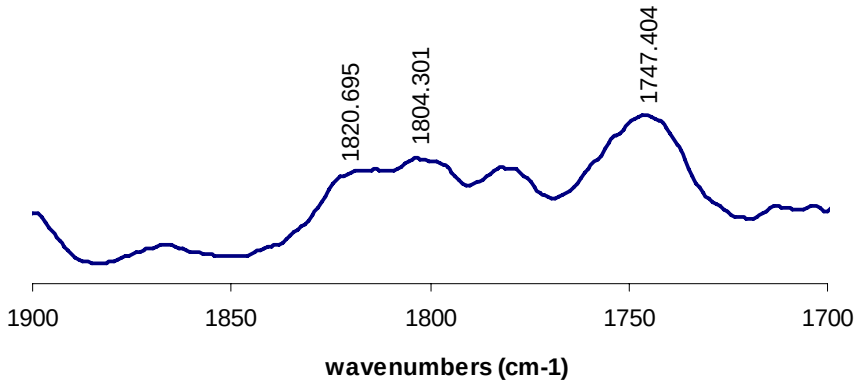

(b)

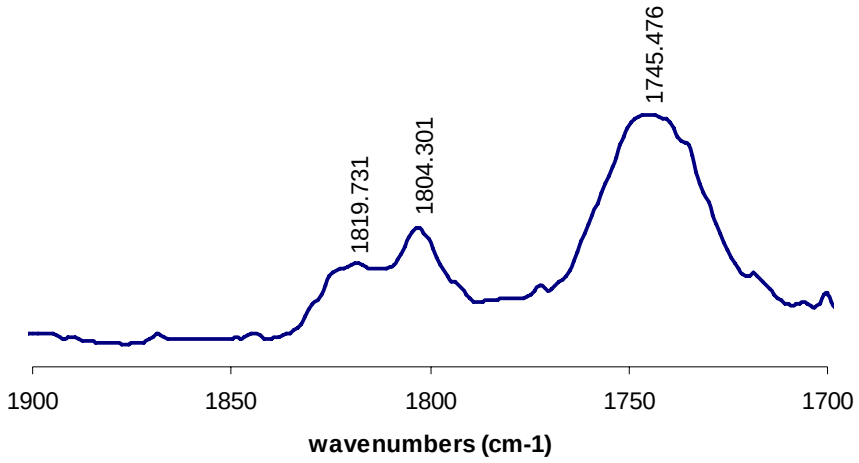

Figure 4-17. IR spectra after copolymerization of cyclohexene oxide and carbon dioxide for 24 hours (a) using **4-6** without cocatalyst and (b) using **4-7** with 1 eq. of tricyclohexylphosphine (PCy_3) as a cocatalyst.

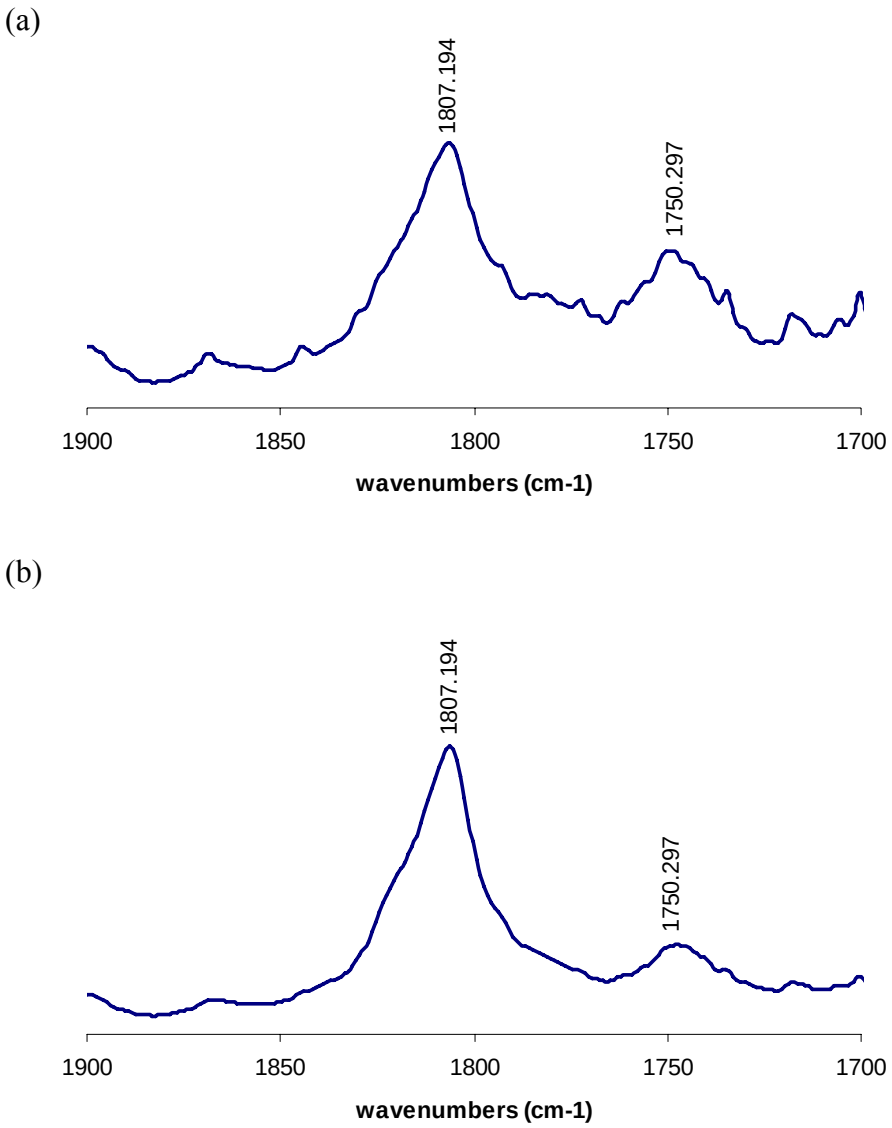

Figure 4-18. IR spectra after copolymerization of cyclohexene oxide and carbon dioxide for 24 hours (a) using **4-8** with 1 eq. of tricyclohexylphosphine (PCy_3) as a cocatalyst and (b) using **4-9** with 1 eq. of tricyclohexylphosphine (PCy_3) as a cocatalyst.

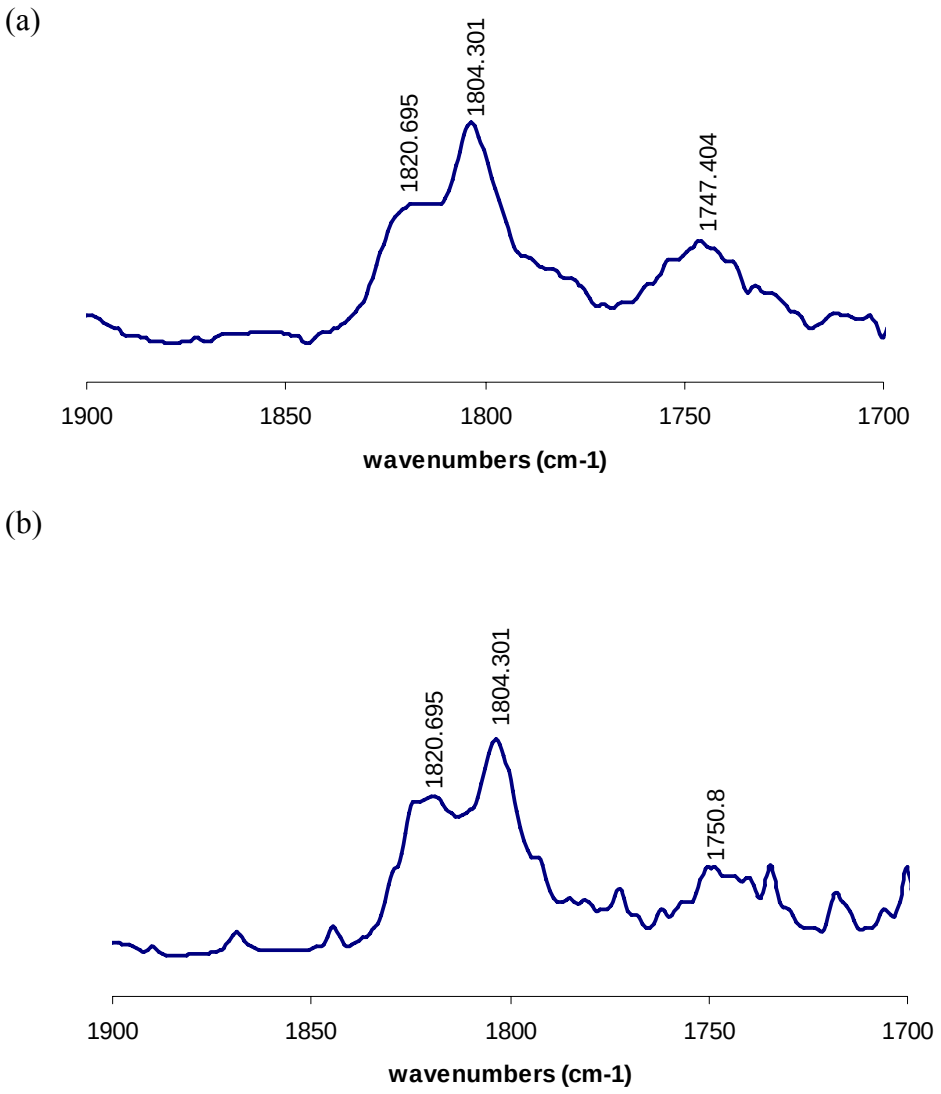

Figure 4-19. IR spectra after copolymerization of cyclohexene oxide and carbon dioxide for 24 hours using **4-10** (a) with 1 eq. of tricyclohexylphosphine (PCy_3) as a cocatalyst and (b) with 1 eq. of N-methylimidazole (NMeI) as a cocatalyst.

Ca(salen) catalyst with cocatalysts (**2-1** and **2-4**) were applied to the copolymerization of carbon dioxide and cyclohexene oxide and resulted in only formation of cis cyclic carbonate (Figure 4-20).

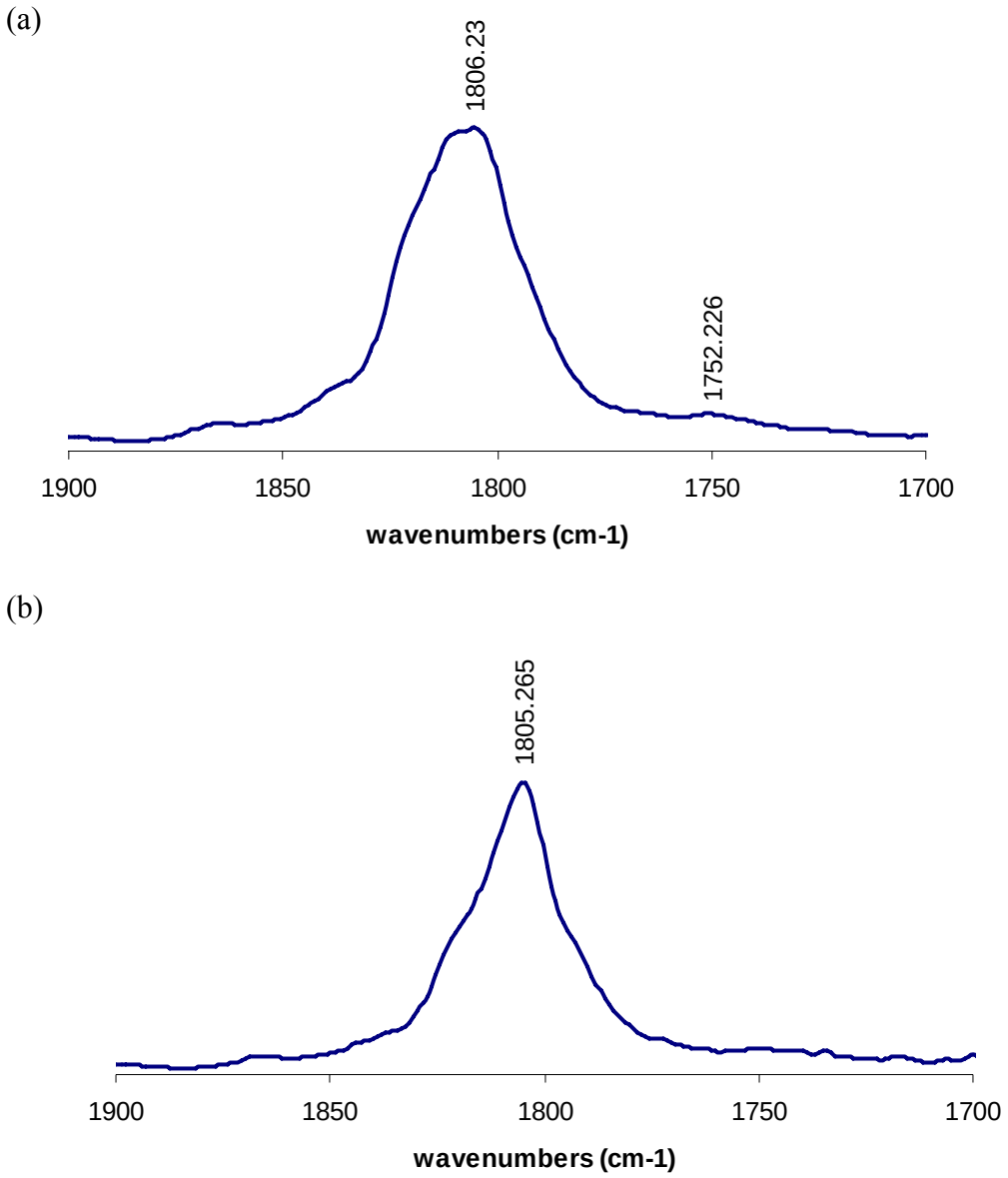

Figure 4-20. IR spectra after copolymerization of cyclohexene oxide and carbon dioxide for 24 hours using (a) **2-1** with 1 eq. n-Bu_4NCl as a cocatalyst and (b) **2-4** with 1 eq. of n-Bu_4NCl as a cocatalyst.

Other catalysts (in Figure 4-21) have also been applied to copolymerization of cyclohexene oxide and carbon dioxide. The IR spectra in Figure 4-22 indicate that catalyst **4-12** produced polycarbonate without cyclic carbonate. This catalyst **4-12** has a

chiral center, thereby tacticity of isolated polycarbonate from catalyst **4-12** was investigated by ^{13}C NMR which indicates atactic polycarbonate (60% of isotactic polycarbonate and 40 % of syndiotactic polycarbonate centers in Figure 4-23).

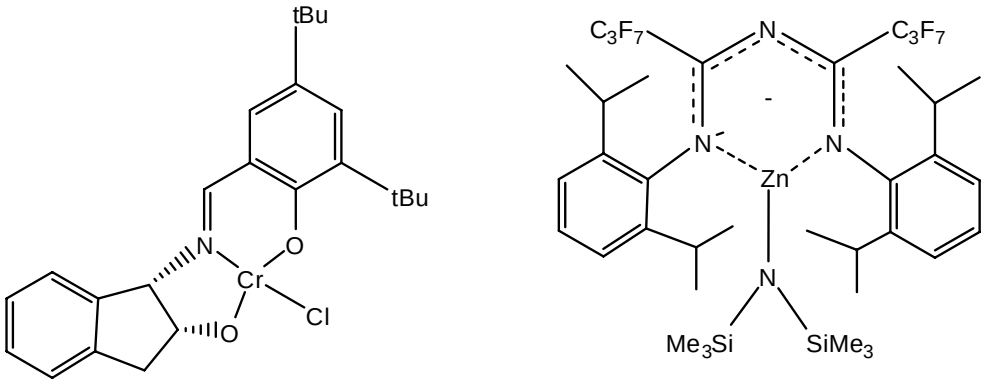

4-12 **4-13**

Figure 4-21. Structures of catalysts of **4-12** and **4-13.**

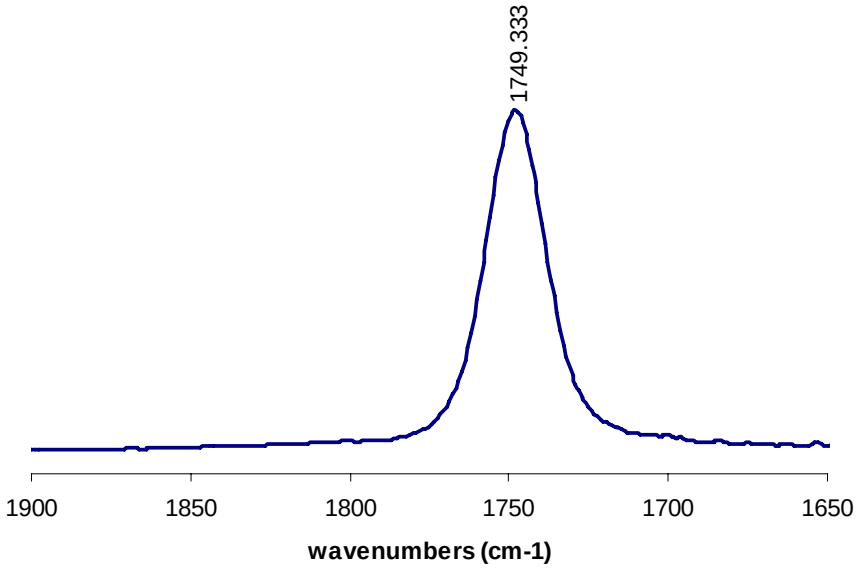

Figure 4-22. IR spectrum after copolymerization of cyclohexene oxide and carbon dioxide for 14 hours using **4-12** with 1 eq. of tricyclohexylphosphine (PCy_3) as a cocatalyst.

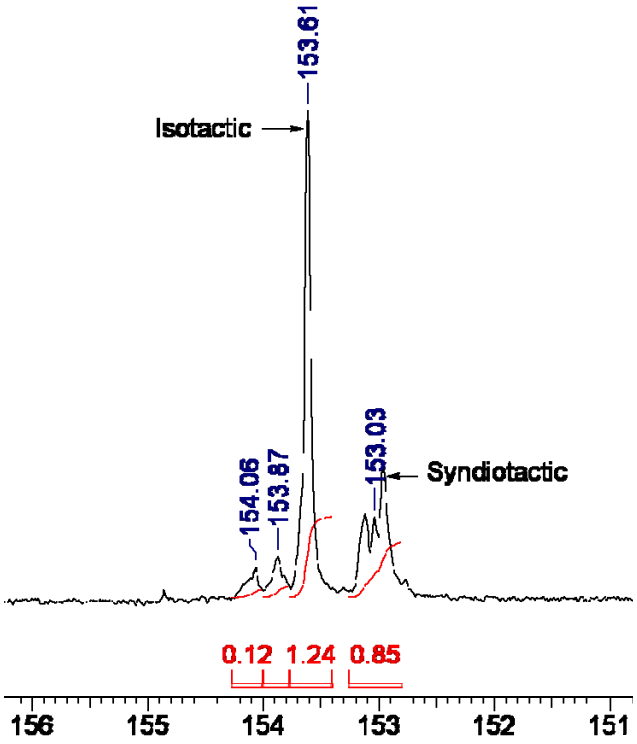

Figure 4-23. ^{13}C NMR spectrum of isolated polycarbonate from copolymerization of cyclohexene oxide and carbon dioxide using **4-12** with 1 eq. of tricyclohexylphosphine (PCy_3) as a cocatalyst (δ = 154.06 corresponds to *cis* cyclic carbonate and δ = 153.87 corresponds to *trans* cyclic carbonate).

Complex **4-13** has a similar structure to zinc(β-diiminate) complex by Coates, which is the most active catalyst for copolymerization of cyclohexene oxide and carbon dioxide so far (Figure 4-5). Copolymerization of cyclohexene oxide and carbon dioxide using catalyst **4-13** was monitored by *in situ* infrared spectroscopy. Initiation was carried out at 50°C and 200 psi CO_2 pressure up to 4 hours and reaction temperature and CO_2 pressure were raised to 80°C and 600 psi. *In situ* IR spectroscopy and reaction profile (Figure 4-24) show that the formation of polycarbonate is slower at 50°C and 200

psi CO_2 pressure, and it is faster at 80°C and 600 psi CO_2 pressure. However, the formation of polycarbonate was not increased after 6 hours and the formation of cyclic carbonate did not change during the reaction period. Therefore, copolymer after 10 hours of reaction time was investigated by ^1H NMR indicating mostly formation of polyether.

Further investigations for copolymerization of carbon dioxide and other available epoxides such as propylene oxide, limonene oxide and [2-(3,4-epoxycyclohexyl)ethyl] trimethoxysilane (TMSO) have been performed. Copolymerization of carbon dioxide and propylene oxide at 40°C and 52 bar CO_2 pressure for 24 hour using catalyst **4-7** with 1 eq. of tricyclohexylphosphine (PCy_3) as a cocatalyst formed no copolymer or no cyclic carbonate. The next trial to increase reaction temperature to 60°C under identical condition above formed mostly cyclic carbonate (Figure 4-25).

(a)

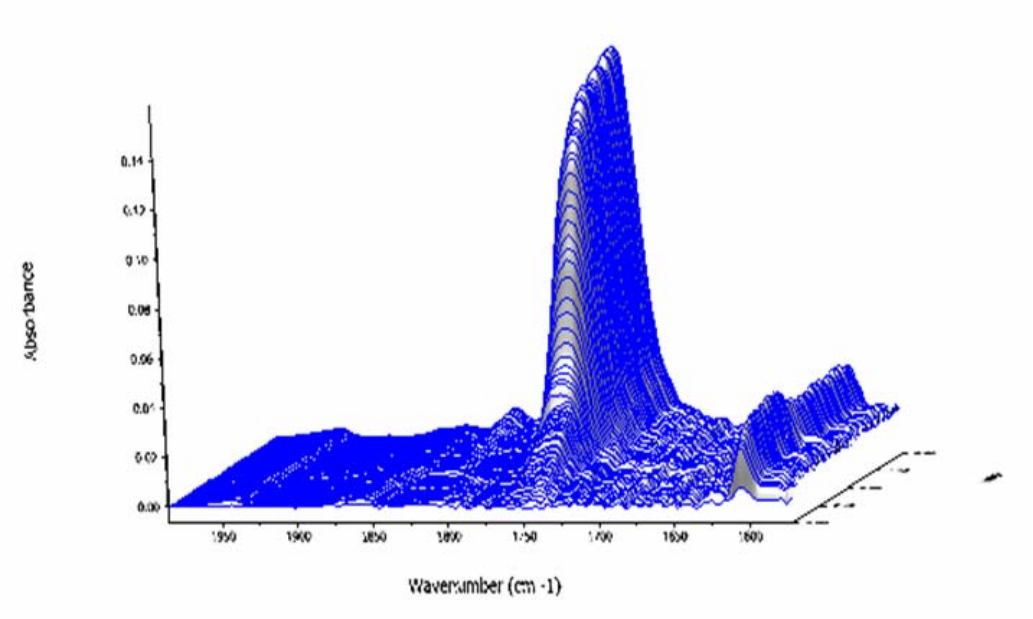

(b)

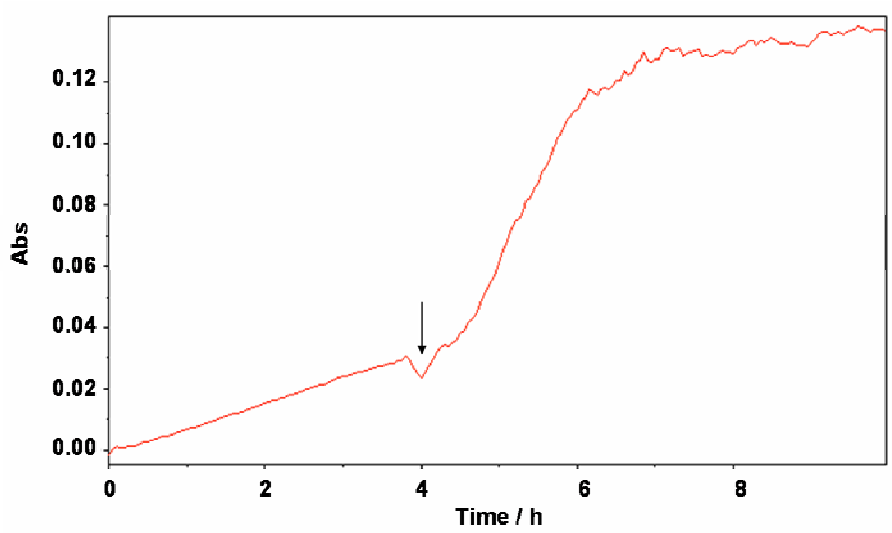

Figure 4-24. (a) Three-dimensional stack plot and (b) reaction profile for the ν(C=O) stretch at 1750 cm^{-1} from the resulting polycarbonate produced from the copolymerization of cyclohexene oxide and carbon dioxide using catalyst **4-13**. Note: Initiation was carried out at 50°C and 200 psi CO_2 pressure up to 4 hours (at arrow on the plot) and reaction temperature and CO_2 pressure were raised to 80°C and 600 psi.

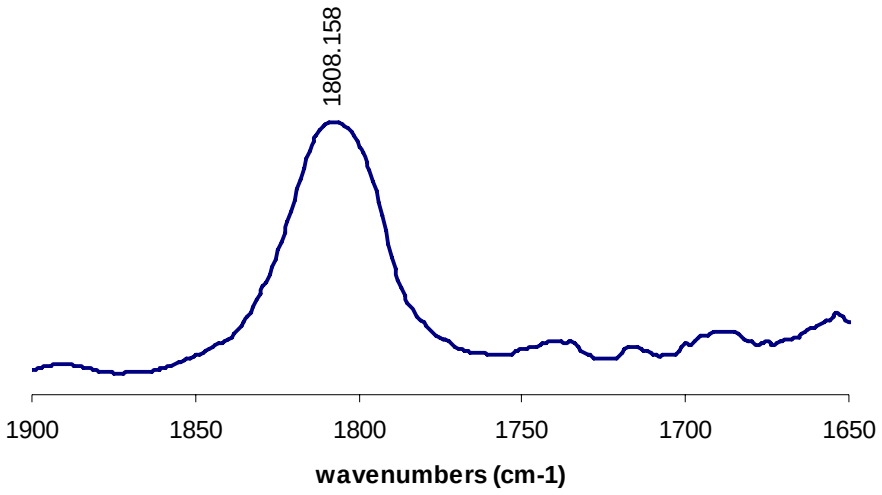

Figure 4-25. IR spectrum after copolymerization of propylene oxide and carbon dioxide for 24 hours using **4-7** with 1 eq. of tricyclohexylphosphine (PCy_3) as a cocatalyst.

Copolymerization of carbon dioxide and limonene oxide or TMSO has been performed with **2-1** catalyst and 2 eq. of nBu_4NCl. Figure 4-26 shows that it produced a small amount of cyclic carbonate from the copolymerization of carbon dioxide and limonene oxide. Figure 4-27 shows that it produced only cyclic carbonate from the copolymerization of TMSO and carbon dioxide.

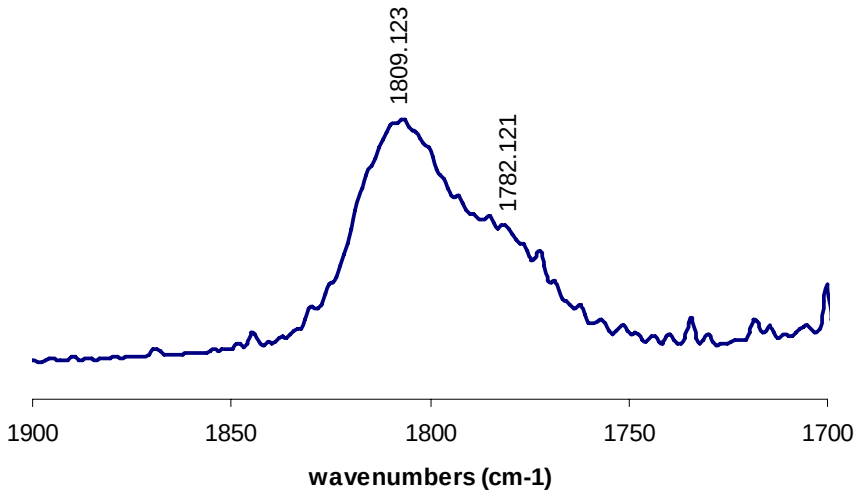

Figure 4-26. IR spectrum after copolymerization of limonene oxide and carbon dioxide for 24 hours using **2-1** with 2 eq. of nBu_4NCl as a cocatalyst.

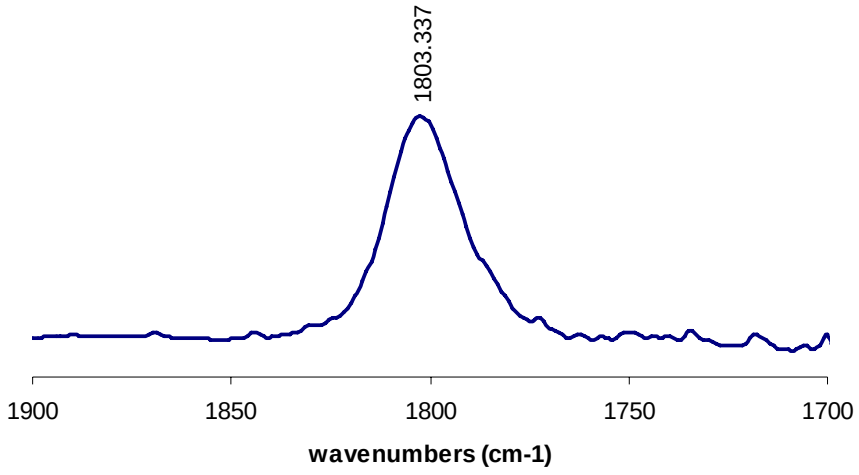

Figure 4-27. IR spectrum after copolymerization of TMSO and carbon dioxide for 15 hours using **2-1** with 2 eq. of nBu_4NCl as a cocatalyst.

CONCLUSIONS

For production of polycarbonate from carbon dioxide and epoxides, various Schiff base metal complexes have been synthesized. Tridentate Schiff base metal complexes have shown much less catalytic activity compared to (salen)Cr(III)X complexes. However, they have formed polycarbonates with more than 60 % of CO_2 linkage. The catalytic activity with these complexes is increased in the order: Cr(III) > Cr(II) > M(II) (M = Co, Zn, Ca or Fe), and with more donating group diimine backbones. (Salen)Ca(II) complexes formed *cis* cyclic carbonate from copolymerization of carbon dioxide and cyclohexene oxide rather than *trans* cyclic carbonate. It has also formed cyclic carbonates from copolymerization of carbon dioxide and limonene oxide as well as copolymerization of carbon dioxide and TMSO.

CHAPTER V

SUMMARY AND CONCLUSIONS

This dissertation consists of two types of polymerization reactions for the formation of polycarbonates and their thermoplastic elastomers: Ring-opening polymerization of cyclic monomers and the copolymerization of carbon dioxide and cyclic ethers. The research is more focused on ring-opening polymerization of cyclic carbonates and cyclic esters to produce polycarbonates, polyesters and their copolymers.

In chapter II, biometal Schiff base derivatives as catalysts for the ring-opening polymerization of trimethylene carbonate and lactides have been designed and synthesized with an issue of the use of biodegradable polymers as medical materials. The catalytic activity varied with metal in the order $Ca^{+2} > Mg^{+2} \approx C_2H_5Al^{+2} > Zn^{+2}$. Tridentate Schiff base calcium(II) complexes have shown higher activities for ring-opening polymerization of trimethylene carbonate as well as lactide than (salen)Ca(II) complexes. Optimization of the calcium(II) system was achieved by changing backbone, substituents in the 3,5-positions of the phenolate rings, and initiators. These calcium systems have shown excellent catalytic activity for ring-opening polymerization of trimethylene carbonate or lactide to produce high molecular weight polymers with narrow polydispersities. In addition these catalysts effectively copolymerize these two monomers. The polymerization reaction was shown to be *quasi-living* as illustrated by a linear relationship between M_n and % conversion and a low polydispersity index, clearly demonstrating that the level of polymerization control was high.

Solution kinetic studies revealed the polymerization reactions to be first-order in [monomer], [catalyst], and [cocatalyst] (in case of the catalytic system of (salen)Ca and an external initiator). It was observed that ring-opening polymerization of trimethylene carbonates is much faster than that of lactide in homopolymerization reactions while the rate to grow the poly(trimethylene carbonate) chain is much slower than that of lactide in copolymerization.

Stereoselectivity has been investigated for lactide polymerization using the tridentate Schiff base calcium catalyst with di-*tert*-butyl groups in the 3,5-positions of the phenolate rings since polymer tacticity is very important factor for polymer properties. Therefore, the polymer products under various polymerization conditions have been investigated and it was found that the Ca(II) catalyst predominantly produced heterotactic poly(lactide) from *rac*-lactide.

Activation parameters for trimethylene carbonate and lactides homopolymerization have been obtained from Eyring plots and it was found that ROP of TMC is a less energetic process than that of lactide. Activation parameters for copolymerization of lactide and trimethylene carbonate have also been determined and compared with those for homopolymerization. Interestingly, it is noticed that the feed ratios in copolymerization reaction influence not only polymer properties and degradation, but also copolymerization rate. Larger negative $\Delta S^{\neq}$ for ring-opening polymerization of trimethylene carbonate than that of lactide was consistent with binding studies between metal complex and monomer *via* IR spectroscopy.

In chapter III, copolymerization of carbon dioxide and oxetane to produce poly(trimethylene carbonate) has been addressed. (Salen)CrX complexes have been found to be very active catalyst for carbon dioxide and epoxides such as cyclohexene oxide and propylene oxide. Therefore, these catalysts have been applied for copolymerization of carbon dioxide and oxetane, which is a less active monomer because of less ring strain than epoxides, and these studies have shown that metal salen derivatives of chromium and aluminum, along with *n*-Bu_4NX (X = Cl or N_3) salts are effective catalysts for the selective coupling of CO_2 and oxetane (trimethylene oxide) to provide the corresponding polycarbonate with only trace quantities of ether linkages. These results have shown that the selectivity for copolymer formation from oxetane and CO_2 is very high (97 %) in all instances, even at 110°C.

However, reaction profiles for copolymerization of carbon dioxide and epoxide *vs*. copolymerization of carbon dioxide and oxetane are different since cyclic carbonate from copolymerization of carbon dioxide and oxetane, that is trimethylene carbonate, is thermodynamically less stable than poly(trimethylene carbonate) while cyclic carbonate from copolymerization of carbon dioxide and epoxide is more stable than the corresponding polycarbonate. These are two possible mechanisms in copolymerization of carbon dioxide and oxetane: direct formation of poly(trimethylene carbonate) from carbon dioxide and oxetane, and formation via the intermediate trimethylene carbonate (direct formation of trimethylene carbonate and then poly(trimethylene carbonate) is produced from ring-opening polymerization of trimethylene carbonate). The formation of copolymer is suggested, based on circumstantial evidence, not to proceed via the

intermediacy of trimethylene carbonate, which was observed as a minor product of the coupling reaction. To support these evidences, ring-opening polymerization of trimethylene carbonate has been performed and it was found that the kinetic parameters are different from those values from copolymerization of carbon dioxide and oxetane. It was also observed that the process of ring-opening polymerization of trimethylene carbonate to produce poly(trimethylene carbonate) favors high temperature while selectivity to produce poly(trimethylene carbonate) from copolymerization of carbon dioxide and oxetane is increased at lower reaction temperature.

For a reaction catalyzed by (salen)CrCl in the presence of *n*-Bu_4NN_3 as the cocatalyst, both matrix-assisted laser desorption ionization time-of-flight mass spectroscopy and infrared spectroscopy revealed an azide end group in the copolymer.

In the last chapter, copolymerization reactions of carbon dioxide and various epoxides such as cyclohexene oxide, propylene oxide, limonene oxide, and [2-(3,4-epoxycyclohexyl)ethyl]trimethoxysilane (TMSO) have been tried with various metal complexes. The tridentate Schiff base metal complexes were shown to be much less catalytically active than the (salen)Cr(III)X complexes. However, they were found to form polycarbonates with more than 60 % CO_2 linkages. The catalytic activity of these complexes increased in the order: Cr(III) > Cr(II) > M(II) (M = Co, Zn, Ca or Fe), with more donating group diimine backbones. (Salen)Ca(II) complexes formed *cis* cyclic carbonate from the reaction of carbon dioxide and cyclohexene oxide rather than *trans* cyclic carbonate. It also formed cyclic carbonates from the reaction of carbon dioxide and limonene oxide or TMSO.

These catalysts, which were synthesized for the ring-opening polymerization of cyclic monomers and copolymerization of carbon dioxide and cyclic ethers, can be applied as catalysts for other polymerization reactions. They can be utilized for the ring-opening polymerization of other cyclic monomers such as cyclic carbonates, cyclic esters, cyclic acid anhydrides, cyclic ethers, aziridine, cyclic phosphinite etc., and their copolymers or copolymers with carbon dioxide.

REFERENCES

1. A Case Study by the Weinberg Group, **2001**, Polycarbonates and Their Socio-Economic Impact.

2. Plast Europe *Special: Plastics Market* **2001**, *10*, 110-112.

3. Inoue. S.; Koinuma. H.; and Tsuruta, T. *Die. Makromolekulare. Chemie.* **1969,** *130*, 210.

4. MatWeb (database of material properties data at http://www.matweb.com/ reference), May 2007, the properties of polycarbonate.

5. Darensbourg, D. J.; Yarbrough, J. C.; Ortiz, C.; and Fang, C. C. *J. Am. Chem. Soc.* **2003,** *125*(25), 7586.

6. (a) Soga, K. *et al*. *Polym. Sci., Part A: Polym. Chem.* **1976,** *14*, 161. (b) Harris, R. F. *J. Appl. Polym. Sci*. **1989**, *37*, 1491. (c) Vogdanis, L.; and Heitz, W. *Makromol. Chem., Rapid Commun*. **1986**, *7*, 543. (d) Storey, R. F.; and Hoffman, D. C. *Macromolecules* **1992**, *25*, 5369. (e) Lee, J. C.; and Lett, M. H. *Macromolecules* **2000**, *33*, 1618.

7. Clements, J. H. *Ind. Eng. Chem. Res.* **2003**, *42*, 663-674.

8. Powell, D. P. *Medical Plastics and Biomaterials* September, 1998, p.13.

9. Ying, H.; Tang, H.; and Lin, C. *Macromolecules* **2006**, *39*, 3745.

10. (a) Cameron, P. A.; Gibson, V. C.; Redshaw, C.; Segal, J. A.; Bruce, M. D.; White, A. J. P.; and Williams, D. J. *Chem. Commun*. **1999**, 1883. (b) Cameron, P. A.; Gibson, V. C.; Redshaw, C.; Segal, J. A.; White, A. J. P.; and Williams, D. J. *J. Chem. Soc. Dalton Trans*. **2002**, 415.

11. O'Reilly, R. K.; Gibson, V. C.; White, A. J. P.; and Williams, D. J. *J. Am. Chem. Soc.* **2003**, *125*, 8450.

12. (a) Hansen, T. V. and Skattebøl *Tetrahedron Letters* **2005**, *46*, 3829. (b) Casiraghi, G.; Casnati, G.; Puglia, G.; Sartori, G., and Tereghi, G. *J.C.S. Perkin I*, **1979**, 1862.

13. (a) Darensbourg, D. J.; and Holtcamp, M. W. *Macromolecules* **1995,** *28*, 7577. (b) Darensbourg, D. J.; Holtcamp. M. W.; Struck, G. E.; Zimmer, M. S.; Niezgoda, S. A.; Rainey, P.; Robertson, J. B.; Graper, J. D.; Reibenspies, J. H. *J. Am. Chem. Soc.* **1999,** *121*, 107. (c) Darensbourg, D. J.; Wilderson, J. R.; Yarbrough, J. C.; and Reibenspies, J. H. *J. Am. Chem. Soc.* **2000,** *122*, 12487. (d) Darensbourg, D. J.; Zimmer, M. S.; Rainey, P.; Larkins, D. L. *Inorg. Chem*. **2000**, *39*, 1578. (e) Darensbourg, D. J.; Wildeson, J. R.; Lewis, S. A.; Yabrough, J. C. *J. Am. Chem. Soc*. **2002**, *124*, 7075.

14. Penco, M.; Donetti, R.; Mendrichi, R.; Ferruti, P. *Macromol. Chem. Phys*. **1998**, *199*, 1737-1745. (b) Smith, A.; Hunneyball, I. M. *Int. J. Pharm*. **1986**, *30*, 215-220.

15. (a) Pêgo, A. P.; Siebum, B.; VanLuyn, M. J. A.; Gellego, K. J.; Van Seijen, Y.; Poot, A. A.; Grijpma, D. W.; Feijen, J. *Tissue Eng*. **2003**, *9*, 981-994. (b) Marler, J. J.; Upton, J.; Langer, R.; Vacanti, J. P. *Adv. Drug Delivery Rev*. **1998**, *33*, 165-182.

16. Seal, B. L.; Otero, T. C.; Panitch, A. *Mater. Sci. Eng.* **2001**, R34, 147-230.

17. Beiser, I. H.; Konat, I. O. *J. Am. Podiatric Med. Assoc*. **1990**, *80*, 272-275.

18. Rokicki, G. *Prog. Polym. Sci.* **2000**, *25*, 259-342.

19. Darensbourg, D. J.; Ganguly, P.; and Billodeaux, D. *Macromolecules* **2005**, *38*, 5406.

20. Yang, J.; Yu,Y.; Li, Q.; Li, Y.; Cao, A. *J. Polym. Sci. Part A: Polym. Chem.* **2005**, *43*, 373.

21. Wurm, B.; Keul, H.; Hocker, H. *Makromol. Chem. Rapid Commun.* **1992**, *13*, 9.

22. Dobrzynski, P.; Malgorzata P.; Bero, M. *J. Polym. Sci. A, Polym. Chem.* **2005**, *43*, 1913.

23. (a) Darensbourg, D. J.; Choi, W.; Ganguly, P.; and Richers, C. P. *Macromolecules* **2006**, *39*, 4374. (b) Chisholm, M. H.; Gallucci, J. C.; and Phomphrai, K. *Inorg. Chem.* **2004**, *43*, 6717. (c) Westerhausen, M.; Schneiderbauer, S.; Kneifel, A. N.; Söltl, Y.; Mayer, P.; Nöth, H.; Zhong, Z.; Dijkstra, P.; and Feijen, J. *Eur. J. Inorg. Chem.* **2003**, 3432. (d) Zhong, Z.; Dijkstra, P. J.; Grig, C.; Westerhausen, M.; and Feijen, J. *Macromolecules* **2001**, *34*, 3863.

24. (a) Pospiech, D.; Komber, H.; Jehnichen, D.; Häussler, L.; Eckstein, K.; Scheibner, H.; Janke, A.; Kricheldorf, H. R.; and Petermann, O. *Biomacromolecules* **2005**, *6*, 439. (b) Kricheldorf, H. R. and Striker, A. *Macromol. Chem. Phys.* **1999**, *200*, 1726. (c) Yuan, A. and Ruckenstein, E. *J. of Appl. Poly. Sci.* **1998**, *69*, 1429. (d) Kim, J-H.; and Lee J. H. *Poly. J.* **2002,** *34*, 203. (e) Cai, J.; Zhu, K. J.; and Yang, S. L. *Polymer*, **1988**, *39*, 4409.

25. Simic, V.; Pensec, S.; and Spassky, N. *Macromol. Symp.* **2000**, *153*, 109.

26. (a) Nakayama, Y.; Yasuda, H.; Yamamoto, K.; Tsutsumi, C.: Jerome, R.; and Lecomte, P. *Reactive & Functional Polymers* **2005**, *63*, 95. (b) Agarwal, S.; and Puchner, M. *European Polymer Journal* **2002**, *38*, 2365. (c) Tsutsumi, C.; Yamamoto, K.; Ichimaru, A.; Nodono, M.; Nakagawa, K.; and Yashuda, H. *J. of Polym. Sci. Part A: Polym. Chem.* **2003,** *41*, 3572. (d) Tsutsumi, C.; Nakagawa, K.; Shirahama, H.; and Yashuda, H. *Polym. Int.* **2003,** *52*, 439. (e) Ling, J.; Shen, Z.; and Huang, Q. *Macromolecules* **2001**, *34*, 7613.

27. O'Keefe, B. J.; Breyfogle, L. E.; Hillmyer, M. A.; and Tolman, W. B. *J. Am. Chem. Soc.* **2002**, *124*, 4384.

28. Russell, S.; Gamble, C. L.; Gibbins, K.; Jurl, K. C. S.; Mitchel, W. S.; Tumas, A. J.; and Hofmeister, G. E. *Macromolecules* **2005**, *38*, 10336.

29. Shueh, M.; Wang, Y.; Huang, B.; Kuo, C.; and Lin, C. *Macromolecules* **2004**, *37*, 5155.

30. (a) Zhong, Z.; Dijkstra, P. J.; and Feijen, J. *J. Am. Chem. Soc.* **2003**, *125*, 11291. (b) Cameron, P. A.; Jhurry, D.; Gibson, V. C.; Andrew, J. P. W.; Williams, D, J.; and Williams, S. *Macromol. Rapid Commun.* **1999**, *20*, 616.

31. (a) Chisholm, M. H.; Gallucci, J. C.; and Phomphrai, K. *Inorg. Chem.* **2005**, *44*, 8004. (b) Chisholm, M. H.; Gallucci, J. C.; and Zhen, H. *Inorg. Chem.* **2001**, *40*, 5051.

32. (a) Reeve, M. S.; McCarthy, S. P.; Downey, M. J.; Gross, R. A. *Macromolecules* **1994**, *27*, 825. (b) Sarasua, J. R.; Prud'homme, R. E.; Wisniewski, M.; Le Borgne, A.; Spassky, N. *Macromolecules* **1998**, *31*, 3895. (c) Radano, C. P.; Baker, G. L.; Smith, M. R. *J. Am. Chem. Soc.* **2000**, *122*, 1552. (d) Spassky, N.; Wisniewski, M.; Pluta, C.; Le Borgne, A. *Macromol. Chem. Phys.***1996**, *197*, 2627. (e) Ovitt, T. M. and Coates, G. W. *J. Am. Chem. Soc.* **1999**, *121*, 4072. (f) Zhong, S.; Dijkstra, P. J.; Feijen, J. *J. Biomater. Sci. Polymer Edn.* **2004**, *15*, 929.

(g) Zhong, S.; Schneiderbauer, S.; Dijkstra, P. J.; Westerhausen, M.; .Feijen J. *J. Polym. Environ*. **2001**, *9*, 31.

33. Spassky, N.; Wisniewski, M.; Pluta, C.; Le Borgne, A. *Macromol. Chem. Phys.* **1996**, *197*, 2627.

34. Ovitt, T. M. and Coates, G. W. *J. Am. Chem. Soc.* **1999**, *121*, 4072.

35. Demadis, K. D.; Meyer, T. J.; White, P. S. *Inorg. Chem.* **1998**, *37*, 3610-3619.

36. Darensbourg, D. J.; Mackiewicz, R.; Rodgers, J. L.; Fang, C. C.; Billodeaux, D. R.; Reiebenspies, J. H. *Inorg. Chem.* **2004**, *23*, 6024-6034.

37. (a) Lu, X. B.; Feng, X. J.; He, R. *Applied Catalysis A: General* **2002**, *234*, 25. (b) Singer, A. L.; Atwood, D. A. *Inorg. Chim. Acta* **1998**, *277*, 157.

38. Darensbourg, D. J.; Billodeaux, D. R. *Inorg. Chem.* **2005**, *44*, 1433-1442.

39. SMART 1000CCD, Bruker Analytical X-Ray Systems, Madison, WI, 1999.

40. Bruker, SAINT-PLUS, Version 6.02, Madison, WI, 1999.

41. Sheldrick, G. *SHELXS-86*: *Program for Crystal Structure Solution;* Institut für Anorganische Chemie der Universitat Tammanstrasse 4, D-3400 Göttingen, Germany, 1986.

42. Sheldrick, G. *SHELXS-97*: *Program for Crystal Structure Refinement;* Institut für Anorganische Chemie der Universitat Tammanstrasse 4, D-3400 Göttingen, Germany, 1997.

43. Bruker, SHELXTL, Version 5.0, Madision, WI, 1999.

44. Koinuma, H.; Hirai, H. *Makromol. Chem.* **1977**, *178*, 241.

45. Darensbourg, D. J.; Mackiewicz, R. M.; Rodgers, J. L. *J. Am. Chem. Soc.* **2005**, *127*, 14026-14038.

46. Ling, J.; Shen, Z.; Huang, Q. *Macromolecules* **2001**, *34*, 7613-7616.

47. Sánchez, M.; Harvey, M. J.; Nordstrom, F.; Parkin, S.; Atwood, D. A. *Inorg. Chem.* **2002**, *41*, 5397-5402.

48. Zell, M. T.; Padden, B. E.; Paterick, A. J.; Thakur, K. A. M.; Kean, R. T.; Hillmyer, M. A.; and Munson, E. J. *Macromolecules* **2002**, *35*, 7700.

49. (a) Fernández-García, M.; Fernández-Sanz, M.; and Madruga, E. L. *J. of Polym. Sci. Part A: Polym. Chem.* **2004**, *42*, 130. (b) Fernández-García, M.; Fernández-Sanz, M.; and Madruga, E. L. *Macromol. Chem. Phys.* **1999**, *200*, 199.

50. Chisholm, M. H.; Patmore, N. J. and Zhou, Z. *Chem. Commun*., **2005**, 127.

51. Inoue, S.; Koinuma, H.; Tsuruta, T. *J. Polym. Sci., Part B: Polym. Phys.* **1969**, *7*, 287-292.

52. (a) Moore, D. R.; Coates, G. W. *Angew. Chem. Int. Ed.* **2004**, *43*, 6618-6639. (b) Darensbourg, D. J.; Mackiewicz, R. M.; Phelps, A. L.; Billodeaux, D. R. *Acc. Chem. Res.* **2004**, *37*, 836-844. (c) Sugimoto, H.; Inoue, S. *J. Polym. Sci., Part A: Polym. Chem.* **2004**, *42*, 5561-5573. (d) Chisholm, M. H.; Zhou, Z. *J. Mater. Chem.* **2004**, *14*, 3081-3092. (e) Super, M. S.; Beckman, E. J. *Trends Polym. Sci.* **1997**, *5*, 236-240. (f) Kuran, W. *Prog. Polym. Sci.* **1998**, *23*, 919-992. (g) Paddock, R. L.; Nguyen, S. T. *Macromolecules* **2005**, *38*, 6251-6253. (h) Cohen, C. T.; Chu, T.; Coates, G. W. *J. Am. Chem. Soc.* **2005**, *127*, 10869-10878.

53. (a) Kruper, W. J.; Dellar, D. V. *J. Org. Chem.* **1995**, *60*, 725-727. (b) Kuran, W.; Listós, T. *Macromol. Chem. Phys.* **1994**, *195*, 1011-1015.

54. (a) Kricheldorf, H. R.; Jenssen, J. *J. Macromol. Sci., Pure Appl. Chem.* **1989**, *A26*, 631-644. (b) Ariga, T.; Takata, T.; Endo, T. *J. Polym. Sci., Part A: Polym. Chem.* **1993**, *31*, 581-584. (c) Matsumura, S.; Tsukada, K.; Toshima, K. *Macromolecules*, **1997**, *30*, 3122-3124.

55. Sawada, H. *J. Macromol. Sci. Rev. Macromol. Chem.* **1970**, *C5*, 151-174.

56. Koinuma, H.; Hirai, H. *Makromol. Chem.* **1977**, *178*, 241-246.

57. (a) Baba, A.; Kashiwagi, H.; Matsuda, H. *Tetrahedron Lett.* **1985**, *26*, 1323-1324. (b) Baba, A.; Meishou, H.; Matsuda, H. *Makromol. Chem., Rapid Commun.* **1984**, *5*, 665-668. (c) Baba, A.; Kashiwagi, H.; Matsuda, H. *Organometallics* **1987**, *6*, 137-140.

58. Matsuo, J.; Sandra, F.; Endo, T. *J. Polym. Sci., Part A: Polym. Chem*. **2000**, 35, 1375.

59. Takeda, N.; Inoue, S. *Makromol. Chem*. **1978**, *179*, 1377.

60. (a) Cheng, M.; Lobkovsky, E. B.; Coates, G. W. *J. Am. Chem. Soc.* **1998**, *120*, 11018. (b) Cheng, M.; Darling, N. A.; Lobkovsky, E. B.; Coates, G. W. *Chem. Commun*. **2000**, 2007. (c) Cheng, M.; Moore, D. R.; Reczek, J. J.; Chamberlain, B. M.; Lobkovsky, E. B.; Coates, G. W. *J. Am. Chem. Soc*. **2001**, *123*, 8783. (d) Moore, D. R.; Cheng, M.; Lobkovsky, E. B.; Coates, G. W. *Angew. Chem. Int. Edit*. **2002**, *41*, 2599. (e) Allen, S. D.; Moore, D. R.; Lobkovsky, E. B.; Coates, G. W. *J. Am. Chem. Soc*. **2002**, *124*, 14284.

61. (a) Stinziano-Eveland, R. A.; Nguyen, S. T.; Lable-Sands, Lialbe-Sands, L. M.; Reingold, A. L. *Inorg. Chem.* **2000**, *39*, 2452. (b) Morris, G. A.; Zhou, H.; Stern, C. L.; Nguyen, S. T. *Inorg. Chem*. **2001**, *40*, 3222.

62. Byrne, C. M.; Allen, S. D.; Lobkovsky, E. B.; and Coates, G. W. *J. Am. Chem. Soc. Commun.* **2004**. *126*, 12404.

63. Crivello, J. V.; Mao, Z. *Chem. Mater*. **1997**, *9*, 1554.

64. Darensbourg, D. J.; Rogers, J. D.; and Fang, C. C. *Inorg. Chem*. **2003**, *42*, 4498.

65. Ruck, R. T.; and Jacobsen, E. N. *J. Am. Chem. Commun*. **2002**, *124*, 2882.

66. (a) Dias, H. V. R.; and Singh, S. *Inorg. Chem*. **2004**, *43,* 5786. (b) Siedle, A. R.; Webb, R. J.; Behr, F. E.; Mewark, R. A.; Weil, D. A.; Erickson, K.; Naujok, R.; Brostrom, M.; Mueller, M.; Chou, S.; and Young, V. G. *Inorg. Chem*. **2003**, *42*, 932.

APPENDIX A

SUPPLEMENTARY MATERIAL FOR CRYSTAL STRUCTURES IN CHAPTER II

Table A-1. Atomic coordinates (x 10^4) and equivalent isotropic displacement parameters (Å^2 x 10^3) for salen-naph. U(eq) is defined as one third of the trace of the orthogonalized U^{ij} tensor.

	x	y	z	U(eq)
O(2)	4993(2)	6537(2)	2212(1)	32(1)
O(1)	2166(3)	9815(2)	2359(1)	33(1)
N(1)	1871(3)	8718(3)	3624(2)	31(1)
N(2)	4720(3)	7035(3)	3561(2)	30(1)
C(12)	156(4)	10536(3)	1598(2)	25(1)
C(27)	7370(4)	5973(3)	1570(2)	25(1)
C(13)	771(4)	9961(3)	2263(2)	28(1)
C(28)	7006(4)	6511(3)	2814(2)	29(1)
C(29)	6425(4)	6350(3)	2201(2)	27(1)
C(30)	8833(4)	5816(3)	1590(2)	27(1)
C(31)	8482(4)	6341(3)	2796(2)	31(1)
C(14)	-1272(4)	10662(3)	1532(2)	29(1)
C(11)	543(4)	8927(3)	3493(2)	30(1)
C(1)	2439(4)	8079(3)	4287(2)	29(1)
C(15)	175(4)	11596(3)	317(2)	32(1)
C(2)	3946(4)	7243(3)	4254(2)	29(1)
C(16)	-1511(4)	9715(3)	2713(2)	32(1)
C(26)	6080(4)	6863(3)	3484(2)	30(1)
C(17)	-2149(4)	10270(3)	2075(2)	30(1)
C(18)	-71(4)	9554(3)	2817(2)	29(1)
C(19)	1051(4)	10998(3)	986(2)	29(1)
C(32)	6774(4)	5760(3)	892(2)	27(1)
C(33)	9439(4)	5988(3)	2186(2)	29(1)
C(34)	8004(4)	5344(3)	273(2)	32(1)
C(3)	2272(4)	7630(3)	5598(2)	35(1)
C(4)	4406(5)	6164(4)	6218(2)	44(1)
C(5)	1634(4)	8269(3)	4945(2)	34(1)

Table A-1. (Continued)

	x	y	z	U(eq)
C(35)	1059(4)	5808(3)	2146(2)	31(1)
C(20)	2453(4)	9919(4)	747(2)	35(1)
C(21)	1447(4)	12004(4)	1256(2)	36(1)
C(36)	6176(4)	4728(3)	1075(2)	33(1)
C(6)	3775(4)	6795(3)	5566(2)	35(1)
C(37)	12038(4)	4508(3)	1929(2)	37(1)
C(7)	4578(4)	6615(3)	4883(2)	34(1)
C(38)	5571(4)	6957(3)	597(2)	35(1)
C(22)	-3710(4)	10451(3)	1935(2)	35(1)
C(8)	1468(5)	7796(4)	6288(2)	46(1)
C(9)	3603(5)	6365(4)	6869(2)	47(1)
C(39)	11314(4)	6783(4)	1568(2)	41(1)
C(10)	2124(6)	7174(4)	6903(2)	50(1)
C(40)	11537(4)	5951(4)	2863(2)	42(1)
C(23)	-3618(5)	9502(5)	1420(3)	55(1)
C(24)	-4529(5)	11754(4)	1604(3)	63(2)
C(25)	-4598(5)	10255(6)	2640(3)	64(1)
C(43)	2680(20)	1260(20)	4360(20)	490(30)
Cl(3)	4024(17)	632(16)	4537(9)	606(10)
Cl(4)	2270(20)	2428(18)	3953(11)	816(14)

Table A-2. Bond lengths [Å] and angles [°] for salen-naph.

O(2)-C(29)	1.346(4)
O(1)-C(13)	1.354(4)
N(1)-C(11)	1.287(4)
N(1)-C(1)	1.416(4)
N(2)-C(26)	1.274(4)
N(2)-C(2)	1.419(4)
C(12)-C(14)	1.382(4)
C(12)-C(13)	1.417(5)
C(12)-C(19)	1.537(5)
C(27)-C(30)	1.390(4)
C(27)-C(29)	1.414(5)
C(27)-C(32)	1.545(4)
C(13)-C(18)	1.405(5)
C(28)-C(31)	1.392(5)
C(28)-C(29)	1.405(5)
C(28)-C(26)	1.458(5)
C(30)-C(33)	1.398(5)
C(31)-C(33)	1.385(5)
C(14)-C(17)	1.406(5)
C(11)-C(18)	1.446(5)
C(1)-C(5)	1.372(5)
C(1)-C(2)	1.428(5)
C(15)-C(19)	1.535(5)
C(2)-C(7)	1.379(5)
C(16)-C(17)	1.377(5)
C(16)-C(18)	1.397(5)
C(17)-C(22)	1.525(5)
C(19)-C(20)	1.534(5)
C(19)-C(21)	1.544(5)
C(32)-C(36)	1.537(5)
C(32)-C(38)	1.532(5)
C(32)-C(34)	1.546(5)
C(33)-C(35)	1.527(5)
C(3)-C(8)	1.423(5)
C(3)-C(5)	1.421(5)
C(3)-C(6)	1.424(5)
C(4)-C(9)	1.363(6)
C(4)-C(6)	1.415(5)
C(35)-C(40)	1.519(5)
C(35)-C(37)	1.533(5)

Table A-2. (Continued)

C(35)-C(39)	1.547(5)
C(6)-C(7)	1.411(5)
C(22)-C(24)	1.515(6)
C(22)-C(25)	1.535(6)
C(22)-C(23)	1.536(6)
C(8)-C(10)	1.363(6)
C(9)-C(10)	1.398(6)
C(43)-Cl(3)	1.30(3)
C(43)-Cl(4)	1.41(4)
Cl(3)-Cl(3)#1	2.61(3)
C(11)-N(1)-C(1)	120.7(3)
C(26)-N(2)-C(2)	119.7(3)
C(14)-C(12)-C(13)	116.9(3)
C(14)-C(12)-C(19)	122.3(3)
C(13)-C(12)-C(19)	120.8(3)
C(30)-C(27)-C(29)	117.2(3)
C(30)-C(27)-C(32)	122.3(3)
C(29)-C(27)-C(32)	120.5(3)
O(1)-C(13)-C(12)	119.5(3)
O(1)-C(13)-C(18)	120.7(3)
C(12)-C(13)-C(18)	119.8(3)
C(31)-C(28)-C(29)	120.6(3)
C(31)-C(28)-C(26)	118.4(3)
C(29)-C(28)-C(26)	121.0(3)
O(2)-C(29)-C(28)	120.7(3)
O(2)-C(29)-C(27)	120.1(3)
C(28)-C(29)-C(27)	119.2(3)
C(27)-C(30)-C(33)	125.0(3)
C(33)-C(31)-C(28)	122.0(3)
C(12)-C(14)-C(17)	124.9(3)
N(1)-C(11)-C(18)	122.5(3)
C(5)-C(1)-N(1)	123.3(3)
C(5)-C(1)-C(2)	119.9(3)
N(1)-C(1)-C(2)	116.8(3)
C(7)-C(2)-N(2)	122.1(3)
C(7)-C(2)-C(1)	119.7(3)
N(2)-C(2)-C(1)	118.1(3)
C(17)-C(16)-C(18)	121.8(3)
N(2)-C(26)-C(28)	123.6(3)
C(16)-C(17)-C(14)	116.4(3)

Table A-2. (Continued)

C(16)-C(17)-C(22)	123.5(3)
C(14)-C(17)-C(22)	120.0(3)
C(16)-C(18)-C(13)	120.1(3)
C(16)-C(18)-C(11)	118.7(3)
C(13)-C(18)-C(11)	121.1(3)
C(15)-C(19)-C(20)	107.9(3)
C(15)-C(19)-C(12)	112.2(3)
C(20)-C(19)-C(12)	110.3(3)
C(15)-C(19)-C(21)	106.7(3)
C(20)-C(19)-C(21)	110.4(3)
C(12)-C(19)-C(21)	109.2(3)
C(36)-C(32)-C(38)	110.4(3)
C(36)-C(32)-C(34)	107.0(3)
C(38)-C(32)-C(34)	107.0(3)
C(36)-C(32)-C(27)	110.2(3)
C(38)-C(32)-C(27)	110.8(3)
C(34)-C(32)-C(27)	111.3(3)
C(31)-C(33)-C(30)	116.0(3)
C(31)-C(33)-C(35)	123.3(3)
C(30)-C(33)-C(35)	120.8(3)
C(8)-C(3)-C(5)	122.5(4)
C(8)-C(3)-C(6)	118.3(3)
C(5)-C(3)-C(6)	119.2(3)
C(9)-C(4)-C(6)	120.8(4)
C(1)-C(5)-C(3)	121.0(3)
C(40)-C(35)-C(33)	113.0(3)
C(40)-C(35)-C(37)	107.6(3)
C(33)-C(35)-C(37)	109.9(3)
C(40)-C(35)-C(39)	108.4(3)
C(33)-C(35)-C(39)	108.7(3)
C(37)-C(35)-C(39)	109.3(3)
C(7)-C(6)-C(4)	122.3(4)
C(7)-C(6)-C(3)	118.7(3)
C(4)-C(6)-C(3)	119.0(3)
C(2)-C(7)-C(6)	121.5(3)
C(24)-C(22)-C(25)	107.4(4)
C(24)-C(22)-C(17)	110.5(3)
C(25)-C(22)-C(17)	111.7(3)
C(24)-C(22)-C(23)	110.2(4)
C(25)-C(22)-C(23)	108.5(4)
C(17)-C(22)-C(23)	108.6(3)

Table A-2. (Continued)

C(10)-C(8)-C(3)	120.7(4)
C(4)-C(9)-C(10)	120.4(4)
C(8)-C(10)-C(9)	120.8(4)
Cl(3)-C(43)-Cl(4)	122.2(19)
C(43)-Cl(3)-Cl(3)#1	153(3)

Symmetry transformations used to generate equivalent atoms:
#1 -x+1,-y,-z+1

Table A-3. Anisotropic displacement parameters ($A^2 \times 10^3$) for salen-naph. The anisotropic displacement factor exponent takes the form: $-2\pi^2[h^2 a^{*2} U^{11} + ... + 2 h k a^* b^* U^{12}]$.

	U^{11}	U^{22}	U^{33}	U^{23}	U^{13}	U^{12}
O(2)	28(1)	42(2)	25(1)	-7(1)	0(1)	-12(1)
O(1)	31(1)	40(2)	31(1)	6(1)	-12(1)	-16(1)
N(1)	36(2)	27(2)	28(2)	-4(1)	-6(1)	-10(1)
N(2)	34(2)	34(2)	21(1)	-3(1)	-1(1)	-11(1)
C(12)	26(2)	20(2)	30(2)	-3(1)	-6(1)	-8(1)
C(27)	30(2)	21(2)	25(2)	1(1)	-6(1)	-10(1)
C(13)	26(2)	24(2)	34(2)	-3(1)	-8(1)	-9(1)
C(28)	34(2)	26(2)	27(2)	-1(1)	-7(1)	-10(2)
C(29)	30(2)	25(2)	26(2)	-1(1)	-4(1)	-11(1)
C(30)	29(2)	23(2)	28(2)	-3(1)	-1(1)	-9(1)
C(31)	32(2)	33(2)	30(2)	-6(2)	-6(2)	-13(2)
C(14)	30(2)	23(2)	36(2)	-3(1)	-11(2)	-9(1)
C(11)	32(2)	26(2)	29(2)	-4(1)	2(1)	-9(2)
C(1)	41(2)	24(2)	23(2)	-1(1)	-2(1)	-13(2)
C(15)	35(2)	31(2)	33(2)	2(2)	-10(2)	-14(2)
C(2)	37(2)	27(2)	22(2)	-2(1)	-4(1)	-10(2)
C(16)	29(2)	28(2)	37(2)	-4(2)	-3(2)	-11(2)
C(26)	31(2)	32(2)	26(2)	-2(1)	-9(1)	-9(2)
C(17)	27(2)	26(2)	38(2)	-6(2)	-5(2)	-9(1)
C(18)	31(2)	25(2)	32(2)	-6(1)	-2(1)	-10(1)
C(19)	30(2)	28(2)	30(2)	1(1)	-9(1)	-10(2)
C(32)	29(2)	29(2)	25(2)	-5(1)	-4(1)	-11(2)
C(33)	31(2)	24(2)	34(2)	-3(1)	-6(2)	-10(1)
C(34)	37(2)	32(2)	27(2)	-6(2)	-2(2)	-15(2)
C(3)	51(2)	26(2)	23(2)	-5(1)	1(2)	-12(2)
C(4)	61(3)	35(2)	29(2)	-1(2)	-5(2)	-13(2)
C(5)	39(2)	28(2)	31(2)	-7(2)	-1(2)	-6(2)
C(35)	28(2)	28(2)	39(2)	-5(2)	-8(2)	-10(2)
C(20)	30(2)	38(2)	33(2)	0(2)	-4(2)	-11(2)
C(21)	40(2)	36(2)	37(2)	4(2)	-10(2)	-21(2)
C(36)	41(2)	34(2)	27(2)	-5(2)	-4(2)	-17(2)
C(6)	49(2)	30(2)	24(2)	-3(2)	-4(2)	-14(2)
C(37)	31(2)	32(2)	46(2)	-4(2)	-9(2)	-10(2)

Table A-3. (Continued)

	U^{11}	U^{22}	U^{33}	U^{23}	U^{13}	U^{12}
C(7)	40(2)	30(2)	28(2)	-2(2)	-4(2)	-8(2)
C(38)	37(2)	35(2)	31(2)	-3(2)	-9(2)	-9(2)
C(22)	31(2)	32(2)	45(2)	-2(2)	-7(2)	-15(2)
C(8)	64(3)	37(2)	31(2)	-9(2)	5(2)	-14(2)
C(9)	78(3)	31(2)	29(2)	-1(2)	-7(2)	-16(2)
C(39)	37(2)	33(2)	55(3)	-3(2)	-3(2)	-18(2)
C(10)	78(3)	41(2)	28(2)	-9(2)	7(2)	-22(2)
C(40)	35(2)	43(2)	51(2)	-9(2)	-11(2)	-15(2)
C(23)	43(2)	62(3)	70(3)	-15(2)	-13(2)	-26(2)
C(24)	33(2)	41(3)	115(4)	18(3)	-27(3)	-15(2)
C(25)	36(2)	96(4)	68(3)	-8(3)	-2(2)	-34(3)
C(43)	243(19)	340(30)	970(70)	-430(40)	340(30)	-200(20)
Cl(3)	760(30)	700(30)	490(20)	-122(18)	101(19)	-430(30)
Cl(4)	1090(40)	660(30)	710(20)	190(20)	-115(19)	-410(30)

Table A-4. Hydrogen coordinates (x 10^4) and isotropic displacement parameters (A^2 x 10^3) for salen-naph.

	x	y	z	U(eq)
H(2)	4587	6728	2614	48
H(1)	2399	9438	2755	50
H(30)	9456	5577	1174	33
H(31)	8835	6470	3206	37
H(14)	-1684	11033	1096	35
H(11)	-44	8665	3846	36
H(15A)	-65	10991	120	48
H(15B)	758	11902	-43	48
H(15C)	-716	12269	454	48
H(16)	-2053	9439	3084	38
H(26)	6506	6967	3875	36
H(34A)	8778	4590	437	47
H(34B)	8391	5976	135	47
H(34C)	7605	5207	-138	47
H(4)	5382	5605	6201	52
H(5)	657	8824	4964	41
H(20A)	3029	9538	1155	52
H(20B)	3018	10223	376	52
H(20C)	2189	9320	559	52
H(21A)	559	12674	1401	54
H(21B)	1989	12307	872	54
H(21C)	2038	11656	1662	54
H(36A)	5347	4986	1427	50
H(36B)	6934	3991	1270	50
H(36C)	5874	4563	642	50
H(37A)	13050	4417	1880	55
H(37B)	11764	4391	1476	55
H(37C)	11911	3901	2297	55
H(7)	5555	6062	4857	41
H(38A)	5249	6816	163	53
H(38B)	5958	7594	488	53
H(38C)	4753	7212	955	53
H(8)	484	8334	6321	55
H(9)	4042	5962	7294	57
H(39A)	10737	7597	1713	61
H(39B)	11025	6700	1110	61

Table A-4. (Continued)

	x	y	z	U(eq)
H(39C)	12339	6655	1522	61
H(10)	1581	7290	7349	60
H(40A)	10948	6762	3011	63
H(40B)	12555	5844	2805	63
H(40C)	11411	5338	3226	63
H(23A)	-4592	9552	1364	82
H(23B)	-3035	8685	1618	82
H(23C)	-3171	9677	955	82
H(24A)	-4428	12338	1886	95
H(24B)	-5553	11901	1600	95
H(24C)	-4125	11848	1116	95
H(25A)	-4579	10783	2986	96
H(25B)	-4171	9407	2834	96
H(25C)	-5598	10453	2540	96
H(43A)	2050	1376	4805	584
H(43B)	2425	731	4088	584

APPENDIX B

1. Degradations of homopolymers

For the biodegradations of poly(trimethylene carbonate) and poly(*L*-lactide), each polymer was put into a vial filled with a sodium phosphate buffered saline (pH 7.4). NaN_3 was then added to the mixtures at a concentration of 0.02 % (wt./vol.) to prevent bacterial growth. Every three weeks, the polymers were dried under vacuum. Weight losses, molecular weights and PDIs were determined by GPC in THF (Table B-1).

Table B-1. Degradations of poly(trimethylene carbonate) and poly(*L*-lactide).

	Mn		weight		PDI	
3 weeks	initial	final	initial	final	initial	final
high Mn PTMC	145,000	-	-	-	1.207	-
low Mn PTMC	55,000	-	-	-	1.411	-
high Mn PLLA	124,600	90,100	0.1002	0.0939	1.327	1.022
high Mn PLLA	89,400	61,300	0.1003	0.0846	1.042	1.014
6 weeks						
high Mn PTMC	145,000	123,300	0.096	0.0959	1.207	1.504
low Mn PTMC	55,000	58,800	0.1044	0.1043	1.411	1.324
high Mn PLLA	124,600	87,500	0.1007	0.0992	1.327	1.042
low Mn PLLA	89,400	51,000	0.1	0.0975	1.042	1.026
9 weeks						
high Mn PTMC	145,000	69,400	0.1031	0.1028	1.207	1.411
low Mn PTMC	55,000	35,000	0.1042	0.1032	1.411	1.705
high Mn PLLA	124,600	67,700	0.1003	0.0996	1.327	1.274
low Mn PLLA	89,400	41,400	0.1001	0.096	1.042	1.294

Table B-1. (Continued)

	Mn		weight		PDI	
12 weeks	initial	final	initial	final	initial	final
H Mn PTMC	145,000	59,900	0.1031	0.1031	1.207	1.617
L Mn PTMC	55,000	28,700	0.1049	0.1048	1.411	1.936
H Mn PLLA	124,600	65,100	0.1006	0.098	1.327	1.299
low Mn PLLA	89,400	40,400	0.1001	0.0965	1.042	1.324
15 weeks						
H Mn PTMC	145,000	69,800	0.1032	0.1026	1.207	1.493
L Mn PTMC	55,000	39,600	0.1049	0.1047	1.411	1.617
H Mn PLLA	124,600	52,800	0.1008	0.0995	1.327	1.514
L Mn PLLA	89,400	28,100	0.1	0.0992	1.042	1.857
18 weeks						
H Mn PTMC	145,000	63,900	0.102	0.0976	1.207	1.65
L Mn PTMC	55,000	25,500	0.1033	0.101	1.411	1.785
H Mn PLLA	124,600	53,600	0.1007	0.0968	1.327	1.509
L Mn PLLA	89,400	40,000	0.1	0.0978	1.042	1.308
21 weeks						
H Mn PTMC	145,000		0.1033	0.099	1.207	
L Mn PTMC	55,000		0.1037	0.1037	1.411	
H Mn PLLA	124,600	50,400	0.1001	0.098	1.327	1.652
L Mn PLLA	89,400	19,400	0.1004	0.0985	1.042	2.546

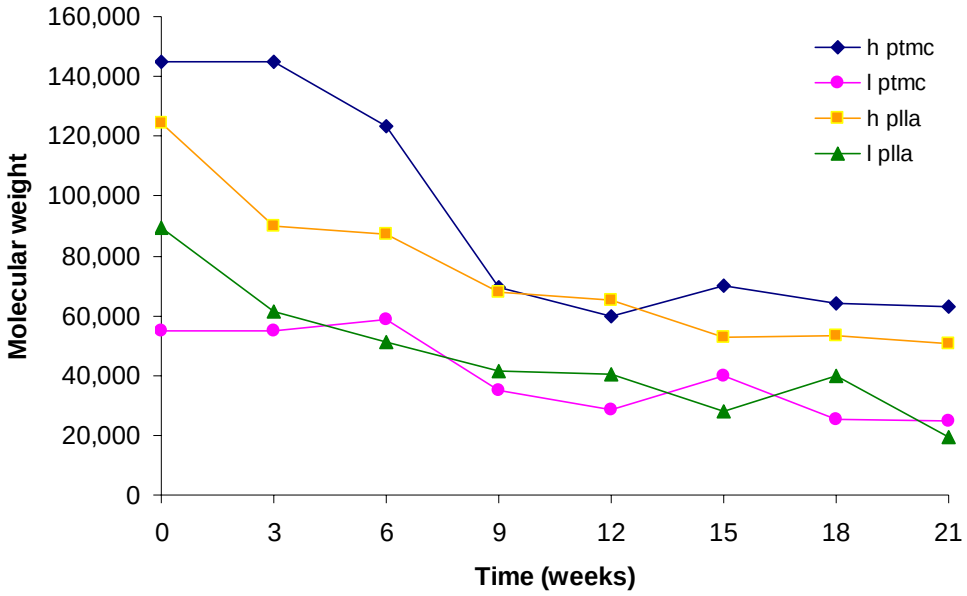

Figure B-1. Molecular weight changes for poly(trimethylene carbonate) and poly(*L*-lactide), where h ptmc is high molecular weight poly(trimethylene carbonate), l ptmc is low molecular weight poly(trimethylene carbonate), h plla is high molecular weight poly(*L*-lactide), and l plla is low molecular weight poly(*L*-lactide).

2. Degradations of copolymers

For the degradations of copolymers, random copolymerization reactions with different compositions of trimethylene carbonate and *L*-lactide have been performed using catalyst **2-9**. The produced random copolymers are listed in Table B-2. For the degradation studies, each copolymer was put into a vial filled with a sodium phosphate buffered saline (pH 7.4). NaN_3 was then added to the mixtures at a concentration of 0.02 % (wt./vol.) to prevent bacterial growth. Every three weeks, the copolymers were dried under vacuum. Weight losses, and composition changes have been determined by ^{1}H NMR (Table B-2).

Table B-2. Random copolymers produced from *L*-lactide and trimethylene carbonate using catalyst **2-9**.

random copolymers[a]	feed ratio (mol LLA : mol TMC)	conversion (%)[b]		composition[c] (mol PLLA : mol PTMC)
		LLA	TMC	
1	50 : 50	98.7	42.2	63 : 37
2	25 : 75	74.6	35.3	27 : 73
3	75 : 25	53.8	15.8	90 : 10

[a] Random copolymerization reactions were performed in melt maintaining a nomomer : initiator ratio as 350:1 at 110°C for 60 minutes. [b] Obtained from ^{1}H NMR after copolymerization reactions. [c] Obtained from ^{1}H NMR after precipitating in 5% HCl and MeOH, and drying in a vacuum oven.

Table B-3. Degradations of random copolymer **1**.

time (weeks)	weight (g)	composition (%)	
		PLLA	PTMC
0	0.0887	37	63
3	0.0885	37	63
6	0.0872	32	68

Table B-4. Degradations of random copolymer **2**.

time (weeks)	weight (g)	composition (%)	
		PLLA	PTMC
0	0.0930	90	10
3	0.0929	89	11
6	0.0827	73	22

Table B-5. Degradations of random copolymer **3**.

time (weeks)	weight (g)	composition (%)	
		PLLA	PTMC
0	0.1000	27	73
3	0.0993	22	78
6	0.1158	27	73

APPENDIX C

SUPPLEMENTARY MATERIAL FOR CRYSTAL STRUCTURES IN CHAPTER IV

Table C-1. Atomic coordinates (x 10^4) and equivalent isotropic displacement parameters (Å^2 x 10^3) for **4-4**. U(eq) is defined as one third of the trace of the orthogonalized U^{ij} tensor.

	x	y	z	U(eq)
C(7S)	10100(40)	3330(50)	9180(30)	260(40)
Cr(1)	-1242(2)	3234(2)	5812(1)	36(1)
Cl(1)	-365(4)	2898(3)	4544(2)	41(1)
Cl(2)	-2330(4)	3617(3)	6958(2)	46(1)
O(1W)	-1459(9)	5150(8)	5877(6)	41(2)
O(1)	638(9)	3653(8)	6589(6)	39(2)
N(1)	-1168(10)	1320(9)	5692(6)	28(2)
N(2)	-3199(11)	2502(10)	4924(6)	34(3)
C(1)	1408(14)	2976(12)	7015(8)	31(3)
C(2)	1051(13)	1596(12)	6837(8)	35(3)
C(3)	1965(13)	885(11)	7324(8)	31(3)
C(4)	3162(13)	1479(12)	7976(8)	33(3)
C(5)	3506(14)	2851(12)	8146(8)	35(3)
C(6)	2698(16)	3606(12)	7693(8)	40(3)
C(7)	-181(14)	843(12)	6170(8)	33(3)
C(8)	-2357(13)	481(11)	5059(8)	30(3)
C(9)	-3459(14)	1146(13)	4675(8)	33(3)
C(10)	-4730(14)	445(14)	4036(9)	42(3)
C(11)	-4881(15)	-930(14)	3813(9)	45(4)
C(12)	-3844(14)	-1576(13)	4176(7)	37(3)

Table C-1. (Continued)

	x	y	z	U(eq)
C(13)	-2581(13)	-893(11)	4792(7)	30(3)
C(14)	-4184(16)	3187(14)	4596(9)	47(4)
C(15)	-5475(15)	2551(15)	3959(9)	48(4)
C(16)	-5721(14)	1213(14)	3715(9)	44(4)
C(17)	3157(14)	5085(12)	7906(9)	41(3)
C(18)	1990(16)	5931(13)	8233(9)	52(4)
C(19)	3381(15)	5336(12)	7070(8)	44(4)
C(20)	4571(16)	5557(13)	8633(10)	56(4)
C(21)	4096(15)	790(13)	8555(8)	42(3)
C(22)	3686(17)	1191(13)	9451(8)	53(4)
C(23)	3843(14)	-705(12)	8137(9)	44(4)
C(24)	5719(14)	1156(13)	8724(10)	55(4)
O(1S)	8457(10)	7147(9)	7374(6)	47(2)
C(1S)	8020(20)	7092(17)	8136(10)	73(5)
C(2S)	8790(30)	8220(20)	8868(12)	110(8)
C(3S)	9560(20)	8990(20)	8562(15)	131(10)
C(4S)	9426(17)	8286(14)	7626(10)	56(4)
C(6S)	9110(60)	4180(40)	9380(20)	210(30)
C(5S)	8740(40)	5410(60)	9900(30)	190(20)

Table C-2. Bond lengths [Å] and angles [°] for **4-4**.

C(7S)-C(6S)	1.34(7)
C(7S)-C(5S)#1	1.79(7)
C(7S)-H(7S)	0.9500
Cr(1)-O(1)	1.903(9)
Cr(1)-N(1)	1.976(10)
Cr(1)-O(1W)	2.013(8)
Cr(1)-N(2)	2.053(11)
Cr(1)-Cl(2)	2.295(5)
Cr(1)-Cl(1)	2.355(5)
O(1W)-H(1W)	0.8400
O(1)-C(1)	1.278(13)
N(1)-C(7)	1.296(14)
N(1)-C(8)	1.416(14)
N(2)-C(14)	1.316(16)
N(2)-C(9)	1.365(15)
C(1)-C(2)	1.419(16)
C(1)-C(6)	1.441(17)
C(2)-C(3)	1.428(16)
C(2)-C(7)	1.431(16)
C(3)-C(4)	1.355(16)
C(3)-H(3)	0.9500
C(4)-C(5)	1.411(16)
C(4)-C(21)	1.513(16)
C(5)-C(6)	1.383(16)
C(5)-H(5)	0.9500
C(6)-C(17)	1.529(17)
C(7)-H(7)	0.9500
C(8)-C(13)	1.377(15)
C(8)-C(9)	1.413(16)
C(9)-C(10)	1.422(17)
C(10)-C(16)	1.377(18)
C(10)-C(11)	1.382(18)

Table C-2. (Continued)

C(11)-C(12)	1.344(17)
C(11)-H(11)	0.9500
C(12)-C(13)	1.398(16)
C(12)-H(12)	0.9500
C(13)-H(13)	0.9500
C(14)-C(15)	1.416(18)
C(14)-H(14)	0.9500
C(15)-C(16)	1.346(18)
C(15)-H(15)	0.9500
C(16)-H(16)	0.9500
C(17)-C(18)	1.533(19)
C(17)-C(20)	1.536(17)
C(17)-C(19)	1.541(18)
C(18)-H(18A)	0.9800
C(18)-H(18B)	0.9800
C(18)-H(18C)	0.9800
C(19)-H(19A)	0.9800
C(19)-H(19B)	0.9800
C(19)-H(19C)	0.9800
C(20)-H(20A)	0.9800
C(20)-H(20B)	0.9800
C(20)-H(20C)	0.9800
C(21)-C(23)	1.502(17)
C(21)-C(22)	1.542(18)
C(21)-C(24)	1.545(18)
C(22)-H(22A)	0.9800
C(22)-H(22B)	0.9800
C(22)-H(22C)	0.9800
C(23)-H(23A)	0.9800
C(23)-H(23B)	0.9800
C(23)-H(23C)	0.9800
C(24)-H(24A)	0.9800

Table C-2. (Continued)

C(24)-H(24B)	0.9800
C(24)-H(24C)	0.9800
O(1S)-C(4S)	1.407(16)
O(1S)-C(1S)	1.430(16)
C(1S)-C(2S)	1.43(2)
C(1S)-H(1S1)	0.9900
C(1S)-H(1S2)	0.9900
C(2S)-C(3S)	1.38(2)
C(2S)-H(2S1)	0.9900
C(2S)-H(2S2)	0.9900
C(3S)-C(4S)	1.45(2)
C(3S)-H(3S1)	0.9900
C(3S)-H(3S2)	0.9900
C(4S)-H(4S1)	0.9900
C(4S)-H(4S2)	0.9900
C(6S)-C(5S)	1.41(5)
C(6S)-H(6S)	0.9500
C(5S)-C(7S)#1	1.79(7)
C(5S)-H(5S)	0.9500
C(6S)-C(7S)-C(5S)#1	82(4)
C(6S)-C(7S)-H(7S)	138.8
C(5S)#1-C(7S)-H(7S)	138.8
O(1)-Cr(1)-N(1)	91.2(4)
O(1)-Cr(1)-O(1W)	92.9(4)
N(1)-Cr(1)-O(1W)	176.0(4)
O(1)-Cr(1)-N(2)	171.8(4)
N(1)-Cr(1)-N(2)	81.0(4)
O(1W)-Cr(1)-N(2)	95.0(4)
O(1)-Cr(1)-Cl(2)	93.4(3)
N(1)-Cr(1)-Cl(2)	91.5(3)
O(1W)-Cr(1)-Cl(2)	88.2(3)

Table C-2. (Continued)

N(2)-Cr(1)-Cl(2)	89.2(3)
O(1)-Cr(1)-Cl(1)	92.4(3)
N(1)-Cr(1)-Cl(1)	91.2(3)
O(1W)-Cr(1)-Cl(1)	88.7(3)
N(2)-Cr(1)-Cl(1)	85.5(3)
Cl(2)-Cr(1)-Cl(1)	173.62(17)
Cr(1)-O(1W)-H(1W)	109.5
C(1)-O(1)-Cr(1)	130.7(8)
C(7)-N(1)-C(8)	121.0(10)
C(7)-N(1)-Cr(1)	124.8(8)
C(8)-N(1)-Cr(1)	114.1(7)
C(14)-N(2)-C(9)	119.0(12)
C(14)-N(2)-Cr(1)	127.5(10)
C(9)-N(2)-Cr(1)	113.5(8)
O(1)-C(1)-C(2)	122.2(12)
O(1)-C(1)-C(6)	120.1(11)
C(2)-C(1)-C(6)	117.7(11)
C(1)-C(2)-C(3)	119.7(12)
C(1)-C(2)-C(7)	123.5(11)
C(3)-C(2)-C(7)	116.8(11)
C(4)-C(3)-C(2)	122.8(11)
C(4)-C(3)-H(3)	118.6
C(2)-C(3)-H(3)	118.6
C(3)-C(4)-C(5)	116.9(10)
C(3)-C(4)-C(21)	124.5(11)
C(5)-C(4)-C(21)	118.5(11)
C(6)-C(5)-C(4)	123.9(12)
C(6)-C(5)-H(5)	118.0
C(4)-C(5)-H(5)	118.0
C(5)-C(6)-C(1)	118.9(11)
C(5)-C(6)-C(17)	120.8(12)
C(1)-C(6)-C(17)	120.3(11)

Table C-2. (Continued)

N(1)-C(7)-C(2)	125.9(11)
N(1)-C(7)-H(7)	117.0
C(2)-C(7)-H(7)	117.0
C(13)-C(8)-C(9)	116.5(12)
C(13)-C(8)-N(1)	128.0(11)
C(9)-C(8)-N(1)	115.5(10)
N(2)-C(9)-C(8)	115.8(11)
N(2)-C(9)-C(10)	121.9(11)
C(8)-C(9)-C(10)	122.3(12)
C(16)-C(10)-C(11)	125.9(13)
C(16)-C(10)-C(9)	116.5(13)
C(11)-C(10)-C(9)	117.6(12)
C(12)-C(11)-C(10)	120.7(13)
C(12)-C(11)-H(11)	119.6
C(10)-C(11)-H(11)	119.6
C(11)-C(12)-C(13)	121.9(13)
C(11)-C(12)-H(12)	119.1
C(13)-C(12)-H(12)	119.1
C(8)-C(13)-C(12)	121.0(12)
C(8)-C(13)-H(13)	119.5
C(12)-C(13)-H(13)	119.5
N(2)-C(14)-C(15)	121.9(14)
N(2)-C(14)-H(14)	119.0
C(15)-C(14)-H(14)	119.0
C(16)-C(15)-C(14)	118.7(13)
C(16)-C(15)-H(15)	120.7
C(14)-C(15)-H(15)	120.7
C(15)-C(16)-C(10)	121.9(13)
C(15)-C(16)-H(16)	119.0
C(10)-C(16)-H(16)	119.0
C(6)-C(17)-C(18)	109.2(11)
C(6)-C(17)-C(20)	112.3(11)

Table C-2. (Continued)

C(18)-C(17)-C(20)	108.1(11)
C(6)-C(17)-C(19)	110.3(11)
C(18)-C(17)-C(19)	109.6(11)
C(20)-C(17)-C(19)	107.4(11)
C(17)-C(18)-H(18A)	109.5
C(17)-C(18)-H(18B)	109.5
H(18A)-C(18)-H(18B)	109.5
C(17)-C(18)-H(18C)	109.5
H(18A)-C(18)-H(18C)	109.5
H(18B)-C(18)-H(18C)	109.5
C(17)-C(19)-H(19A)	109.5
C(17)-C(19)-H(19B)	109.5
H(19A)-C(19)-H(19B)	109.5
C(17)-C(19)-H(19C)	109.5
H(19A)-C(19)-H(19C)	109.5
H(19B)-C(19)-H(19C)	109.5
C(17)-C(20)-H(20A)	109.5
C(17)-C(20)-H(20B)	109.5
H(20A)-C(20)-H(20B)	109.5
C(17)-C(20)-H(20C)	109.5
H(20A)-C(20)-H(20C)	109.5
H(20B)-C(20)-H(20C)	109.5
C(23)-C(21)-C(4)	111.1(11)
C(23)-C(21)-C(22)	108.3(11)
C(4)-C(21)-C(22)	107.8(11)
C(23)-C(21)-C(24)	106.7(11)
C(4)-C(21)-C(24)	113.3(11)
C(22)-C(21)-C(24)	109.5(11)
C(21)-C(22)-H(22A)	109.5
C(21)-C(22)-H(22B)	109.5
H(22A)-C(22)-H(22B)	109.5
C(21)-C(22)-H(22C)	109.5

Table C-2. (Continued)

H(22A)-C(22)-H(22C)	109.5
H(22B)-C(22)-H(22C)	109.5
C(21)-C(23)-H(23A)	109.5
C(21)-C(23)-H(23B)	109.5
H(23A)-C(23)-H(23B)	109.5
C(21)-C(23)-H(23C)	109.5
H(23A)-C(23)-H(23C)	109.5
H(23B)-C(23)-H(23C)	109.5
C(21)-C(24)-H(24A)	109.5
C(21)-C(24)-H(24B)	109.5
H(24A)-C(24)-H(24B)	109.5
C(21)-C(24)-H(24C)	109.5
H(24A)-C(24)-H(24C)	109.5
H(24B)-C(24)-H(24C)	109.5
C(4S)-O(1S)-C(1S)	109.1(10)
O(1S)-C(1S)-C(2S)	106.1(14)
O(1S)-C(1S)-H(1S1)	110.5
C(2S)-C(1S)-H(1S1)	110.5
O(1S)-C(1S)-H(1S2)	110.5
C(2S)-C(1S)-H(1S2)	110.5
H(1S1)-C(1S)-H(1S2)	108.7
C(3S)-C(2S)-C(1S)	109.5(16)
C(3S)-C(2S)-H(2S1)	109.8
C(1S)-C(2S)-H(2S1)	109.8
C(3S)-C(2S)-H(2S2)	109.8
C(1S)-C(2S)-H(2S2)	109.8
H(2S1)-C(2S)-H(2S2)	108.2
C(2S)-C(3S)-C(4S)	107.8(15)
C(2S)-C(3S)-H(3S1)	110.2
C(4S)-C(3S)-H(3S1)	110.2
C(2S)-C(3S)-H(3S2)	110.2
C(4S)-C(3S)-H(3S2)	110.2

Table C-2. (Continued)

H(3S1)-C(3S)-H(3S2)	108.5
O(1S)-C(4S)-C(3S)	107.1(14)
O(1S)-C(4S)-H(4S1)	110.3
C(3S)-C(4S)-H(4S1)	110.3
O(1S)-C(4S)-H(4S2)	110.3
C(3S)-C(4S)-H(4S2)	110.3
H(4S1)-C(4S)-H(4S2)	108.6
C(7S)-C(6S)-C(5S)	150(5)
C(7S)-C(6S)-H(6S)	105.1
C(5S)-C(6S)-H(6S)	105.1
C(6S)-C(5S)-C(7S)#1	128(3)
C(6S)-C(5S)-H(5S)	116.2
C(7S)#1-C(5S)-H(5S)	116.2

Symmetry transformations used to generate equivalent atoms:
#1 -x+2,-y+1,-z+2

Table C-3. Anisotropic displacement parameters ($Å^2 x\ 10^3$) for **4-4**. The anisotropic displacement factor exponent takes the form: $-2\pi^2[h^2 a^{*2} U^{11} + ... + 2 h k a^* b^* U^{12}]$.

	U^{11}	U^{22}	U^{33}	U^{23}	U^{13}	U^{12}
C(7S)	180(40)	520(100)	320(60)	390(70)	130(40)	170(50)
Cr(1)	35(1)	33(1)	37(1)	13(1)	4(1)	2(1)
Cl(1)	46(2)	36(2)	44(2)	19(2)	13(2)	4(2)
Cl(2)	54(2)	43(2)	42(2)	12(2)	17(2)	-3(2)
O(1W)	35(5)	39(5)	56(6)	24(5)	14(5)	13(4)
O(1)	38(5)	30(5)	50(6)	22(4)	2(5)	-3(4)
N(1)	21(6)	30(6)	30(6)	13(5)	-4(5)	-3(5)
N(2)	29(6)	42(7)	35(6)	21(5)	5(5)	8(5)
C(1)	37(8)	28(7)	29(7)	11(6)	9(6)	4(6)
C(2)	28(7)	30(7)	47(8)	10(6)	13(7)	6(6)
C(3)	40(8)	21(6)	33(7)	14(5)	5(6)	6(6)
C(4)	30(8)	40(8)	33(7)	18(6)	6(6)	6(6)
C(5)	32(8)	32(7)	29(7)	3(6)	-4(6)	-5(6)
C(6)	55(9)	36(8)	38(8)	19(6)	20(7)	10(7)
C(7)	40(8)	28(7)	32(7)	5(6)	20(7)	-5(6)
C(8)	32(8)	27(7)	35(7)	11(6)	13(6)	-2(6)
C(9)	29(7)	41(8)	34(7)	12(6)	15(6)	8(6)
C(10)	36(8)	50(9)	39(8)	18(7)	4(7)	2(7)
C(11)	35(8)	59(10)	35(8)	15(7)	-1(7)	-14(7)
C(12)	40(8)	42(8)	21(7)	1(6)	5(6)	-12(7)
C(13)	33(7)	32(7)	25(7)	9(5)	9(6)	4(6)
C(14)	55(10)	50(9)	42(8)	15(7)	23(8)	4(8)
C(15)	32(8)	61(10)	47(9)	19(8)	1(7)	6(8)
C(16)	27(8)	53(9)	43(8)	12(7)	-1(7)	-9(7)
C(17)	36(8)	29(7)	53(9)	13(6)	-1(7)	-3(6)
C(18)	72(11)	31(8)	55(9)	20(7)	12(9)	2(8)
C(19)	46(9)	29(7)	52(9)	20(7)	-6(7)	-8(6)
C(20)	56(10)	33(8)	66(10)	18(7)	-11(8)	-14(7)
C(21)	47(9)	38(8)	35(8)	11(6)	0(7)	-3(7)

Table C-3. (Continued)

	U^{11}	U^{22}	U^{33}	U^{23}	U^{13}	U^{12}
C(22)	72(11)	43(8)	30(8)	15(6)	-14(8)	10(8)
C(23)	43(9)	38(8)	52(9)	23(7)	3(7)	4(7)
C(24)	39(9)	44(9)	65(10)	16(8)	-19(8)	-10(7)
O(1S)	52(6)	46(6)	39(5)	8(4)	14(5)	-7(5)
C(1S)	89(14)	72(12)	50(10)	8(9)	21(10)	-7(10)
C(2S)	180(30)	94(16)	64(13)	11(12)	62(16)	3(16)
C(3S)	114(19)	105(17)	122(19)	-58(15)	66(16)	-74(14)
C(4S)	64(11)	39(9)	69(11)	15(8)	26(9)	5(8)
C(6S)	390(80)	120(30)	90(20)	40(20)	0(30)	-170(40)
C(5S)	110(20)	330(50)	220(40)	250(40)	0(30)	-20(30)

Table C-4. Hydrogen coordinates (x 10^4) and isotropic displacement parameters ($Å^2$ x 10^3) for **4-4**.

	x	y	z	U(eq)
H(7S)	10156	2490	8753	317
H(1W)	-2329	5292	5810	62
H(3)	1724	-45	7186	37
H(5)	4344	3283	8599	42
H(7)	-286	-92	6069	40
H(11)	-5729	-1426	3400	54
H(12)	-3971	-2523	4008	44
H(13)	-1867	-1384	5030	36
H(14)	-4025	4135	4792	56
H(15)	-6154	3059	3710	58
H(16)	-6604	786	3308	53
H(18A)	2288	6881	8381	78
H(18B)	1846	5767	8763	78
H(18C)	1091	5684	7763	78
H(19A)	2507	5013	6584	65
H(19B)	4184	4857	6892	65
H(19C)	3595	6297	7201	65
H(20A)	4885	6473	8696	84
H(20B)	5306	4963	8468	84
H(20C)	4424	5536	9199	84
H(22A)	3884	2161	9746	79
H(22B)	4250	730	9831	79
H(22C)	2662	937	9344	79
H(23A)	2858	-996	8106	66
H(23B)	4519	-1126	8498	66
H(23C)	3986	-970	7536	66
H(24A)	5946	1059	8157	83
H(24B)	6266	556	9000	83
H(24C)	5974	2083	9122	83

Table C-4. (Continued)

	x	y	z	U(eq)
H(1S1)	8256	6245	8248	88
H(1S2)	6971	7150	8044	88
H(2S1)	8106	8757	9166	132
H(2S2)	9452	7898	9308	132
H(3S1)	10579	9136	8898	158
H(3S2)	9171	9874	8642	158
H(4S1)	9062	8868	7269	68
H(4S2)	10372	8020	7529	68
H(6S)	8226	3736	8973	253
H(5S)	7769	5587	9737	227

VITA

Wonsook Choi was born in Chuncheon, Korea, to Aejin Chung and Younghee Choi. She grew up in Seoul, Korea, and attended Sogang University in Seoul, Korea. She graduated with a B.S. in Chemistry in February of 1995 and with an M.S in Chemistry in February of 1997. She earned her second M.S. at the University of New Mexico in August of 2003. In September of the same year she came to Texas A&M University and started research under the guidance of Dr. Donald J. Darensbourg. She earned her Ph.D at Texas A&M University in August of 2007. Questions and comments may be directed to chwons@hotmail.com or 6-402 Kumho apt. Onui-dong, Chuncheon, Kangwon, Republic of KOREA.